Mixture Preparation, Combustion, and HC Emissions at Different Cranking Speeds

by

Halim G. Santoso

B.S., International Development Engineering in Mechanical Course
Tokyo Institute of Technology, 2000

SUBMITTED TO THE DEPARTMENT OF MECHANICAL ENGINEERING IN PARTIAL
FULFILLMENT OF THE REQUIREMENTS FOR THE DEGREE OF

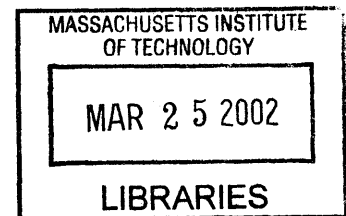MASTER OF SCIENCE IN MECHANICAL ENGINEERING

AT THE

MASSACHUSETTS INSTITUTE OF TECHNOLOGY

FEBRUARY 2002

BARKER

Signature of Author: _____

Department of Mechanical Engineering
January 2002

Certified by: ___

_____
Wai K.Cheng
Professor of Mechanical Engineering
Thesis Supervisor

Accepted by: _____

_____
Ain A. Sonin
Chairman, Departmental Graduate Committee

Mixture Preparation, Combustion, and Hydrocarbon Emissions at Different Cranking Speeds

by

Halim G. Santoso

ABSTRACT

To assess the effect of cranking speeds on hydrocarbon emissions in the engine start-up process, the engine behavior at low speeds were obtained in an engine/dynamometer set up with a pulley speed reduction system. The exhaust and in-cylinder hydrocarbon levels were measured using fast response flame ionization detectors (FFID). Experiments to elucidate the effects of fuel injection amount, cranking speeds, and engine coolant temperatures on mixture preparation, combustion, and hydrocarbon emissions level at these low speeds have been performed using a skip firing strategy.

For the same amount of fuel injection, increasing the cranking speed increased the in-cylinder fuel equivalence ratio, reduced the mass fraction of fuel delivered into the cylinder, and also reduced the engine out hydrocarbon level (EOHC). The engine started to fire with the average in-cylinder fuel equivalence ratio (ϕ) as low as 0.65, although robust combustion was not observed until the average in-cylinder fuel equivalence ratio reached 0.8 or above. The minimum level of HC level observed during the experiment was 1300 $ppmC_1$. The results of heat release analysis showed that the heat release per unit crank angle was much faster at lower engine speed. The MBT timing shifted from $10°$ BTDC to $20°$ BTDC when the engine speed was varied from 300 to 900 rpm. Higher engine coolant temperature resulted in higher in-cylinder fuel equivalence ratio for the same amount of fuelling and lower HC emissions level.

Acknowledgements

TABLE OF CONTENTS

LIST OF FIGURES & TABLES

COMBUSTION

HYDROCARBON EMISSIONS

LIST OF TABLES

NOMENCLATURE

ATDC	After Top Dead Center
BDC	Bottom Dead Center
BTDC	Before Top Dead Center
CAD	Crank Angle Degree
CAP II	California Phase II fuel
CP	Constant Pressure
CVI	Closed Valve Injection
COV	Coefficient of Variation
ECU	Electronic Control Unit
ECT	Engine Coolant Temperature
EGR	Exhaust Gas Recirculation
EOHC	Engine Out Hydrocarbon
EVO	Exhaust Valve Open
EVC	Exhaust Valve Close
FFID	Fast Flame Ionization Detector
FPW	Fuel Pulse Width
FTP	Federal Test Procedure
GDI	Gasoline Direct Injection
GImep	Gross Imep
HC	Hydrocarbon
HSM	Head Sampling Module
Imep	Indicated Mean Effective Pressure
IVC	Intake Valve Close
IVO	Intake Valve Open
LHC	Line Heater Controller
MAP	Manifold Absolute Pressure
MBT	Maximum Brake Torque
MCU	Main Control Unit
MON	Motor Octane Number
OVI	Open Valve Injection
PFI	Port Fuel Injection
RON	Research Octane Number
RVP	Reid Vapor Pressure
SI	Spark Ignition
SSP	Sampling Spark Plug
TDC	Top Dead Center
VAC	Vacuum

m_a	Mass of air
m_f	Mass of fuel
M_a	Molecular weight of air

M_f	Molecular weight of fuel
n_a	Mole of air
n_f	Mole of fuel
OF	Overlap Factor
P_{in}	Intake Pressure
R_a	Gas Constant for air
r_c	Geometric Compression Ratio
stoich	Stoichiometric
T_a	Air temperature
V_{ivc}	Cylinder Volume at Intake Valve Closing
X_f	Fuel Mass Fraction
X_r	Residual Mass Fraction
Y_f	Fuel Mole Fraction
λ	Lambda, Air Fuel Equivalence Ratio
ϕ	Phi, Fuel Air Equivalence Ratio

Chapter 1

INTRODUCTION

1.1 Background

High performance automotive catalyst has significantly reduced hydrocarbon (HC) emissions level under normal operating condition. When the engine is first started, however, the catalyst has not reached its light-off temperature (around 250°C) and therefore ineffective. The HC emissions in this light-off period (typically about 2 minutes for US model year 2000 vehicle) are the dominant components of a trip emission. With fast light-off catalyst (less than 10 seconds light-off time), the HC emissions during the cranking process become significant. This research assesses the effects of increasing cranking speed on hydrocarbon emissions in a PFI spark ignition engine during start-up

It is worth mentioning that there is a fundamental difference in how exhaust emissions are viewed in the U.S. and the rest of the world. While the rest of the world primarily concerns with CO_2 for its greenhouse effect, US puts more emphasis on air quality which is related to the smog produced by automotive exhaust hydrocarbons and nitrogen oxides reacting in sunlight. Therefore hydrocarbon emissions reduction is one of the first priority in engine design process in the US.

The engine-out HC emissions in cranking are significantly higher than those in normal operating condition. This fact can be traced back to how current engine designers meter the amount of fuel injection for the cranking cycles. In current start-up strategies for port fuel injected engines, the Engine Control Unit (ECU) employs an over-fueled bank-injection method in order to avoid engine stalling. Once the ECU senses crankshaft rotation, it waits approximately 30° of crank rotation and then simultaneously injects a large amount of fuel to each cylinder (up to more than 10 times the amount that would make a stoichiometric mixture). During normal engine operation, fueling is based on the estimated amount of air inducted to each cylinder and in the case of engine transient, on the calibrated fuel transport behavior. However the cranking cycles which may be considered as an extreme case of transient, many of the engine processes such as the air induction and fuel evaporation are not

well established. In the absence of accurate critical information to start the engine, over-fueled injection method is necessary to ensure that at least one cylinder fires on the first cycle, and that the remaining cycles quickly follow.

The combined effects of catalyst ineffectiveness and over-fueled bank injection method resulted in substantial Engine Out Hydrocarbon (EOHC) in cold start. This phenomenon is illustrated in Fig 1.1 which shows the EOHC level during standard FTP test (bag 1 and 3). The standard FTP test consists of 3 phases: cold start (bag 1), transient (bag 2), and hot start (bag 3). There is a 10 minutes engine shut-down period between bag 2 and 3 and therefore the engine has to be restarted for the test in phase 3. The EOHC levels during the first few seconds in both the cold and hot start are substantially higher than the levels at normal engine operation. To handle this problem several approaches, such as external heating to the catalyst and retarding the spark timing have been tried. There is no apparent solution yet. This research attempts to clarify the processes involved in cranking so that an optimized cranking management strategy can be established. In particular we focused our efforts to assess the effects of cranking speeds on various engine operating performance parameters.

1.2 Previous Works

There is a relatively limited number of technical papers available in the literature on the subject of mixture preparation, combustion, and HC emissions during the cranking cycles. This fact is due to the relatively new development of fast light-off three way catalyst which accentuates the emissions during cranking. Reports are attempts to visualize the first cycle fuel transport [1], investigate the minimum fuel injection for cold starts [2], and to measure in-cylinder mixture strength [3]. Yet no comprehensive conclusions were drawn. Henning et al [4] assessed the fuel injection timing, spark timing, and fuel air ratio influence on hydrocarbon emissions and coefficient of variation (COV) of IMEP during cold start (25°C ambient temperature). Some of their conclusions include: worse HC emissions at OVI, no significant difference in cumulative HC emissions is observed with CVI air-assisted injection, and dual spray injection neither improved combustion stability nor reduced HC for CVI.

This project is very much influenced by the previous work done in the Sloan Automotive Laboratory by Bridgette Castaign for her master thesis [8] and Jim Cowart for his PhD thesis [7]. Their work was started by the notion suggested by Henein et al [5] that initial

piston position was a key parameter in understanding the engine out hydrocarbon emissions during start-up. Besides initial piston position, the importance of regulating the MAP and spark timing to reduce EOHC emissions during start-up was stressed in Ref [5]. While that paper has reported HC emissions during cranking, little was done to gain a systematic understanding of the necessary mixture preparation process which plays a critical role.

The work by Castaing [6] et al has led to some interesting conclusions that initiated this project. One of the conclusions drawn from their work was that the most important effect of the piston starting position in the engine behavior is on the engine instantaneous RPM values of the first cycle. The instantaneous speed influences the IMEPg of the first cycle through its effect on combustion phasing (with a fixed the spark timing strategy), which affects both the work transfer schedule and the charge heat lost. The piston position which has a higher engine speed at ignition point will have a greater IMEP. Therefore as a direct result of their work, the engine speed has been identified to play a major role in the first cycle combustion process. Since their experimental set-up did not allow for arbitrary engine speed control it was difficult to look at the pure effect of engine speed. This project is aimed to continue their previous works by elucidating the effect engine speed on mixture preparation, combustion, and EOHC emissions.

1.3 Objective

The objective of this work is to investigate the effect of cranking speeds on engine start-up performance in a well-controlled condition. In particular, we are interested in looking at how the mixture preparation, combustion, and hydrocarbon emissions are effected by changing the cranking speed. The mixture preparation process during start-up is different from that of normal practice. The dry intake port requires much more fuel injection to form a fuel puddle of significant area in the intake port. Substantial fuel needs to be injected to establish a proper in-cylinder fuel air equivalence ratio for robust combustion. Previous investigation has suggested that the combustion at low cranking speed will require different combustion phasing. This is due to the fact that the heat release rate is very fast in terms of crank angle at such low speed. While higher engine coolant temperature will lead to a lower HC level, the general behavior of HC emissions during the cranking cycle is not established. Analyzing the effect of increasing cranking speed on mixture preparation, combustion, and

HC emissions performance will provide a better understanding of engine start-up performance and will assess the benefit of increasing cranking speed as an approach to reduce the hydrocarbon emissions.

1.4 Method

To achieve good control of engine speed, the typical production engine starting process using a battery and a starter to crank the engine is replaced by a pulley system which is coupled to a dynamometer to provide low engine speed control. The Manifold Absolute Pressure (MAP) is regulated by adjusting the throttle to match a typical closed throttle start-up strategy. Fig 1.2 shows a typical closed-throttle general cranking behavior of a 4-cylinder PFI spark ignition engine which is taken from a Ford Zetec engine [6]. The fuel injection pulse width indicated that tremendous amount of fuel injection is necessary to achieve firing in the first cycle. The injected fuel decreases in the subsequent cycles. The dip in the manifold absolute pressure occurs during the intake process of the cylinders and decreases slowly with increasing rpm. The engine speed increases from 180 rpm to 600 rpm due to the combustion process which can be identified from the pressure trace. The relation between the engine speed and the MAP is replotted in figure 1.3. In order to keep the experimental condition as close as possible to the real cranking condition the engine speed and MAP is coupled as follows: for 300, 600, and 900 rpm, the MAP is set at 0.92 bar, 0.8 bar, and 0.7 bar.

We used a skip firing strategy to simulate the engine start-up behavior at certain cranking speed. The skip firing strategy is done by injecting a certain amount of fuel for single cycle and skip injection for a certain number of cycles before the next injection of fuel is commenced. By adjusting the number of skip injection, we can eliminate the residual gases inside the cylinder and the liquid fuel build up in the intake port. Thus the condition experienced in the first cycle of a typical PFI engine can be simulated. Another benefit is that the simulated start can be repeated for many times without much difficulties to provide statistic for the data. Figure 1.4 shows the typical pressure trace in the skip injection mode. Notice that the increase in pressure signal prior to combustion cycle is due to the fuel injection signal which was superimposed on the pressure signal.
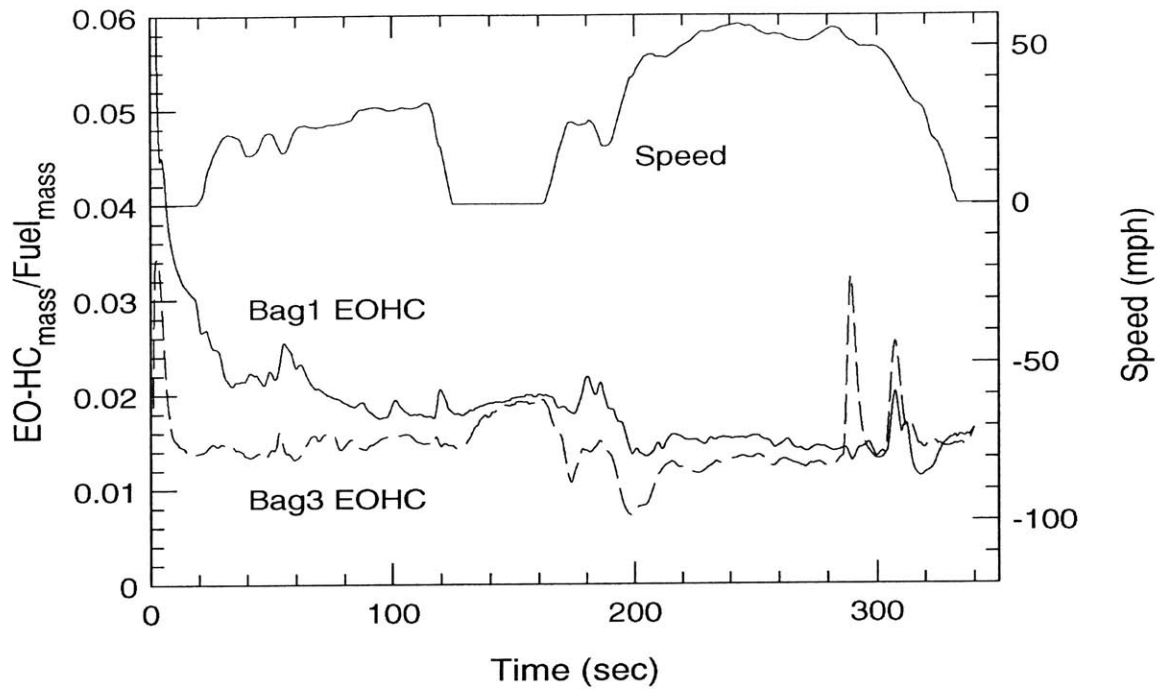
Figure 1.1: EOHC emissions during cranking and start-up from Daimler Chrysler 3.8 L
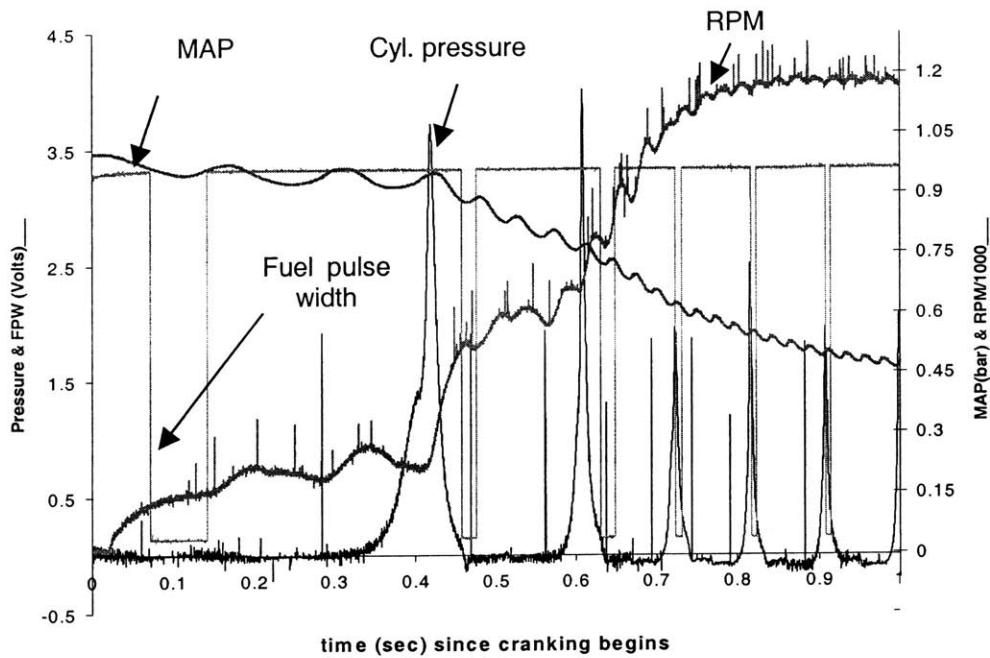
Figure 1.2: General Cranking Behavior from Ford Zetec 4-cylinder Engine
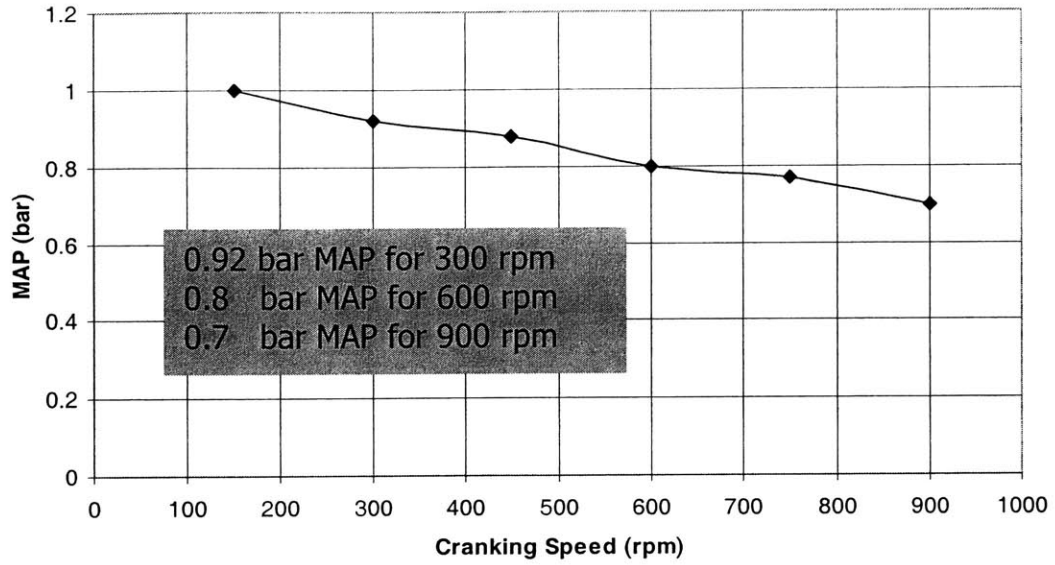
Figure 1.3: Relation between cranking speed and Manifold Absolute Pressure
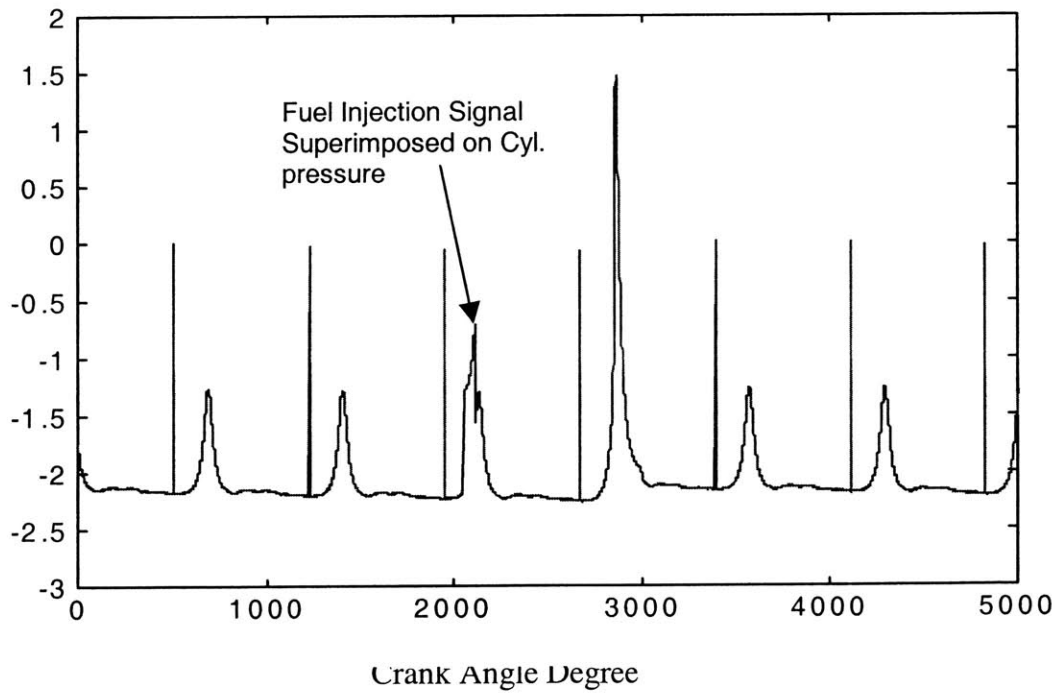
Figure 1.4: Pressure Trace in Skip Injection Mode

Chapter 2

EXPERIMENTAL APPARATUS

2.1 Modified Nissan Engine

The engine used throughout the experiment is a production 4-valve per cylinder, 4 cylinders 2L Nissan SR20DE PFI engine (Figure 2.1 and Table 2.1). To avoid the complexity that resulted from using multi-cylinder engine, the Nissan engine were modified to run only on single cylinder by separating the intake plenum of the firing cylinder from the other cylinders. The non-firing cylinders intake runners were vented to the atmosphere and motored by a dynamometer during the tests. This set up allows for precise control and measurement of the airflow and exhaust gas of the firing cylinder. The effect of the motored cylinders is limited to the friction force that has to be supplied throughout the tests, but the complication of having to consider the effect of firing cycles from other cylinders is eliminated.

The pre-calibrated fuel injector is located 22 cm upstream of the intake valve seat. The amount of fuel injection is controlled by the duration of fuel injection (Fuel Pulse Width). In order to keep the driving pressure differential of the injector constant, the injection pressure is referenced to the MAP pressure. The beginning of the fuel injection is set as 90° BTDC during the compression stroke.

The engine was fitted with a shaft encoder which produces one digital pulse every crank angle as well as one digital pulse every revolution to synchronize the data acquisition system. The spark timing was controlled manually with one crank angle degree precision. During most of the experiments the spark timing was fixed at TDC, except for some cases where the effect of spark timing on the combustion process at cranking speeds was investigated. The engine coolant temperature was controlled with an external heat exchanger which can be varied from 30° to 80°C. Attempts have been taken to lower the engine coolant temperature further with no avail which lead to the conclusion that either a large chiller or different experiment set-up is necessary to run the tests at lower temperature (<10° C).

2.2 Pulley System

A Dynamatic 100HP dynamometer (Figure 2.3) capable of motoring and absorbing the power during firing cycles is used to control the engine speed. Since the stable operating range of the dynamometer is between 600 and 2700 rpm, we need a gear reduction pulley system (Figure 2.2 and 2.4) to run the engine at lower cranking speed. The pulley system has a gear ratio of 3:1 which gives us the operating speed range from 200 to 900 rpm. It consists of 4 pulleys with 1 bushing for each pulley and 2 gearbelts from Browning. Originally the tension of the belt was adjusted by changing the location of the adjusting plate but during the experiments we found that the dynamic of the power pulses especially during high load operation caused the tension of the belts to vary so much that we have to enhance the robustness of the system. Therefore, we added two belt tensioners to reduce the vibration caused by the dynamics of the power pulses at higher engine load. The gear ratio can also be change to accommodate other speed range but the 3 to 1 gear ratio was kept constant throughout the experiments.

2.3 In-cylinder Pressure Measurement

The in-cylinder pressure was measured using a Kistler 6051 piezoelectric pressure transducer located in the cylinder head (Figure 2.5). The output signal from the pressure transducer was magnified using a Kistler charge amplifier and sent to the data acquisition system. The gain of the pressure transducer was bench-calibrated; the calibration curve is shown in figure 2.6. There are 2 additional signals which are superimposed on the pressure signal throughout the experiment, the BDC compression signal and the fuel injection signal. Since the pressure transducer only measures the change in the in-cylinder pressure as opposed to the absolute in-cylinder pressure, we need to have a reference for the pressure signal. A common practice in engine application is to take the pressure at bottom dead center compression as the reference pressure. Since the intake valve is still open at BDC compressions and the piston velocity is zero, the in-cylinder pressure at this point at low and moderate speed is equal to the manifold pressure. A shaft encoder is used to identify the bottom dead center compression during a cycle and gives a digital signal which is superimposed on the pressure signal.

The amount of fuel injection is controlled by changing the fuel pulse width and in order to have the same amount of fuel for a certain pulse width, we need to keep the ΔP of the across the fuel injector constant. Since the experiments were done in skipped injection mode, there is a need to determine the fuel injection cycle and in order to reduce the size of the data file we decided to superimposed the fuel injection signal to the pressure signal.

2.4 Fast Flame Ionization Detector (Fast FID)

A Fast Response Flame Ionization Detector (FID) was used to determine the in-cylinder air fuel ratio and engine out hydrocarbon (EOHC) level. Both the in-cylinder and exhaust hydrocarbon was measured using the Cambustion HFR400 Fast FID (Figure 2.9). The physical origin of the Fast FID signal comes from the fact that when a hydrocarbon is burnt, significant quantities of ions are formed and the number of ions produced is nearly proportional to the number of carbon atoms in the hydrocarbon. The ionization current is measured by the Fast FID. Therefore the output signal of the Fast FID is influenced by the mass flow rate. In the fast FID a sampling system is devised so that the mass flow rate into the detector is independent of the inlet condition. To account for drift it is necessary to perform the calibrations before and after each test.

The Fast FID system consists of a Hydrocarbon Sampling Module (HSM), a gas handling and electronics subsystem, the Main Control Unit (MCU), and for in-cylinder sampling, a heated sampling line, a line heater controller (LHC), an extension volume for the CP chamber and a sampling spark plug (SSP). In the HSM the sample gas is burned with fuel gas (hydrogen) and air mixture, the negative ions generated in the flame are collected at the electrode which is maintain at 180 V with respect to the body of the FID. The signal from the electrode is then transferred and amplified in the MCU. MCU is also used to monitor the temperature and pressure in the HSM and to operate the grow plug starter to light the flame in the HSM. The pressure controller in the MCU consists of 2 parts, the ΔP FID which controls the pressure difference across the sample (FID) tube in mmHg and CP VAC which control the gauge pressure in the CP chamber. To capture the whole intake process the CP VAC must be operated at high value (low absolute pressure). If the FID is operated without a constant pressure system (at atmospheric pressure) then during the intake process when the in-cylinder pressure is lower than atmospheric pressure, there will be no flow from the cylinder to the

HSM. Instead there will be backflow from the HSM to the cylinder which mean that during the intake process the output produced by the Fast FID will be invalid. In order to deal with this problem, we added an extension chamber to the existing vacuum chamber so that higher vacuum pressure (low absolute pressure) could be achieved. Throughout the experiments the CP VAC were set at least at 450 mmHg and ΔP FID at approximately 80 mmHg. Since the lowest intake pressure set during the mixture preparation experiments was 0.7 bar using this experiment set up, we were able to capture the whole intake stroke process.

For in-cylinder HC measurement, a sampling spark plug (SSP) which is an offset spark plug was used to accommodate a heated sample line (TSL-H) capillary tube. The heated line temperature was controlled with a line heater controller (LHC). To avoid the condensation of hydrocarbon in the sampling tube, the sampling tube temperature was kept constant at 180°C. This configuration will delay the carbon deposit formation in the sampling tube and reduce the probability of clogged sampling tube during the experiments. Bench calibration was done for in-cylinder HC measurement. Different ratios of propane and air mixture were introduced to the tip of the sampling line to measure the FID output signals. Instead of having several tanks containing different concentration of propane and air, a volume flow rate controller was used to create a mixture of desired composition (0%, 4%, 8%, 10% C_3H_8). Since the Fast FID signal tends to drift over time, the calibration had to be done twice, before and after the experiments.

The exhaust hydrocarbon calibration is much simpler than the in-cylinder one. Typically a mixture of propane and nitrogen (1500 and 3000 ppm C_3H_8) is used to calibrate the Fast FID output in-situ because it's not difficult to fill the exhaust port with mixture of propane and nitrogen.

2.5 Data Acquisition System

The data acquisition system used in all experiments consisted of a Dell Pentium III computer with National Instruments PCI-6025E multi-function I/O board, National Instrument BNC-2090 BNC connector board, and Labview 5.1 data acquisition program. The Labview program is externally triggered by the crank angle signal from the shaft encoder. Therefore the interval between 2 data point always corresponds to a crank angle degree

regardless the engine speed. Normally only 2 or 3 channels (pressure, in-cylinder HC, exhaust HC) were used in the experiments.

2.6 Engine Operating Condition

The first cycle during cranking is different from that of the subsequent cycles because there is no fuel in the port and no residual burned gas in the cylinder in the first cycle of cranking. To eliminate the residual gases inside the cylinder without having to stop the engine for each test, a skip injection method was selected. In skip injection mode, a suitable fuel injection frequency was chosen so that we could eliminate the residual gas from the cylinder. From the in-cylinder FID signal, skipping the fuel injection for 8 ~ 10 cycles was enough to purge the engine from the residual gas in most of the operating conditions. The spark was left on during the skipped injection operation.

Utilizing this strategy we were able to collect data under a well controlled condition. To assess the effect of changing the cranking speed on engine performance, it was necessary to collect data under conditions similar to the real cranking process. Previous investigation by Jim Cowart and Bridgette Castaing [6] successfully described the general cranking behavior of a production 4-cylinder engine. Our approach was to set the intake pressure for a given speed using the previous cranking data in a production engine [6]. The values chosen for this project were 0.92 bar, 0.8 bar, 0.7 bar intake pressure for 300, 600, and 900 rpm engine speed.

The test procedure was as follows: motored the engine with the dynamometer to the desired speed, adjusted the throttle to set the intake pressure to correspond to the engine speed, injected fuel for a single cycle, skipped injection for 5 ~ 10 cycles to eliminate the residual gas, repeated the test sequence for many cycles. Using this strategy, a condition similar to that of real cranking condition can be simulated and repeated over many cycles without having to stop the engine.

Firing Cylinder and Motored Cylinder Intake Runners
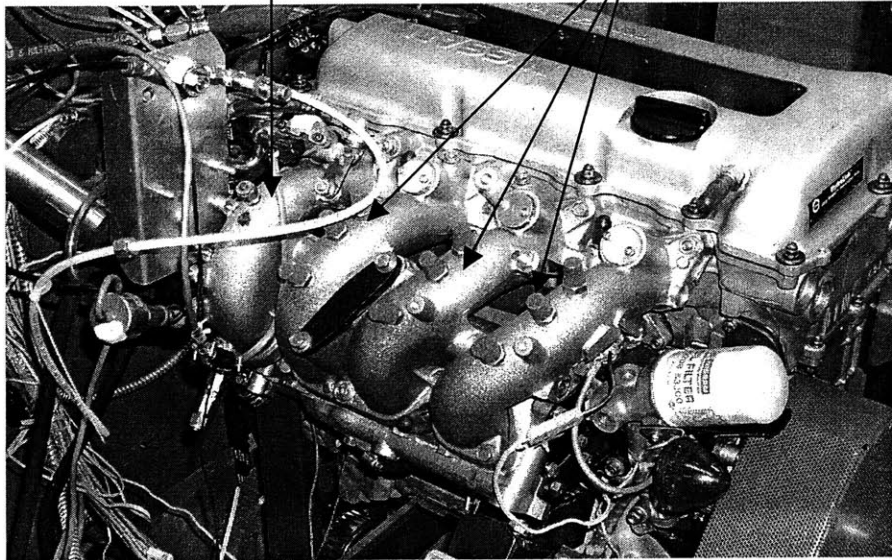
Figure 2.1 Modified Nissan Engine

Modified Nissan Engine	4-valve/cylinder DOHC Aluminum Head/Block
Bore × Stroke (mm)	86 × 86
Displacement Volume (cm^3)	500
Clearance Volume (cm^3)	58.77
Compression Ratio	9.5
Intake Valves (34 mm Diameter / 10.2 mm Max Lift)	Open 13° BTDC Close 235° ATDC
Exhaust Valves (30 mm Diameter / 9.4 mm Max Lift)	Open 483° ATDC Close 723° ATDC
Valve Overlap Period	16 CAD
Connecting Rod Length (mm)	136.3

Table 2.1 Nissan Engine Configuration
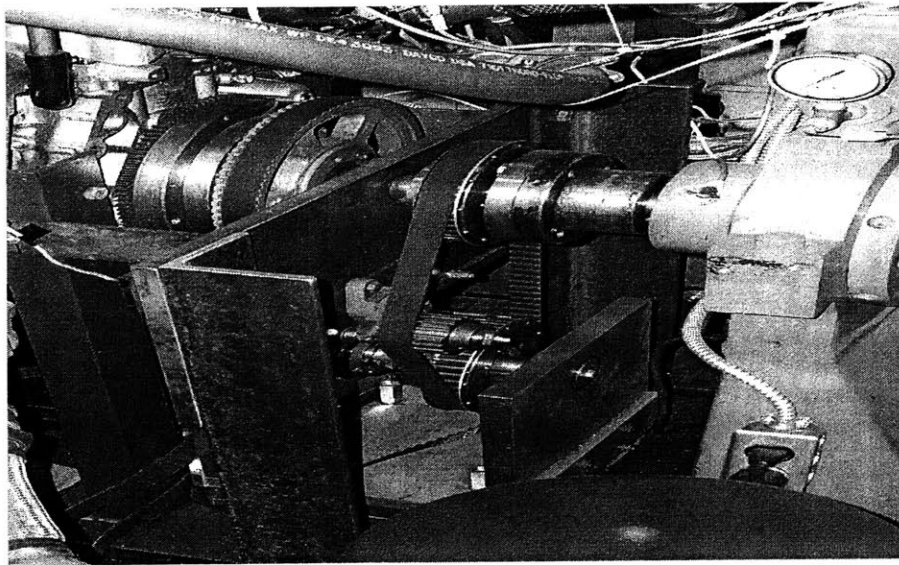
Figure 2.2 Pulley System
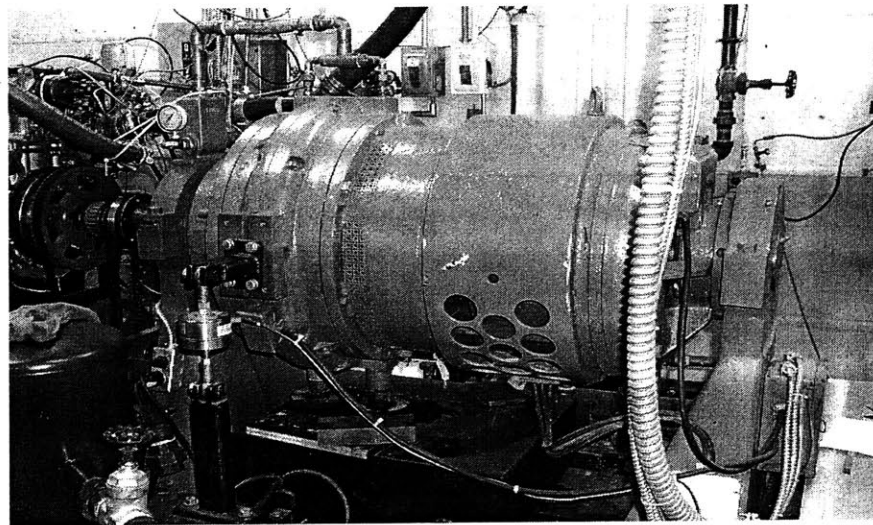
Figure 2.3 Dynamometer
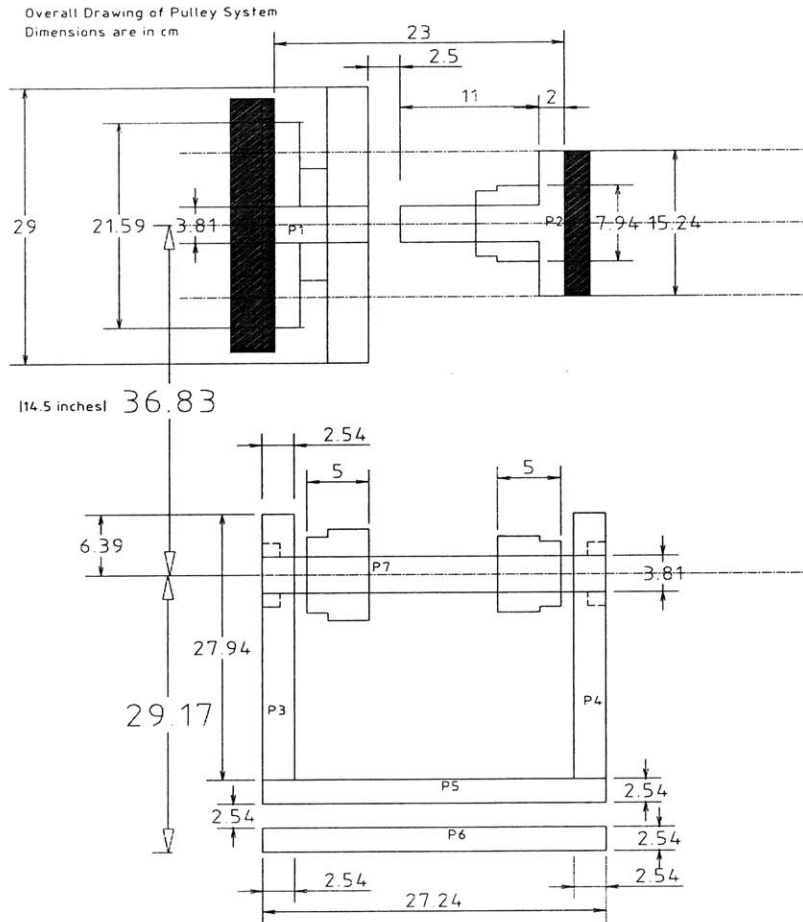
Figure 2.4 Technical Drawing of the Pulley System

Component	Unit
20H100SH Pulley – 1.5" bore	3
60H100SF Pulley – 1.5" bore	1
510H100 Gearbelt	1
420H100 Gearbelt	1
QDSH Bushing	3
QQSF Bushing	1

Table 2.2 Pulley System's Components
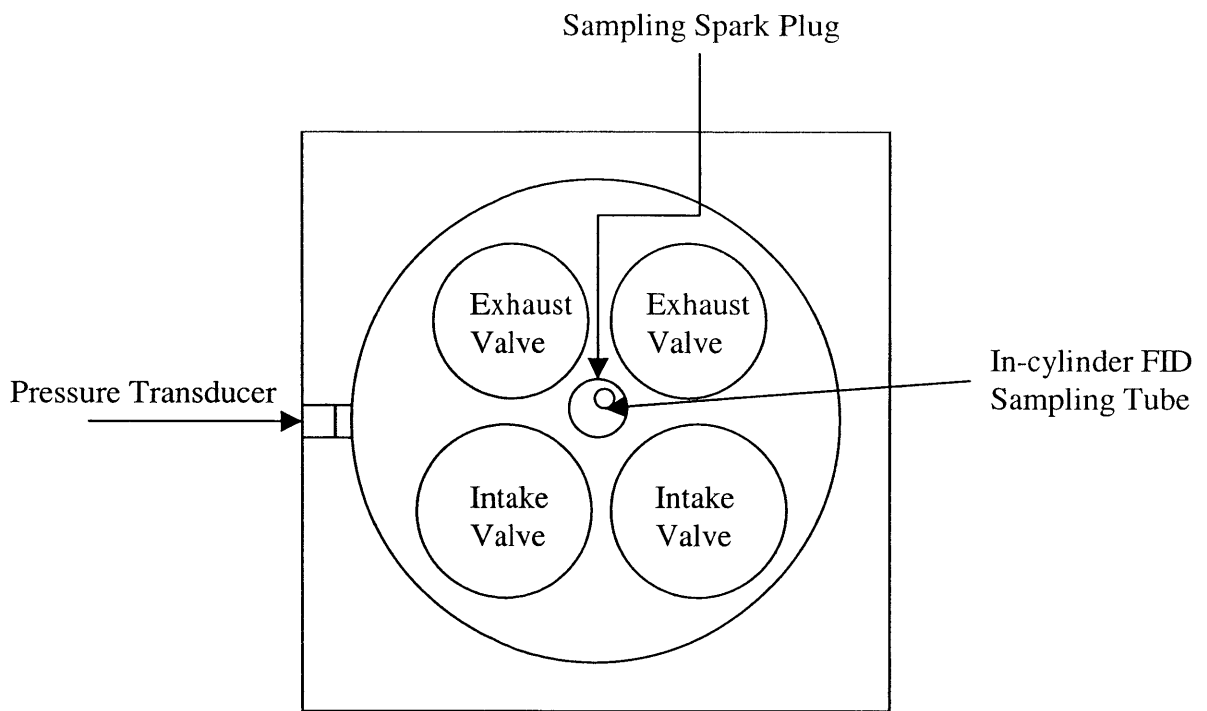
Figure 2.5 Top View of Pressure Transducer and In-cylinder FID Sampling Tube
Locations
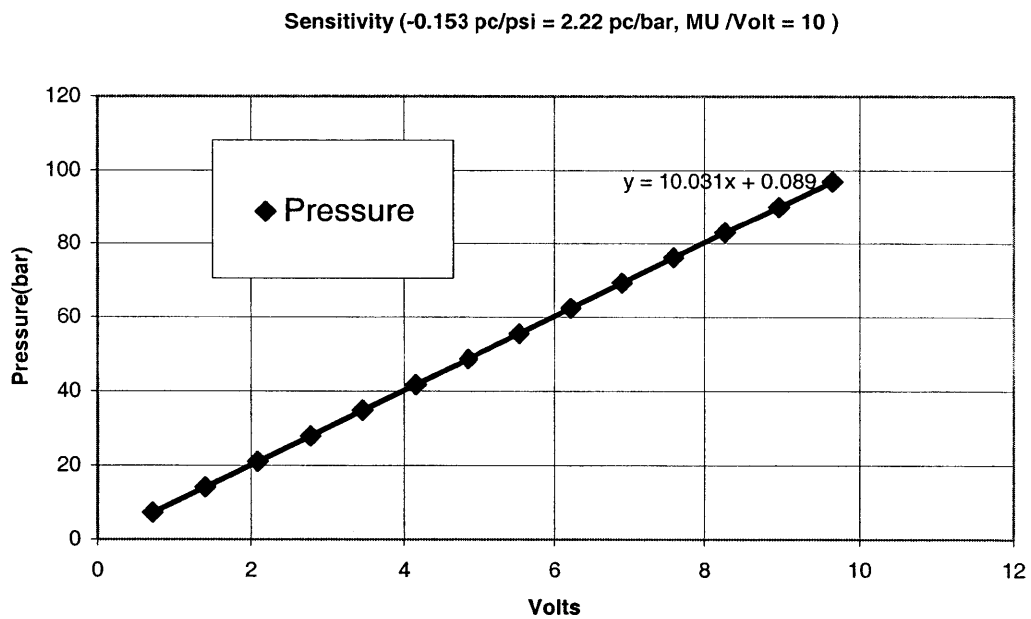
Figure 2.6 Pressure Transducer Calibration Curve
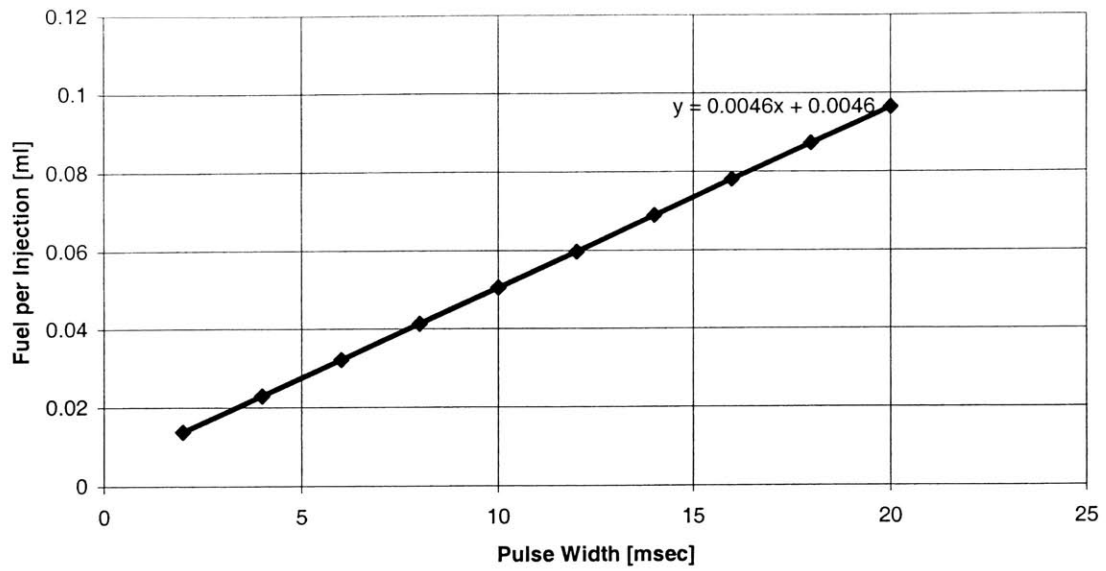
Figure 2.7 Calibration Curve of the Regular Injector
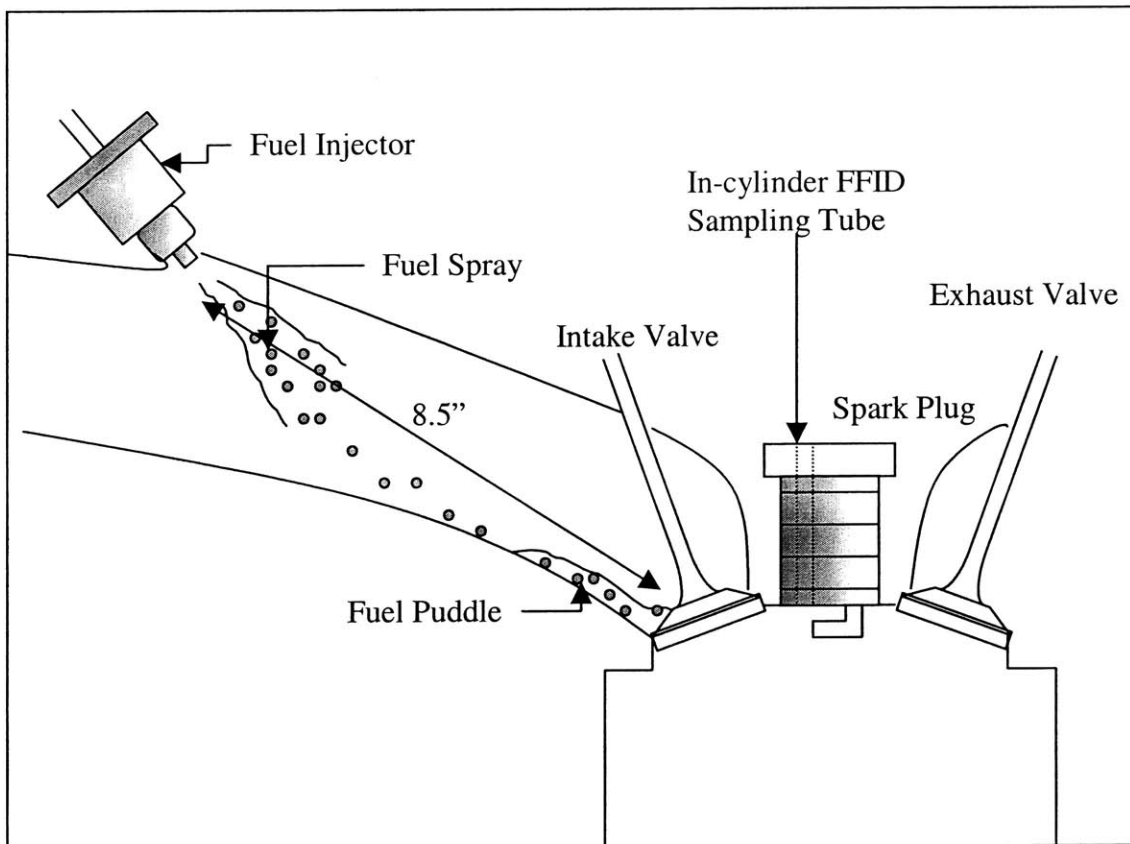
Figure 2.8 Intake Port Geometry for the Nissan Engine

Transfer Sampling Line

Sampling
Tube

Sampling
Head

Line Heater
Controller

Extension Volume
For CP Chamber

Main Control Unit

Compressed Air

Compressed
Hydrogen

Vacuum Pump
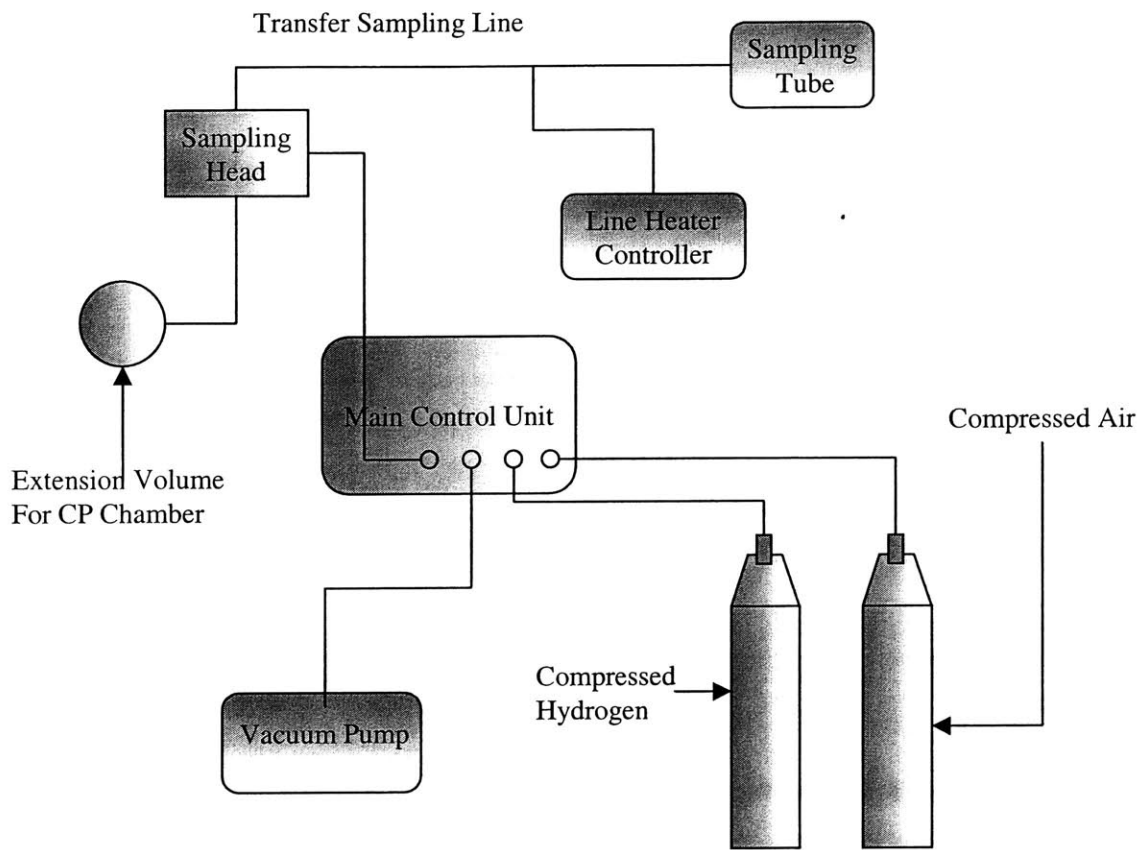
Figure 2.9 Hydrocarbon Sampling System

Chapter 3

MIXTURE PREPARATION

3.1 Mixture Preparation Process Overview

In PFI Spark Ignition Engine, especially during start-up, not all of the fuel injected to the port is delivered into the cylinder for the cycle. Since the combustion process is highly dependent on the in-cylinder fuel air ratio, there is a need to characterize the fuel delivery process during the cranking cycles to avoid misfires which will lead to high level of engine out hydrocarbon level. Mixture preparation is affected by the fuel type, the fuel injection (geometry and atomization), intake port condition, and the intake air flow.

3.1.1 Fuel Properties

Commercial gasoline fuel usually consists of more than 100 chemical species with different boiling temperatures for each species. The low boiling temperature species evaporate faster than fuel species with higher boiling temperature. The fuel used throughout the experiments was California Phase II Reformulated Gasoline with 96.6 Research Octane Number (Table 3.1). The initial boiling point is at 39.4°C; the 10, 50, and 90% distillation points are at 60.6, 94.2, and 148.6° C; the end point is at 191°C.

3.1.2 Fuel Injection and Atomization

Atomizing the liquid fuel into fine droplets facilitates mixture preparation by providing a large area for fuel evaporation. There are three atomization processes in PFI engine: (a) direct atomization of the fuel jet; (b) strip atomization of the liquid wall film by the back flow of the cylinder gases when the intake valve opens; (c) strip atomization of the liquid wall film into the cylinder by the forward intake flow. Because of the low injection pressure (~ 3 bar compared to ~1000 bar in diesel), direct fuel atomization (a) results in droplets of ~ 200 μm. Most of these droplets land on the port-walls and form a liquid wall film. In the first cranking cycle, the backflow is weak because the intake manifold pressure has not been pumped down yet; thus process (b) is not effective. The forward strip atomization (c) is the main process of delivering fuel into the cylinder. Another factor that can influence the atomization process is

the fuel injector type. Shayler et al [11] investigated the influence of fuel injector type on the intake port fuel transport. They found that 4-hole injector had the best performance during the warm-up period (transient) among the 4 types of injector evaluated due to better primary atomization. Air-assisted fuel injection has also been proved as another type of injector that will improve the mixing preparation within the intake port [14]..

3.2   Cranking Speed Effects on Mixture Preparation

3.2.1   Typical in-cylinder FID signal

In order to look at the effect of increasing cranking speed on first and second cycle during cranking, in-cylinder HC level was measured using the sampling spark plug and Fast FID. The intake pressure was set such that for 300, 600, and 900 rpm, the values were at 0.92, 0.8, and 0.7 bar. The start of fuel injection was set at 90° after bottom dead center in the compression stroke which resulted in a closed valve injection. The spark timing was set at TDC throughout the experiments described in this chapter.

Figure 3.1 shows a typical in-cylinder FID signal during skip firing mode with modest amount of fuel injection (34 mg of fuel injection). The fuel injection signal which has been superimposed on the pressure signal shows that the fuel stays in the port for approximately 630 CAD after the start of fuel injection before it is delivered into the cylinder. The in-cylinder fuel delivery can be observed with the increase in the in-cylinder FID signal which corresponds to the fuel (HC) concentration inside the cylinder. The first peak in the in-cylinder FID signal (figure 3.3 and 3.4) mark the rich pocket of fuel vapor which may contain some liquid droplets that enter the cylinder in the early phase of intake stroke. This is to be expected due to the fact that after the injection, most of the fuel resides near the intake valve seat and this fuel rich mixture together with the some of the fuel puddle enter the cylinder during the first phase of intake process. The mixture that enters late in the intake stroke is lean. This phenomena is confirmed by the FID signal which shows low concentrations of HC during the later part of intake stroke. It also shows that the mixing of fuel and air continues in the compression stroke before a nearly homogeneous mixture is created at the onset of spark, as evidenced by the relatively flat signal just before spark. After the spark, the HC level drops very rapidly when the fuel is completely consumed by the flame. Since the in-cylinder sampling tube is located inside the spark plug, the HC level observed is the level of HC

around the spark plug region which is consumed as soon as the combustion process begins. After the combustion, there is almost no fuel left in the cylinder but there is slight increase of HC detected by the FID which describes the out-gassing from crevices in the spark plug and also from the sampling tube. The cycle during which the fuel is first introduced to the cylinder is referred as the first cycle due to the fact that it represents the condition during the first cycle of cranking. The following cycle is referred to as the second, third, and so on. There was substantial exhaust HC from the subsequent cycles although no fuel was injected, see fig 3.2. This HC flow occurred because of the residual fuel left in the intake port being "pumped out" by the engine flow process.

Figure 3.2 represents the in-cylinder FID signal with a large amount of fuel injection (224 mg). For comparison at steady state operation at wide open throttle, the amount of fuel injection is approximately about 30 mg to maintain a stoichiometric in-cylinder fuel air equivalence ratio ($\phi = 1$). This amount of fuel injection is done in order to have a better picture of mixture preparation with a broad range of data and also due to the fact that at lower engine coolant temperature, for example 0°C, this amount of fuel injection is necessary to start the engine. The in-cylinder FID signal from fig.3.2 shows the reason why the engine misfires. The first cycle misfired because the in-cylinder ϕ was too rich (approximately 3.7) but the second and third cycles fired which may be confirmed from the pressure signal. It should also be noted that the HC level after the exhaust stroke of the first cycle never reached zero value before fresh mixture from the intake port rush into the cylinder to contribute to the second cycle in-cylinder fuel air equivalence ratio. The values for the second and third cycle in-cylinder fuel air equivalence ratios were approximately 1.6 and 0.75, which were still in the range of combustible mixture.

3.2.2 Distribution of first cycle in-cylinder ϕ

The first and second cycle in-cylinder fuel air equivalence ratio can be extracted from the in-cylinder FID signal. In this section the main focus will be directed at the first cycle in-cylinder fuel air equivalence ratio. The first cycle in-cylinder fuel air ratio can be found using the equation below:

$$Y_f = \frac{n_f}{n_f + n_a} = \frac{m_f / M_f}{m_f / M_f + m_a / M_a} = \frac{1}{1 + (m_a / m_f)(M_f / M_a)}$$

$$\therefore \quad \frac{m_a}{m_f} = \frac{M_a}{M_f} \times (\frac{1}{Y_f} - 1)$$

Where Y_f, m_a, m_f, M_a, M_f represent fuel mole fraction, mass of air and fuel, molecular weight of air and fuel respectively. The molecular weight of California Phase II fuel used throughout this experiment was approximately 100.1 and the stoichiometric air fuel ratio was 14.4. The only unknown parameter to calculate air fuel ratio (A/F) is, Y_f, which can be found by calibrating the output of the fast FID signal with calibration gas of known mixture. Once the (A/F) ratio is known, we only need to divide it with stoichiometric air fuel ratio to get lambda (λ) which then can easily be inverted to get fuel air equivalence ratio (ϕ).

Figure 3.5 and 3.6 show the distribution of the first and second cycle in-cylinder ϕ over more than 100 cycles. While the distribution is larger than what we expected during steady state operation it is within $\pm 10\%$ over many cycles. There are a lot of factors that contribute to the distribution of in-cylinder ϕ. The pressure oscillation in the intake port is more significant at low cranking speed due to the dynamics of the air motion during intake valve open (air induction to the cylinder) and closed intake valve period where there is almost no detectable air motion. The response of the fuel pressure regulator to this pulsation may not be accurately repeatable; hence there is a spread on the amount of fuel injected. Another reason for the distribution is because of the non-uniformity of the mixture inside the cylinder so that the point measurement by the Fast-FID may not represent the cylinder averaged value. Although Port Fuel Injection usually means a more homogenous in-cylinder mixture but there is still some spatial mixture inhomogeniety which result from incomplete mixing process due to the presence of liquid fuel and hence can contribute to the distribution of in-cylinder ϕ from cycle to cycle.

3.2.3 Mean First Cycle In-Cylinder Fuel Air Equivalence Ratio

Figure 3.7, Figure 3.8, and Figure 3.9 show the effect of increasing cranking speed on the mean first cycle in-cylinder ϕ over 40 to 150 cycles at 40°, 60°, and 80° C engine coolant temperature. Generally increasing the amount of fuel injection increases the in-cylinder ϕ due to larger amount of fuel available in the intake port and to the increase amount of liquid fuel which enters the cylinder. Increasing the cranking speed results in higher in-cylinder fuel air equivalence ratio. There are two contributing factor to this phenomena, first with higher engine speed the intake pressure is lower and lower intake pressure will lead to more fuel vapor generation per unit mass of air in the intake port before the onset of air induction. Secondly, after the start of air induction higher engine speed will lead to higher intake air velocity which will improve the strip atomization which in turn will lead to better fuel delivery. In spite of these two phenomena, however, the effect of increasing cranking speed seems to be modest, with the maximum difference in in-cylinder ϕ of 0.3 and the minimum difference as low as 0.05.

3.2.4 Average First Cycle Fuel Mass Fraction in Charge

The average first cycle in-cylinder ϕ describes the mixture strength inside the cylinder which is essential in controlling the engine combustion. It does not give explicit information on the effectiveness of fuel delivery. The amount of fuel delivered into the cylinder, however, can be calculated if the amount of air trapped inside the cylinder can be estimated. Neglecting the small amount of fuel vapor effect (the fuel vapor pressure value less than 0.04 bar) and since there is no residual in the first cycle, the amount of air trapped inside the cylinder can be estimated by calculating the amount of air that is trapped inside the cylinder at the intake valve closing using the ideal gas law.

$$m_a = \frac{P_{in} V_{ivc}}{R_a T_a}$$

Where V_{ivc} represents the volume of the cylinder at the intake valve closing. The mass of fuel inside the cylinder can then be calculated by equation below:

$$m_f = m_a \times \phi \times (\frac{m_f}{m_a})_{stoic}$$

The fuel mass fraction delivered into the cylinder is then can be expressed as :

$$X_f = \frac{m_f}{m_{f,inj}}$$

Figure 3.10, figure 3.11, and figure 3.12 show the effect of increasing cranking speed on the first cycle fuel mass fraction delivery. In general the fuel mass fraction delivered into the cylinder decreases with higher fuel injection amount. The main reason for this phenomenon is due to the fact that there is limited amount of air available during the intake process which restrict the amount of fuel evaporation mass transfer. The transport process is constrained by the intake pressure and temperature, the available time for the sub-processes, and the air velocity. The fraction of injected fuel which is delivered to the charge decreases with increasing cranking speed. The effect of increasing cranking speed seems to be more significant at higher amount of fuel injection with the maximum difference of fuel mass fraction in charge reaching more than 10%.

3.2.5 Second Cycle In-Cylinder Fuel Air Equivalence Ratio

Since not all of the fuel is delivered into the cylinder during the first cycle, it is only natural to assume that some of the fuel is left in the port and contribute to the mixture preparation of the subsequent cycle. In order to gain some insights of how the fuel left in the port effects mixture preparation, second cycle in-cylinder ϕ was calculated from the corresponding in-cylinder FID signal. The calculation for second cycle in-cylinder phi was somewhat more complicated than the calculation for the first cycle in-cylinder ϕ due to the presence of the residual gases.

$$Y_f = \frac{n_f}{n_f + n_a + n_r} = \frac{m_f/M_f}{m_f/M_f + m_a/M_a + m_r/M_r}$$

$$X_r = \frac{m_r}{m_r + m_f + m_a} \quad \Rightarrow \quad m_r = \frac{X_r(m_a + m_f)}{1 - X_r}$$

$$\frac{F}{A} = \frac{Y_f \left(\dfrac{1}{M_a} + \dfrac{X_r}{M_r\,(1 - X_r)} \right)}{\dfrac{1}{M_f} - \dfrac{Y_f}{M_f} - \dfrac{Y_f\,X_r}{(1 - X_r)\,M_r}}$$

Where X_r and M_r represent the residual gas mass fraction and molecular weight of residual gas. Therefore in order to calculate the second cycle fuel air ratio, appropriate value of residual mass fraction is needed.

The empirical value for residual gas fraction in spark ignition engine has been presented by Rik Waero in his report [15]

$$X_r = \left(0.401 \times \frac{OF}{N} \times f(\xi) + 0.546 \times \frac{1}{r_c} \right) \times \xi^{-0.84} \times \left\{ 1 - \left(\frac{\theta_{spark} - 40}{81.3}\right)^2 \right\}$$

OF   : Overlap Factor β : $1-\xi$

N   : Engine Speed in RPS ξ : ratio of intake to exhaust pressure

$f(\xi)$: $1 - \exp(-4.78\,\beta^{0.7} - 153.8\,\beta^{4.5})$ r_c : compression ratio

θ_{spark} : spark timing before top dead center

Using this formula, X_r can be estimated which immediately lead to the calculation of second cycle in-cylinder ϕ.

Figure 3.13, figure 3.14, and figure 3.15 illustrate the effect of increasing cranking speed on second cycle in-cylinder ϕ. In general, regardless the cranking speed, more injected fuel leads to richer second cycle in-cylinder ϕ. Increasing the cranking speed will instigate higher second cycle in-cylinder ϕ due to the fact that more fuel is left in the port (less fuel mass fraction delivered into the cylinder during the first cycle) and lower intake pressure at higher engine speed. The effect of increasing cranking speed is not substantial at low amount of fuel injection due to the fact that most of the fuel is already delivered into the cylinder during the first cycle. At high amount of fuel injection, increasing the cranking speed led to an increase of second cycle ϕ by 0.2. During the period where the second cycle in-cylinder phi

reached 0.8 ~ 1.9, combustion was observed. Thus there could be another possibility of future cranking strategy by which single fuel injection may result in robust combustion both in the first cycle immediately after fuel injection and the following second cycle. The range of combustible mixture for the second cycle is somewhat smaller than that of the first cycle due to the presence of residual gas.

3.3 Engine Coolant Temperature Effects on Mixture Preparation

3.3.1 First Cycle In-cylinder Fuel Air Equivalence Ratio Effect

Figure 3.16, figure 3.17, and figure 3.18 show the effect of increasing the engine coolant temperature. The in-cylinder fuel air equivalence ratio increases with higher coolant temperature which leads to higher amount of fuel vapor generation per unit mass of air in the intake port. The effect of increasing the coolant temperature is more significant at higher amount of fuel injection due to the fact that at low amount of fuel injection, most of the fuel vapor can be generated in the intake port even at lower engine coolant temperature. Increasing the engine coolant temperature by 20°C will, at large amount of fuel injection, increases the in-cylinder ϕ by more than 1.

3.3.2 Second Cycle In-Cylinder Fuel Air Equivalence Ratio

Figure 3.19, figure 3.20, and figure 3.21 illustrate the effect of engine coolant temperature on second cycle in-cylinder ϕ. At all coolant temperatures, increasing the fuel injection amount will lead to higher second cycle in-cylinder ϕ. When the fuel injection amount reaches 100 mg or more, there was substantial increase in the second cycle ϕ with coolant temperature. This is due to the fact at higher engine coolant temperatures, most of the fuel is already delivered into the cylinder in the first cycle and only a little fuel is left in the port at modest amount of fuel injection. In the second cycle, almost all of the residual fuel evaporated; thus the result was not sensitive to the coolant temperature.

3.3.3 First Cycle Fuel Mass Fraction in Charge

Figure 3.22, figure 3.23, and figure 3.24 illustrate the effect of engine coolant temperature on first cycle fuel mass fraction in charge. The engine coolant temperature plays a major role in determining the fuel mass fraction in charge. High engine temperature will lead to higher fuel mass fraction in charge.

3.3.4 Comparison between Engine Coolant Temperature and Cranking Speed Effect

Figure 3.25 shows the summary of first cycle in-cylinder ϕ. The data for 20°C and 40°C were taken from the Ford Zetec Engine experiments done by Bridgette Castaing and Jim Cowart [6,7,8]. The graph suggests that increasing the engine coolant temperature by 20° C will have greater impact on first cycle in-cylinder ϕ than increasing the cranking speed by 600 rpm. It can also be observed that the slope of first cycle in-cylinder ϕ versus injected fuel amount is also lower at lower engine coolant temperature. At 80° C coolant temperature the change of ϕ is approximately 0.22 for every 10 mg fuel injection increment while, at 40° C the corresponding change in ϕ is as low as 0.07. This fact helps to explain why a substantial amount of fuel injection is necessary to start the engine at lower engine coolant temperature.

There are several publications in the literature which deal with the in-cylinder fuel air equivalence ratio. Quader et al [16] used a laser spectroscopic measurement to evaluate the in-cylinder fuel air equivalence ratio. Although the effect of fuel injection amount was not the main parameter investigated, they found the engine started to fire with the in-cylinder fuel air equivalence ratio as low as 0.63. Another paper by Henein et al [5] investigated the effect of initial piston position. It gave some indication of in-cylinder fuel air equivalence ratio by using the analysis of the exhaust gas composition. Their leanest ϕ value was about 1.1 for consistent firing. This experiment result agrees with the value observed by Quader et al. The threshold of the robust combustion is about 0.8 although in-cylinder ϕ of 0.7 or lower will result in occasional and high covariance combustion. The observed lean limit of combustion was not influenced by the engine coolant temperature and engine speed. The rich limit of combustion is at in-cylinder ϕ of 2.5, which is higher than the rich value expected for steady state operation. This phenomenon is probably due to the fact that there is no residual in the first cycle of cranking which means that combustion limit can be extended. The experimental

result at 0 °C suggests that tremendous amount of fuel has to be injected (approximately 250 mg of fuel) to achieve the combustible range due to the low sensitivity of first cycle in-cylinder ϕ to the amount of injected fuel at such a low temperature.

Figure 3.26 illustrate the summary of the fraction of injected fuel in charge for the first cycle conducted at different engine coolant temperatures and speeds. Figure 3.27 shows the summary of the second cycle in-cylinder ϕ. Higher amount of fuel injection will increase the second cycle in-cylinder ϕ. The effect of engine coolant temperature is less at lower amount of fuel injection but becomes more apparent at higher amount of fuel injection. Higher engine speed will always result in higher second cycle in-cylinder ϕ.

3.4   Mixture Preparation Model

3.4.1   Overview of Available Mixture Preparation Model

Modeling of fuel transport phenomenon in port fuel injected Spark Ignition Engine has been conducted by several individual researchers using different approaches. There are 3 different major approaches used in modeling the mixture preparation : semi-empirical X-τ models, particle tracking models, and continuous physical models [17]. Among these model the X-τ model present the simplest calculation. The X in the X-τ model represent the fuel fraction of the injected fuel mass that is deposited on the intake port as liquid film, where the remaining (1-X) fraction of the injected fuel remain airborne and contribute directly to the fuel flow rate into the cylinder. The τ in the X-τ model represent a characteristic time for the fuel film to enter the cylinder. Both the X and τ values must be determined completely using experimental results and therefore is engine specific. Particle tracking models treats the fuel film in a group and solve the film particle movement using the Lagrangian description of motion which requires sophisticated computation capability and computational time. The result of the particle tracking models is often coupled to a CFD code to assess the effect of different spray impingement and surface tension on liquid film. The continuous physical models approaches the mixture preparation process by solving the heat transfer and mass transfer model simultaneously.

3.4.2 Limited Heat Transfer Model

A model based on the concept of effectively equilibrated air fraction was constructed in order to explain the mixture preparation process better. When liquid fuel is mixed in air, the overall distribution of fuel vapor concentration can generally be described by a probability density function (PDF). The probability density function indicates the probability of the presence of air mass fraction in each charge mass element. Finding the proper probability density function is, in itself, a challenging problem which can not be solved without detailed modeling of the fuel/air mixture process. The concept of effectively equilibrated air fraction simplify this problem by assuming that the available air can be divided into 2 categories: the fraction that interacts with the liquid fuel and the fraction which does not. The air mass fraction that interacts with the fuel can then reach thermal equilibrium with the fuel with the appropriate partition of the fuel into liquid and fuel vapor phases. Figure 3.28 shows the concept. The x axis represent the air mass fraction in charge element which means that the 0 value represents a pure vapor while the value of 1 represents the pure air.

Using this model the amount of fuel vapor can be calculated by estimating the proper amount of air that interacts with liquid vapor. In order to run the thermal equilibrium calculation, we need the thermo-physical properties of the fuel. Since the fuel used throughout the experiments is the California Reformulated Phase II fuel which consists of more than 100 HC species some simplification of the fuel is necessary. The procedure is therefore to represent the behavior of CAP II fuel using 10 major components of the fuel. The thermo-physical properties of the fuel can then be calculated using a computer code and feed to thermal equilibrium calculation input.

Thermal equilibrium calculation is then executed. The initial isothermal model assumes that the mixture preparation is an air-limited evaporation process with only one model parameter which was the effective air mass that is in equilibrium with the fuel. The result of the isothermal flash calculation agrees very well with experimental data at low engine coolant temperature where fuel vapor yield is low but over-estimated the vapor yield at higher temperature. This phenomenon can be attributed to the fact that mixture cooling occurs for in-flight evaporation which is more dominant at higher engine coolant temperature. When a droplet of liquid fuel flies in the intake port, the concentration gradient between the droplet and the surrounding air causes the droplet to evaporate. The heat for the evaporation process

has to be supplied from the droplet itself initially and not by the surrounding air. If the enough time is available and the temperature gradient of the droplet and the surrounding air is large enough, heat will then be supplied from the surrounding air to the droplet. Nevertheless, the initial evaporation process requires the heat to be supplied from the droplet itself and therefore the temperature of the remaining droplet will drop. At higher engine coolant temperature, more fuel fraction is evaporated during the airborne period before hitting the intake port and therefore the fuel droplets temperature will decrease.

The model is then modified to take into account of this effect. The modification is done by introducing an extra parameter which is the fraction of evaporation latent heat supplied by external heat transfer. There are two parameters in this model: the fraction of evaporation latent heat supplied by external heat transfer and the effective air mass that is equilibrated with the fuel. The effective air mass is not a truly an arbitrary parameter since we can estimate the effective air mass by making an educated guess of the boundary layer associated with the heat and mass transfer. The actual calculation requires some iteration before the correction temperature of the fuel can be estimated. One thing worth mentioning is that during the first cycle of cranking, the gas temperature caused by the backflow is low and therefore may not contribute significantly to the fuel vapor generation process and therefore add to the validation of the limited heat transfer model during the first cycle of cranking.

3.4.3 Model and Data Comparison

Fig 3.29 shows the comparison between the limited heat transfer calculation result and the experimental data. The effective air mass was set to 40 mg which represents about 8% of total air mass trapped inside the cylinder, which is approximately equals to about 3 mm of boundary layer thickness of the cylinder wall at the intake valve closing. The model and the experimental result matches very well in spite of the fact that the data for 0° and 20° C engine coolant temperature were taken using the Ford Zetec Engine during a separate experiment. The implication of this result is that the mixture preparation process is indeed limited by the available mass of air and regardless of the engine design and geometry, good estimation of fuel mass fraction in charge can be made as long as the engine coolant temperature and intake pressure are known.

Test	Results	Specification	Method
Specific Gravity, 60/60 F	0.7386	Report	ASTM D-4052
API Gravity	60.05	Report	ASTM D-1298
Average Mole Mass [g/mol]	100.01		
Corrosion 50°C	1A	1 Max	ASTM D-130
Phosphorous [g/gl]	0.001	0.005 Max	ASTM D-3231
Sulfur [ppm]	33	30.0 ~ 40.0	ASTM D-2622
Multi-Substitued Alkyl Aromatic	13.8	12.0 ~ 14.0	
MBTE, LV%	10.9	10.8 ~ 11.2	
Oxygen, WT%	2.00	8	
Carbon, WT%	83.92	Report	ASTM D-611
Hydrogen, WT%	14.08	Report	
Net Heat of Combustion [btu/lb]	18.545	Report	ASTM D-240
Oxidation Stability [min]	1440+	1400 Min.	ASTM D-525
Existent Gums [mg/100ml]	2.2	<5	ASTM D-381
Reid Vapor Pressure [bar]	0.7	0.67 ~ 0.70	ASTM D-323
TEL (ml/gal)	<0.001	0.005 Max	ASTM D-3237
Benzene Content, LV%	0.82	1.0 Max	ASTM D-4815
Research Octane Number	96.6		
Motor Octane Number	87.0		
Antiknock Index	91.8		

Table 3.1 California Phase II Reformulated Gasoline
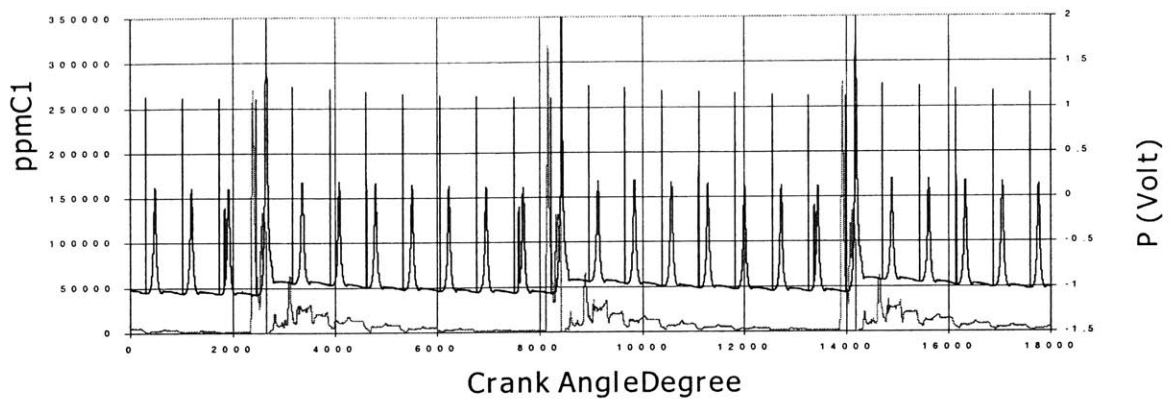
Figure 3.1 In-cylinder FID and Pressure Signal in Skip Injection Mode
300 RPM, 0.92 bar MAP, 80°C ECT, 34 mg Fuel Injection Amount
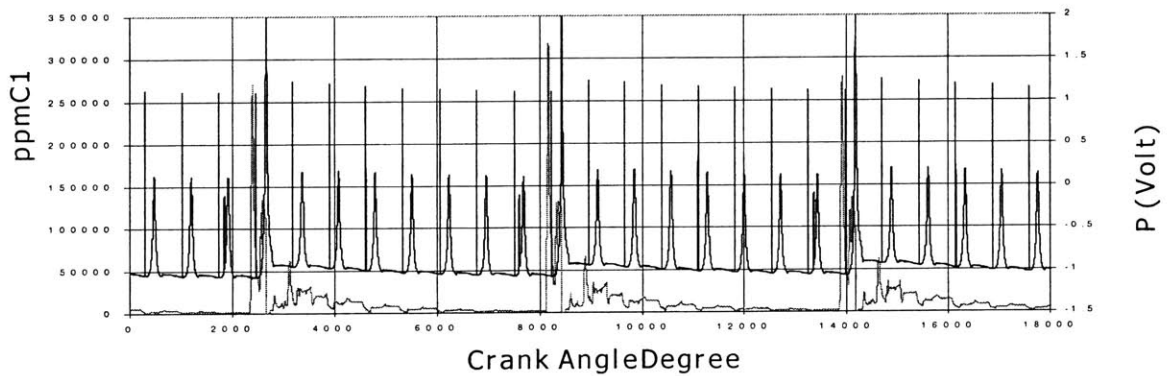

Figure 3.2 In-cylinder FID and Pressure Signal in Skip Injection Mode
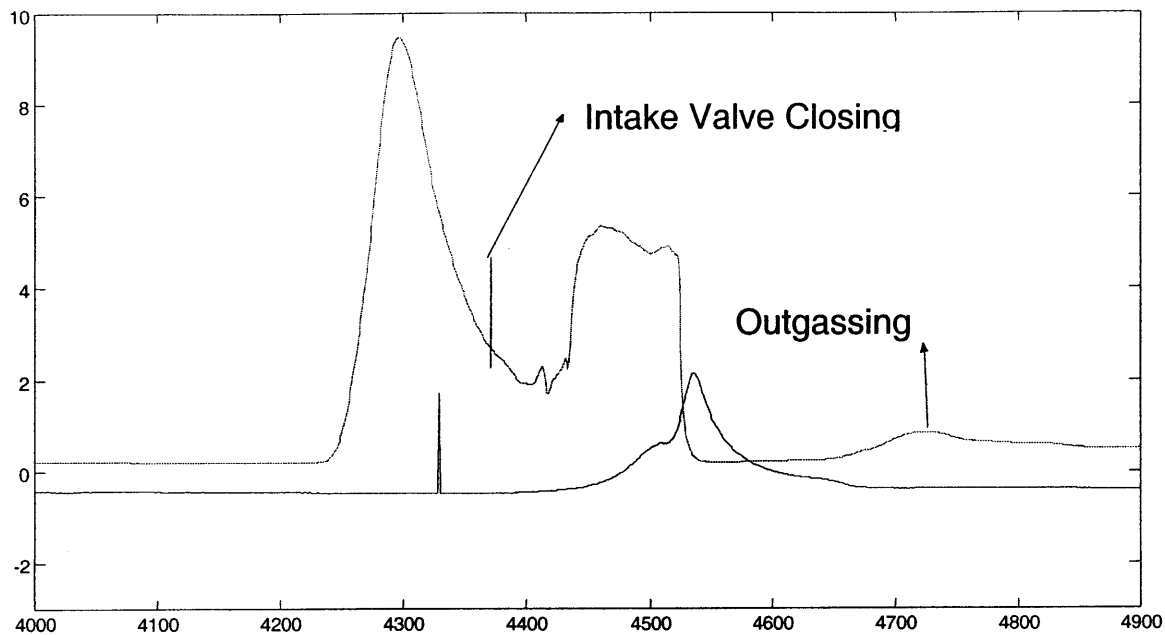300 RPM, 0.92 bar MAP, 80°C ECT, 224 mg Fuel Injection Amount

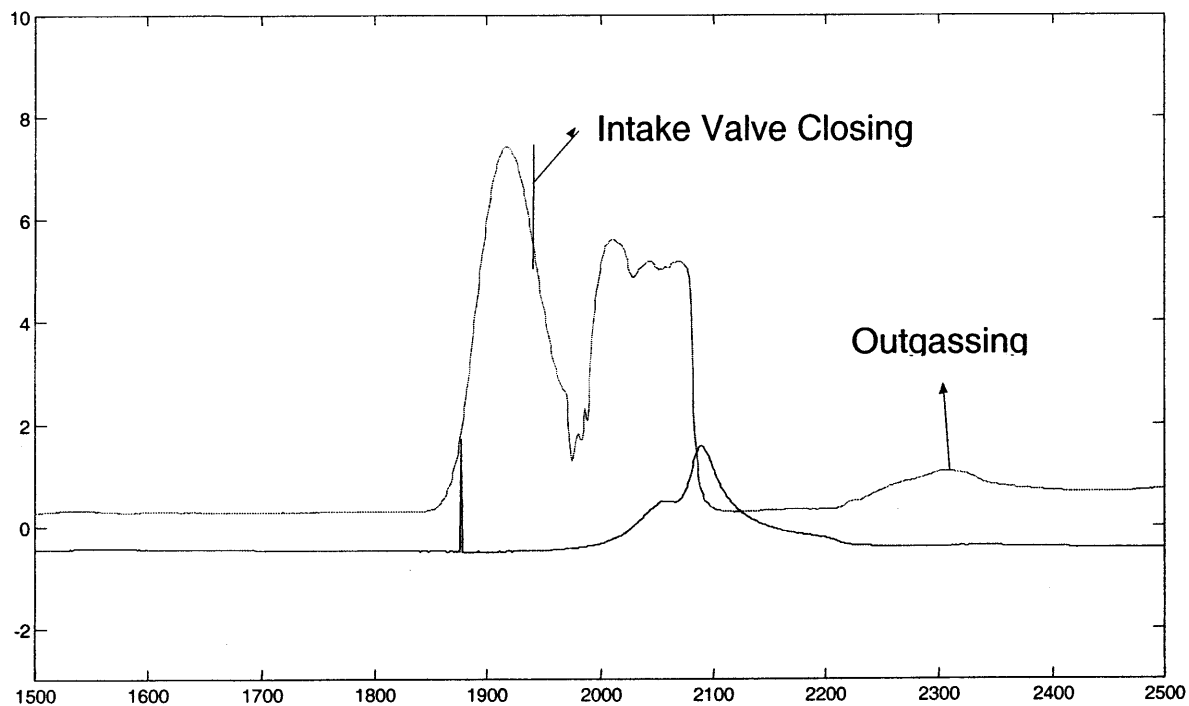Figure 3.3 Typical In-cylinder FID Signal
600 RPM, 0.8 bar MAP, 80 °C ECT

Figure 3.4 Typical In-cylinder FID Signal
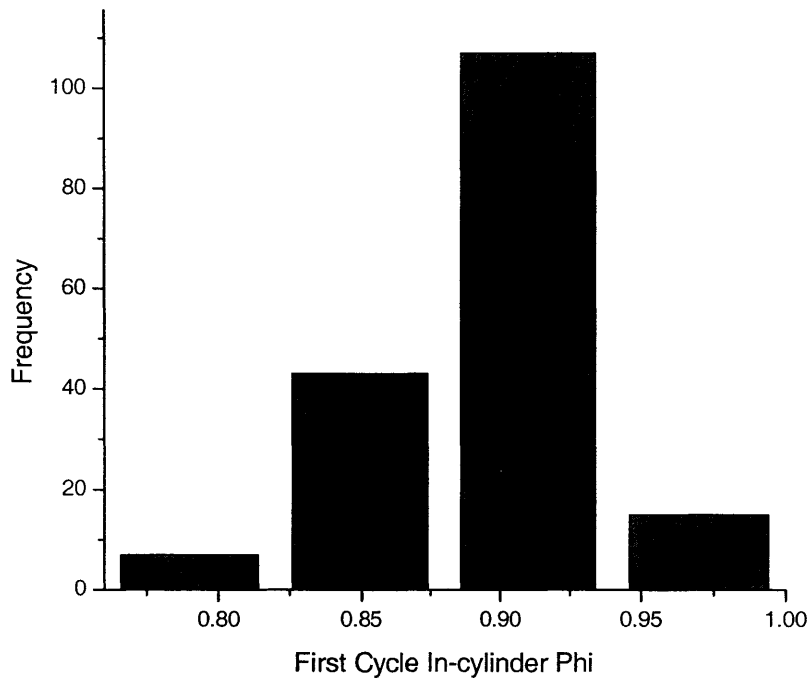900 RPM, 0.7 bar, 80 °C ECT

Figure 3.5 Fuel Injection 38 mg, 300 RPM, 0.92 bar MAP
Average first cycle ϕ = 0.91, 28 mg in-cylinder fuel mass
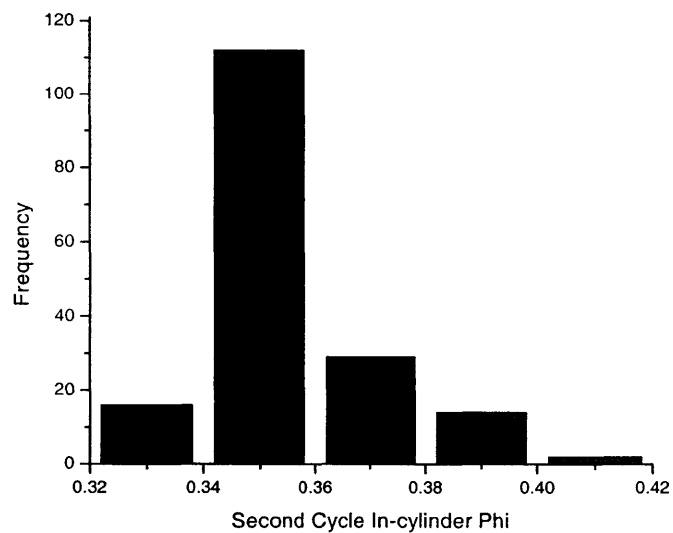
Figure 3.6 Fuel Injection 46 mg, 900 RPM, 0.7 bar MAP
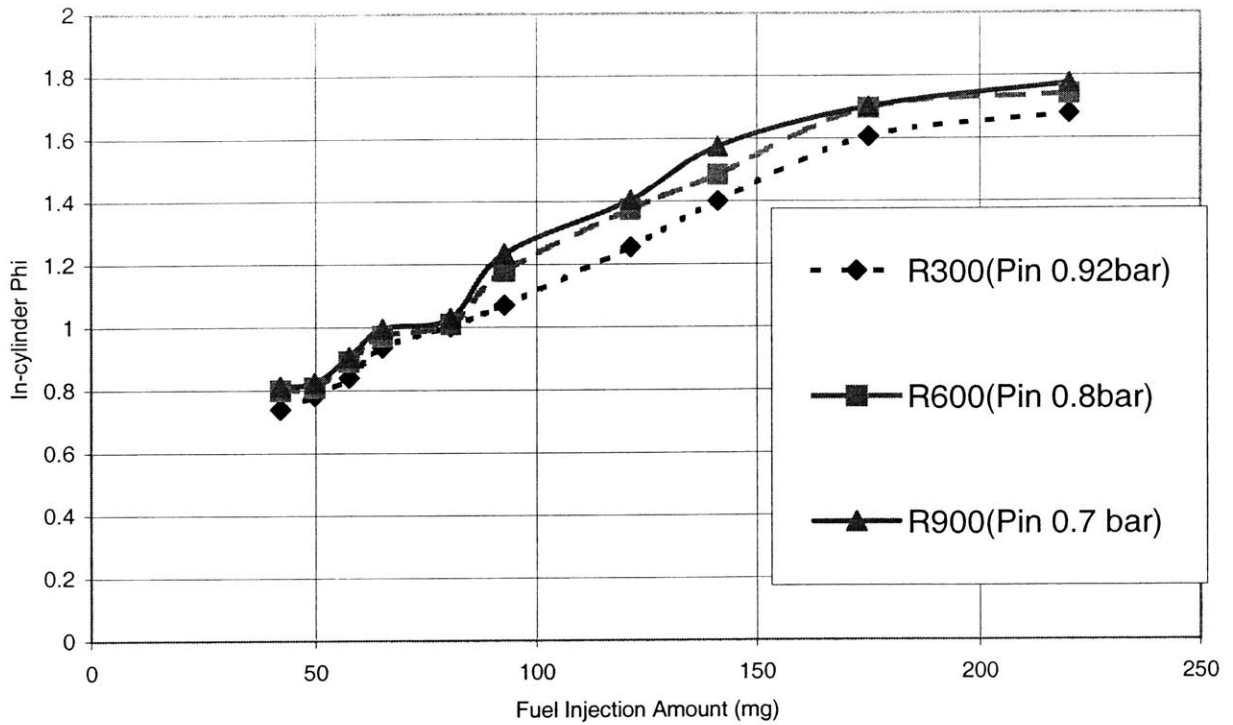Average second cycle ϕ = 0.36, 8.7 mg in-cylinder fuel mass

Figure 3.7 Effect of cranking speed on first cycle in-cylinder ϕ
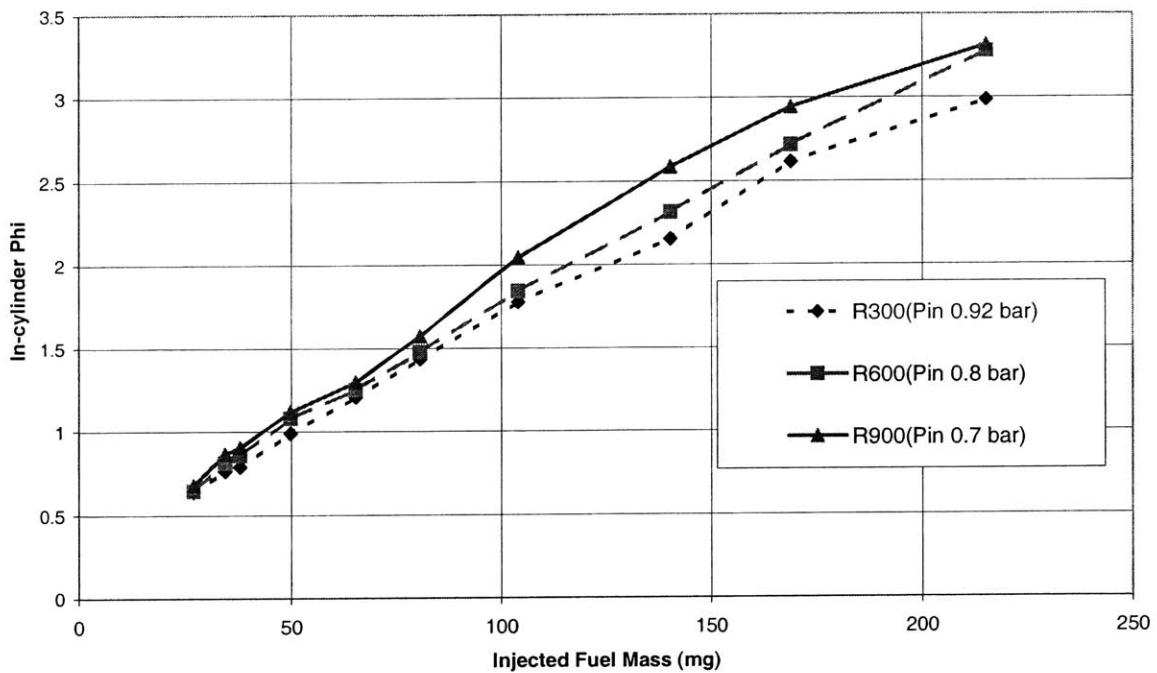Average of 40 ~ 150 cycles, 40 °C ECT

Figure 3.8 Effect of cranking speed on first cycle in-cylinder ϕ
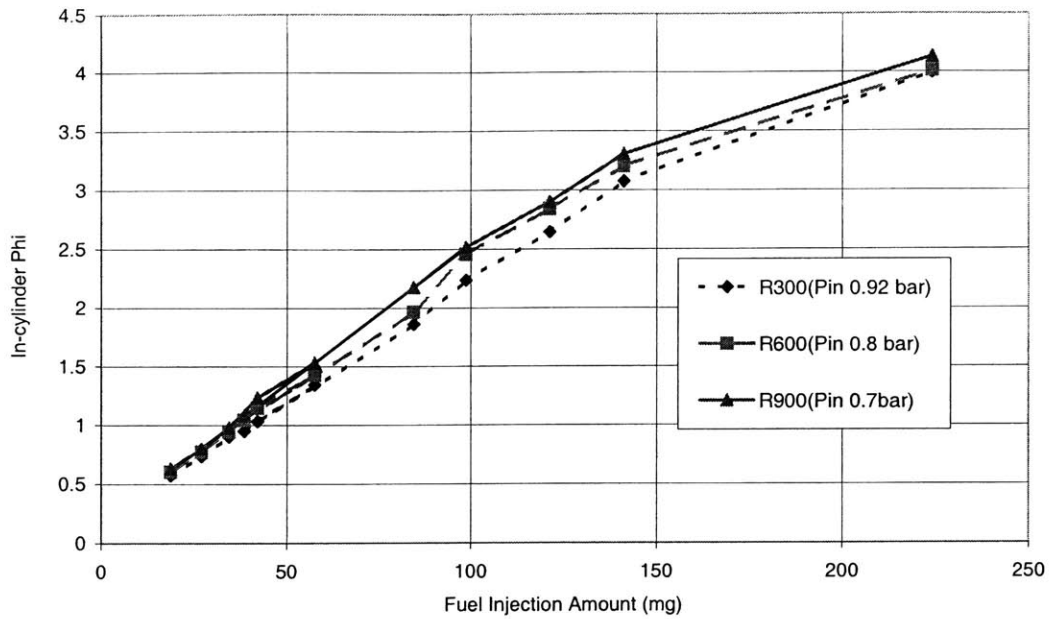Average of 40 ~ 150 cycles, 60 °C ECT

Figure 3.9 Effect of cranking speed on first cycle in-cylinder ϕ
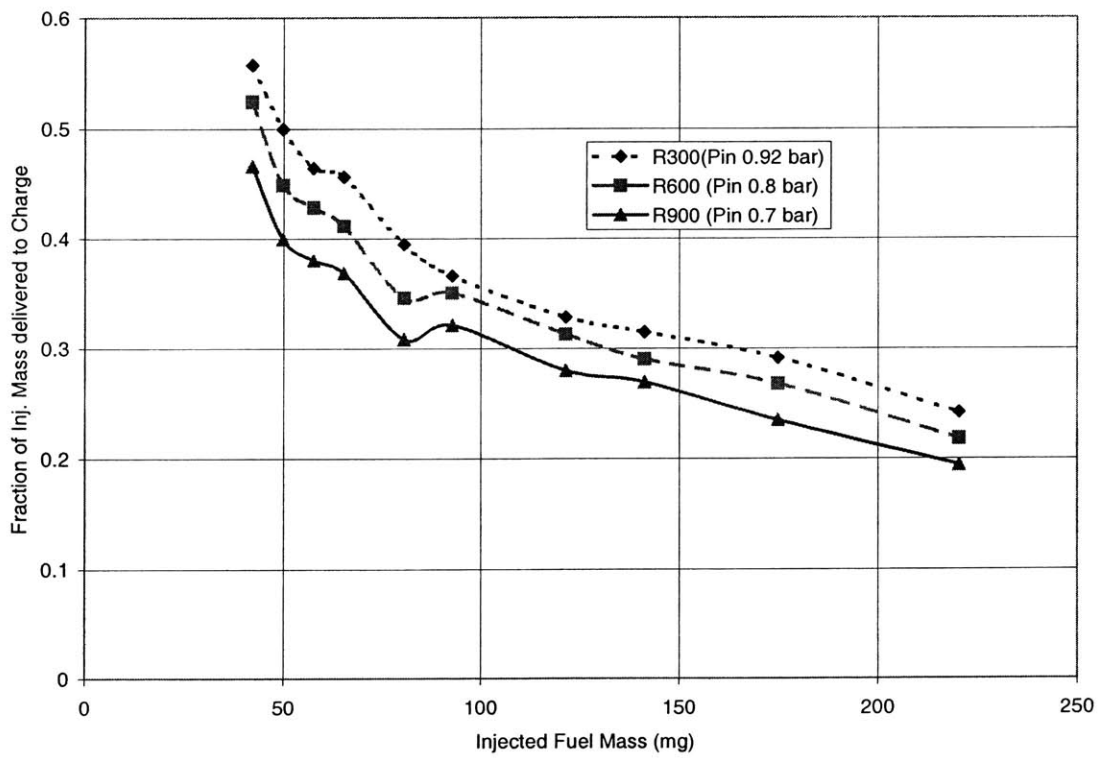Average of 40 ~ 150 cycles, 80 °C ECT

Figure 3.10 Effect of cranking speed on first cycle fraction of inj.mass delivered to charge
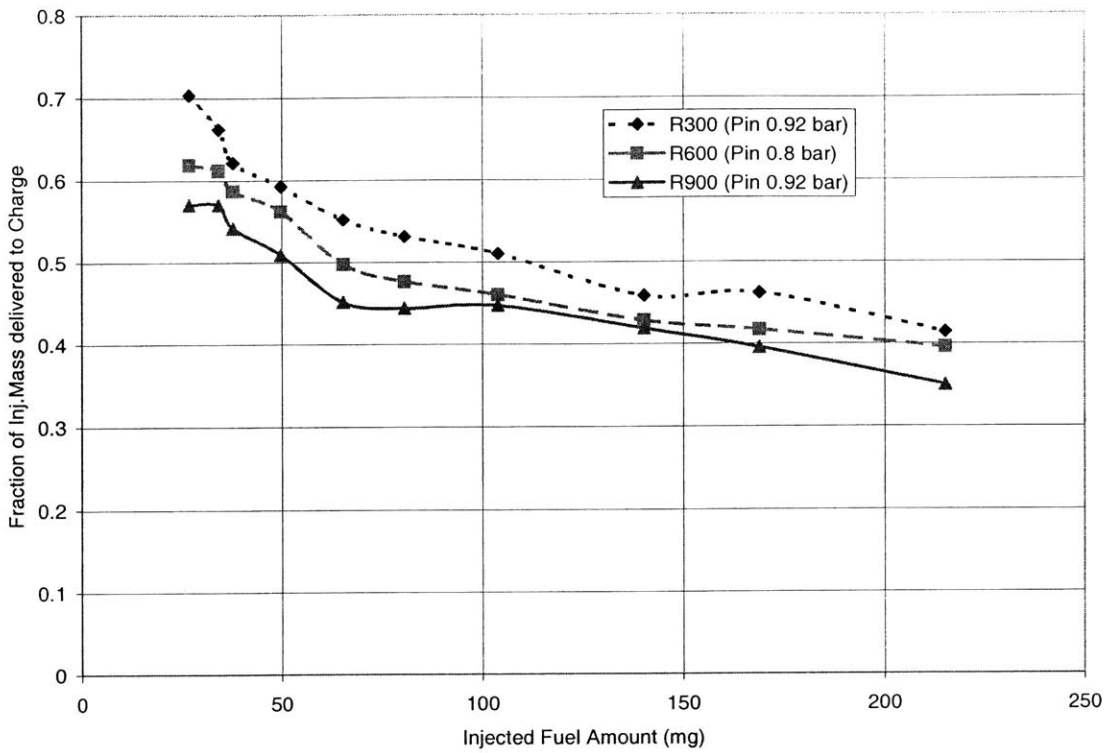Average of 40 ~ 150 cycles, 40 °C ECT

Figure 3.11 Effect of cranking speed on first cycle fraction of inj.mass delivered to charge
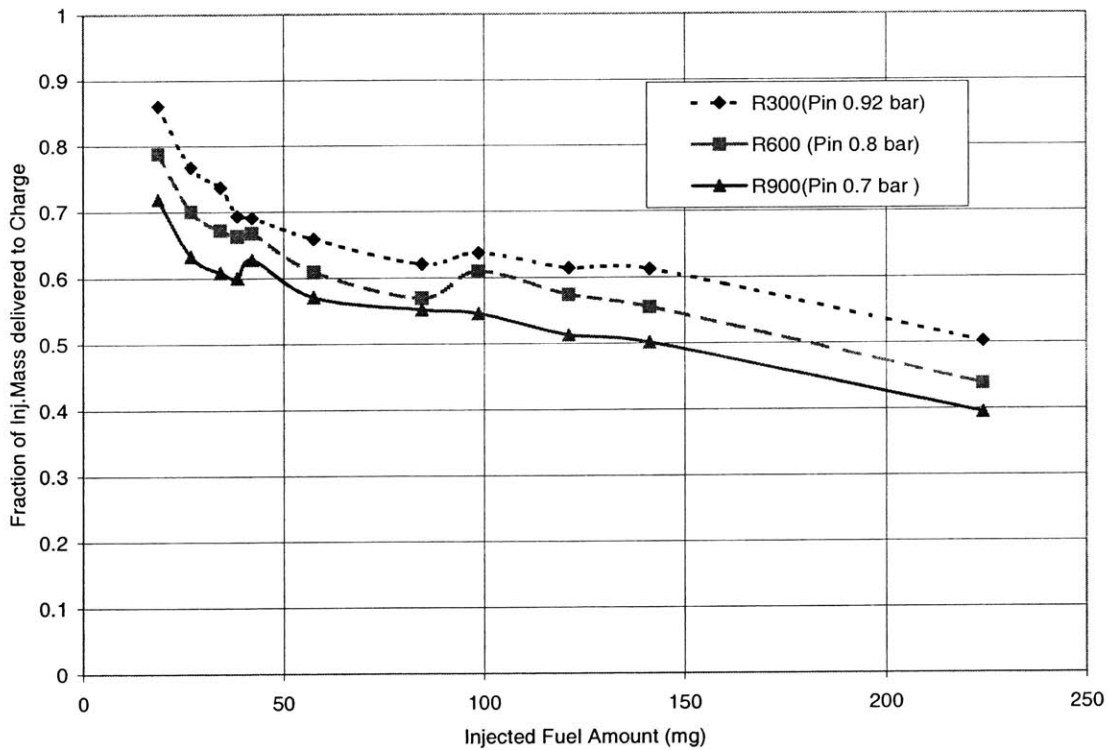Average of 40 ~ 150 cycles, 60 °C ECT

Figure 3.12 Effect of cranking speed on first cycle fraction of inj.mass delivered to charge
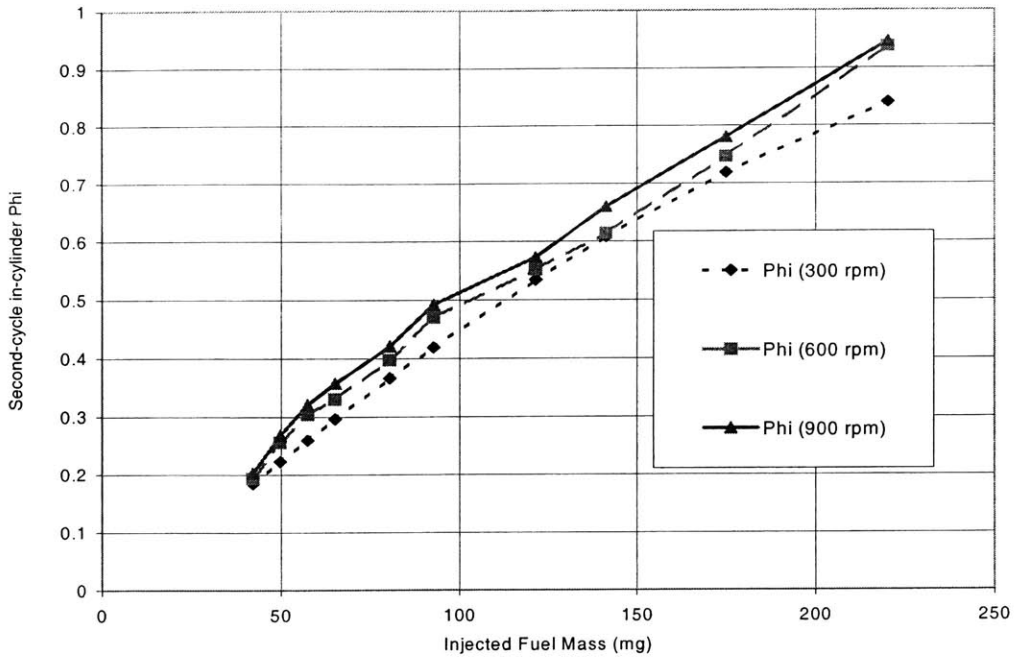Average of 40 ~ 150 cycles, 80 °C ECT

Figure 3.13 Effect of Cranking Speed on Second Cycle In-cylinder ϕ
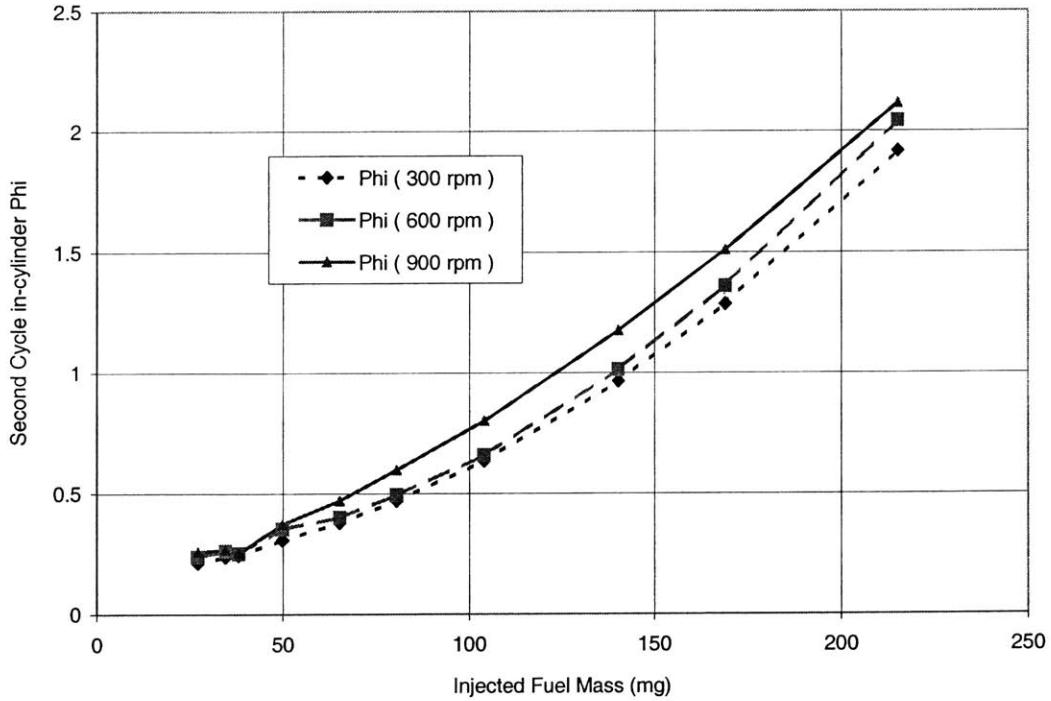Average of 40 ~ 150 cycles, 40 °C ECT

Figure 3.14 Effect of Cranking Speed on Second Cycle In-cylinder ϕ
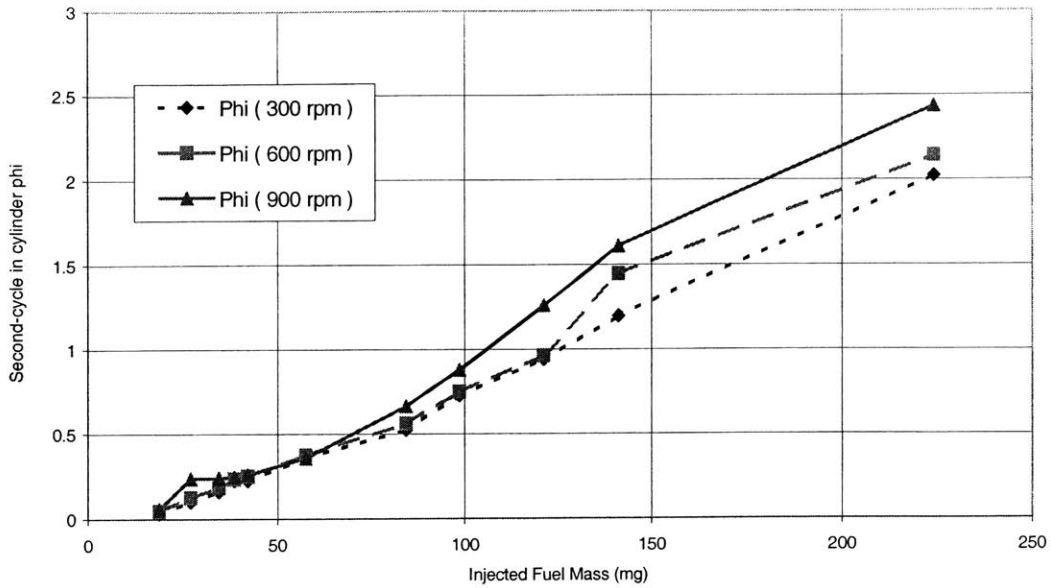Average of 40 ~ 150 cycles, 60 °C ECT

Figure 3.15 Effect of Cranking Speed on Second Cycle In-cylinder Phi
Average of 40 ~ 150 cycles, 80 °C ECT

Figure 3.16 Effect of Engine Coolant Temperature on First Cycle In-cylinder ϕ
Average of 40 ~ 150 cycles, 300 rpm, 0.92 bar MAP

Figure 3.17 Effect of Engine Coolant Temperature on First Cycle In-cylinder ϕ
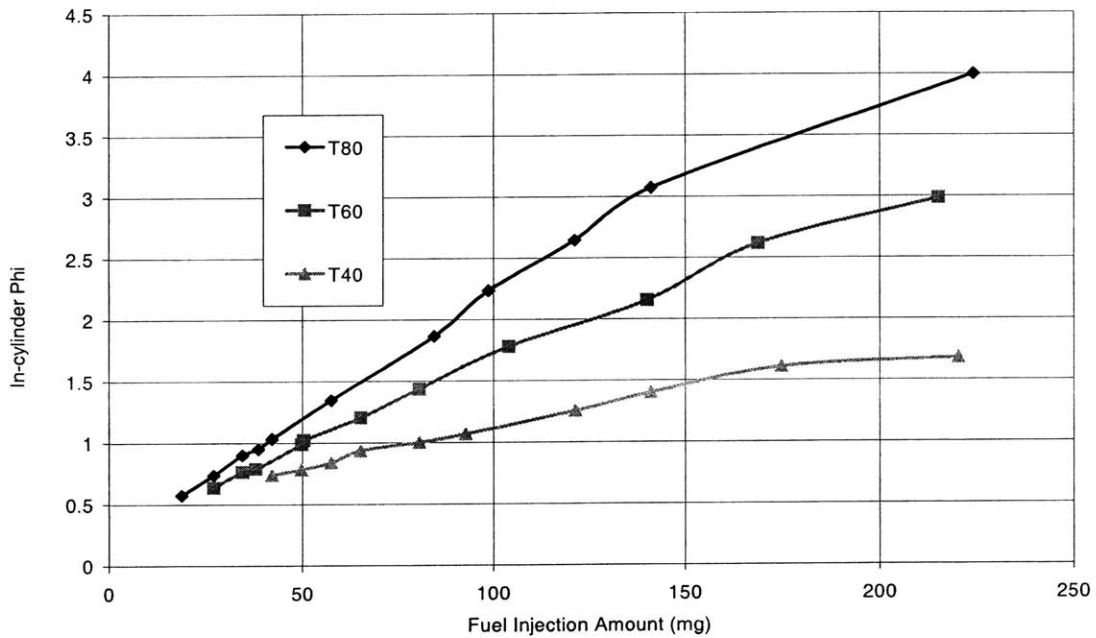Average of 40 ~ 150 Cycles, 600 rpm, 0.8 bar MAP

Figure 3.18 Effect of Engine Coolant Temperature on First Cycle In-cylinder ϕ
Average of 40 ~ 150 Cycles, 900 rpm, 0.7 bar MAP

Figure 3.19 Effect of Engine Coolant Temperature on Second Cycle In-cylinder ϕ
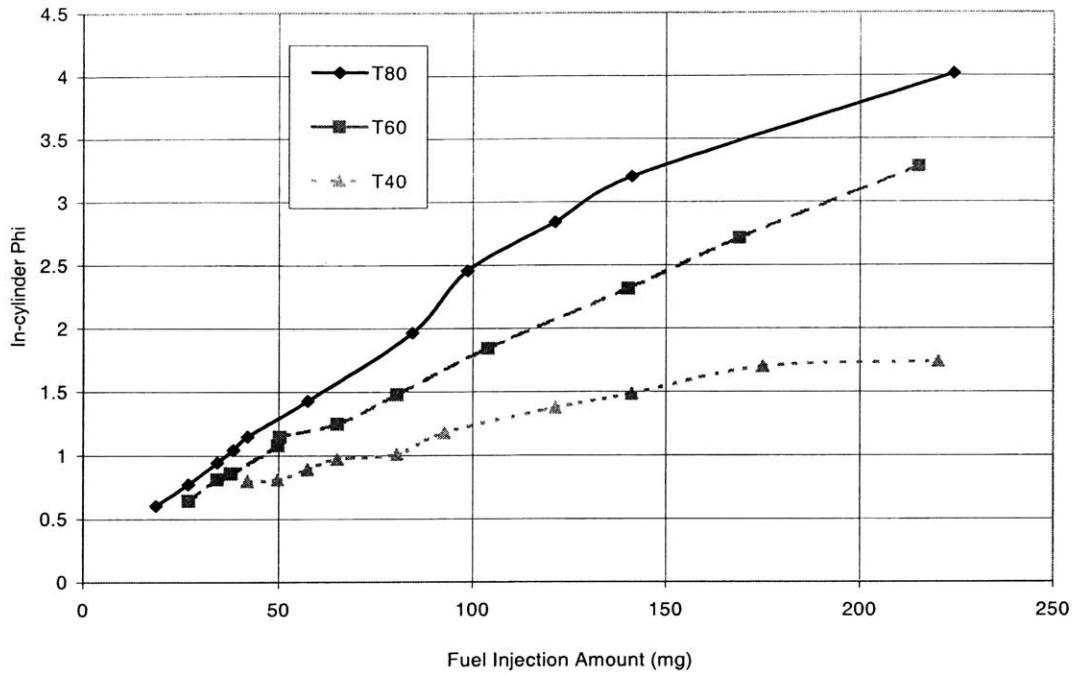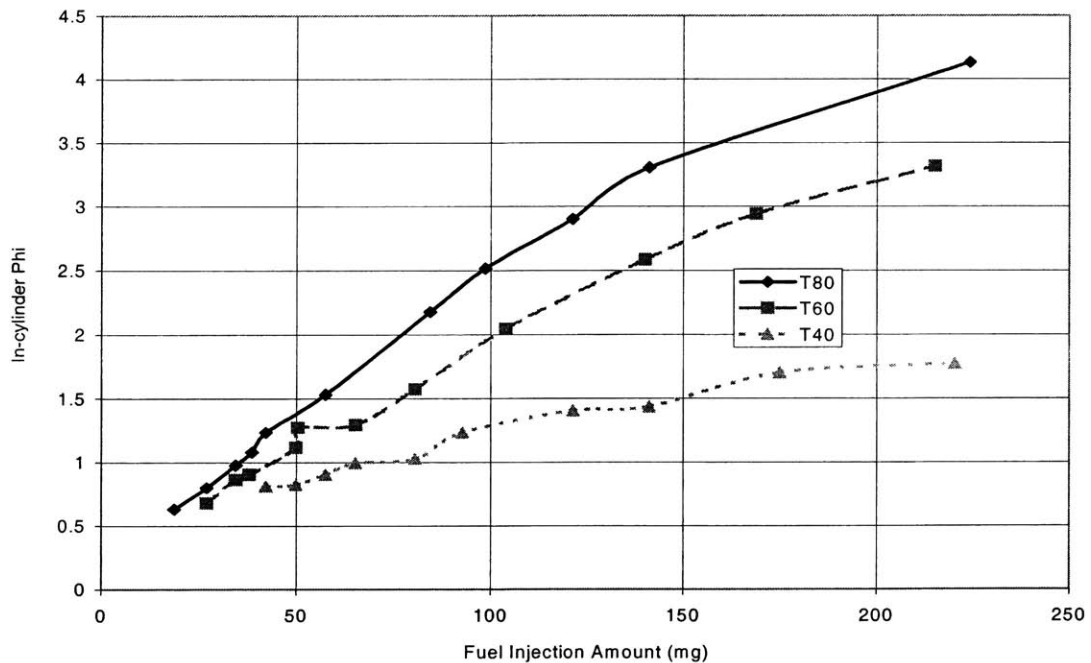Average of 40 ~ 150 Cycles, 300 rpm, 0.92 bar MAP
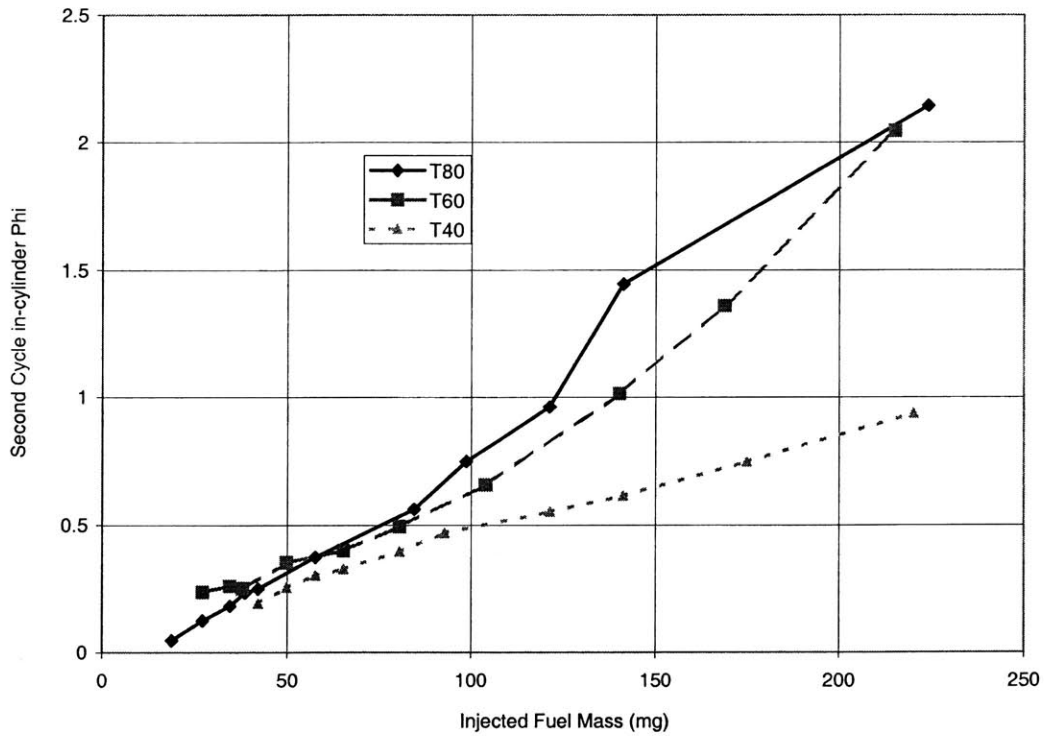
Figure 3.20 Effect of Engine Coolant Temperature on Second Cycle In-cylinder ϕ
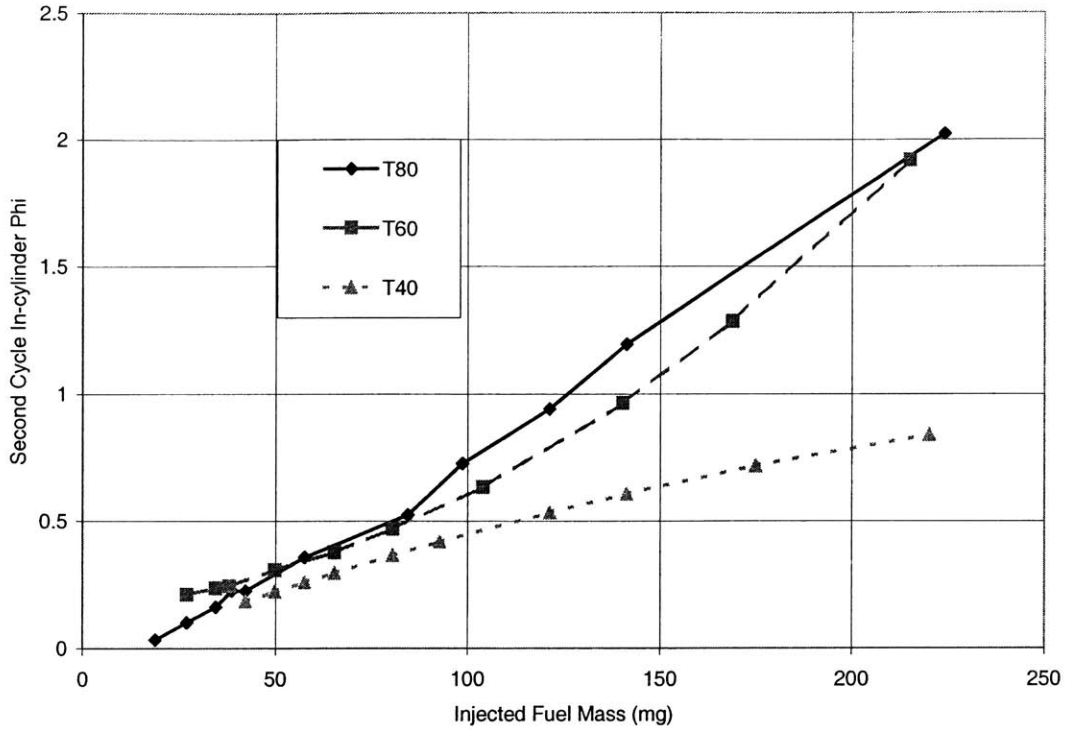Average of 40 ~ 150 Cycles, 600 rpm, 0.8 bar MAP
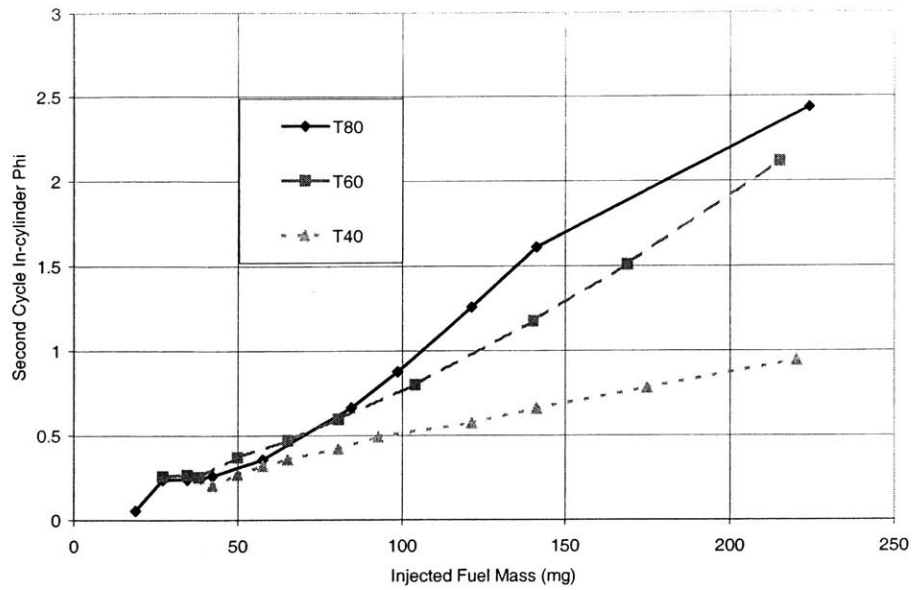
Figure 3.21 Effect of Engine Coolant Temperature on Second Cycle In-cylinder ϕ
Average of 40 ~ 150 Cycles, 900 rpm, 0.7 bar MAP
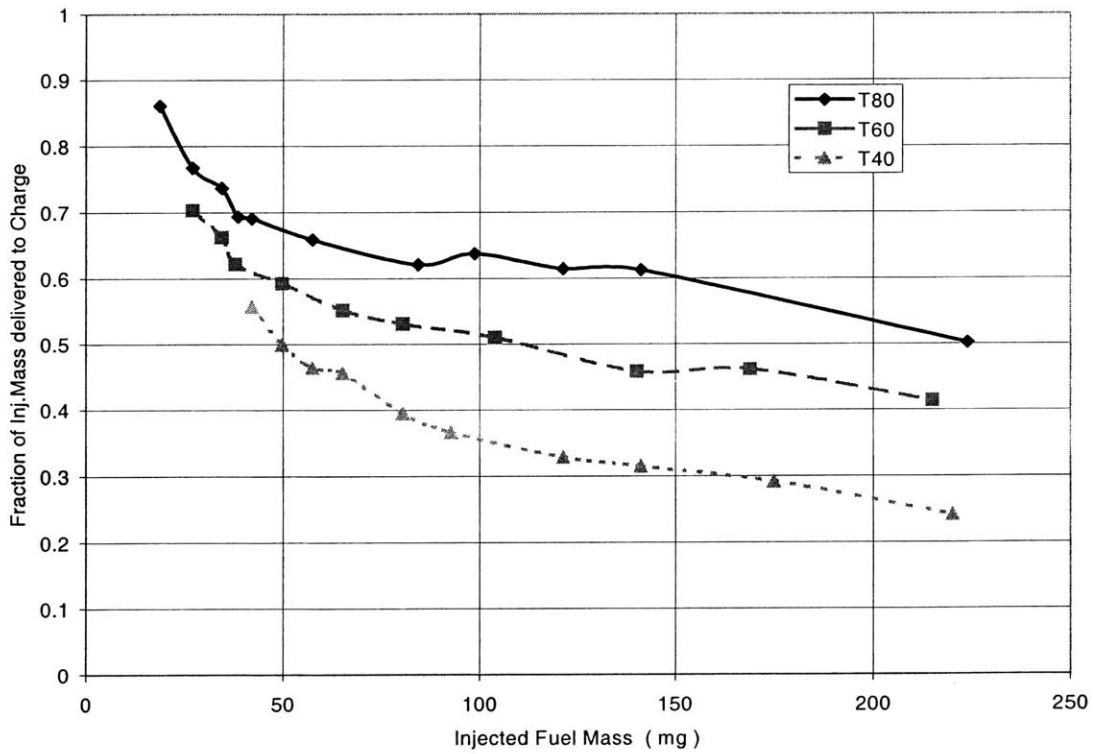
Figure 3.22 Effect of Engine Coolant Temperature on First Cycle Fraction of
Injected.Mass Delivered to Charge
Average of 40 ~ 150 Cycles, 300 rpm, 0.92 bar MAP
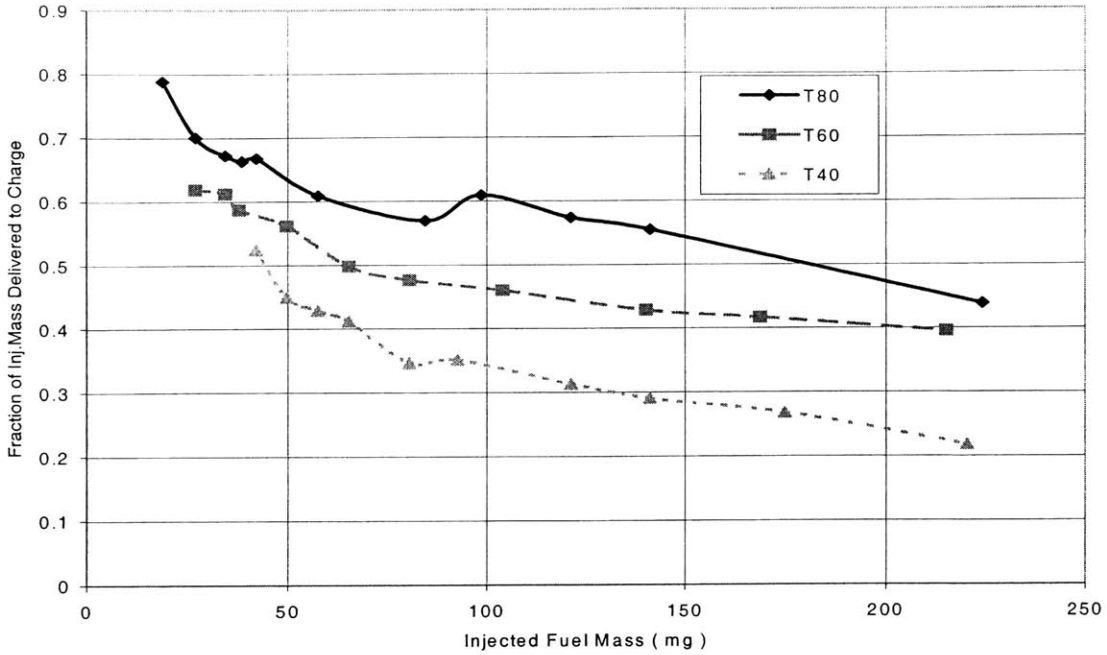
Figure 3.23 Effect of Engine Coolant Temperature on First Cycle Fraction of Injected
Mass Delivered to Charge
Average of 40 ~ 150 Cycles, 600 rpm, 0.8 bar MAP
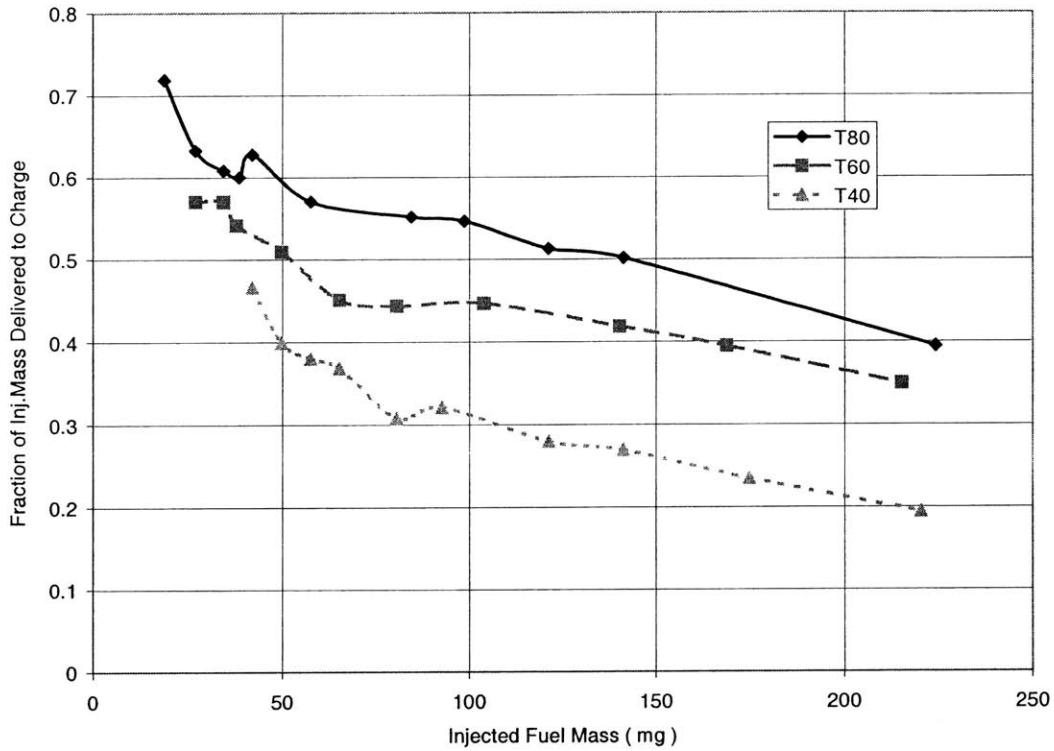
Figure 3.24 Effect of Engine Coolant Temperature on Fuel Mass Fraction in Charge
Average of 40 ~ 150 Cycles, 900 rpm, 0.7 bar MAP
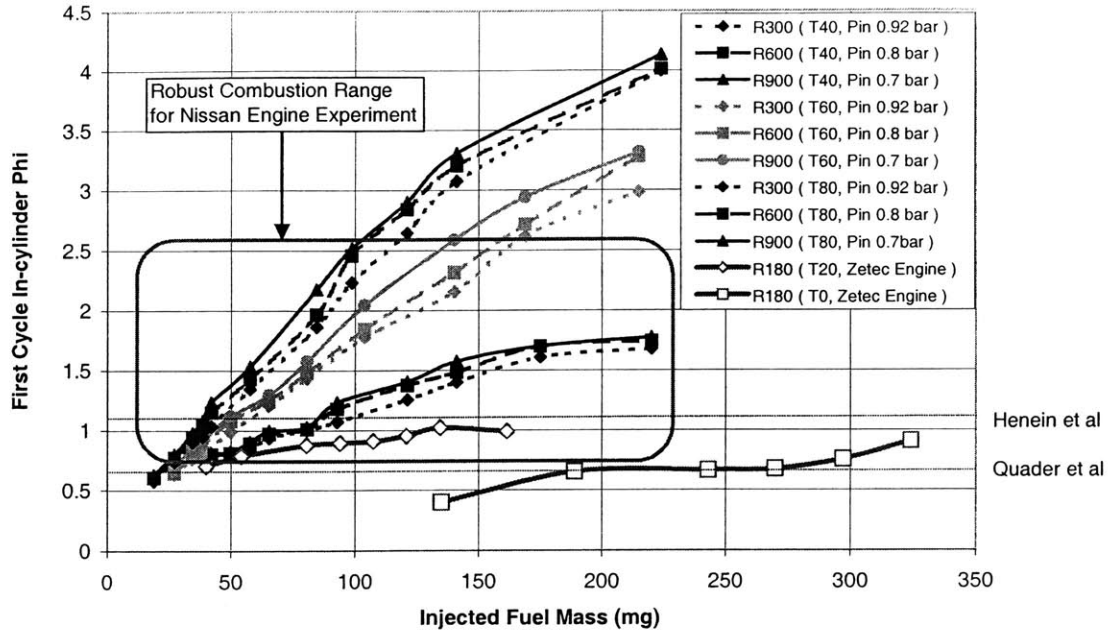
Figure 3.25 Summary of Experimental Results for First Cycle In-cylinder ϕ
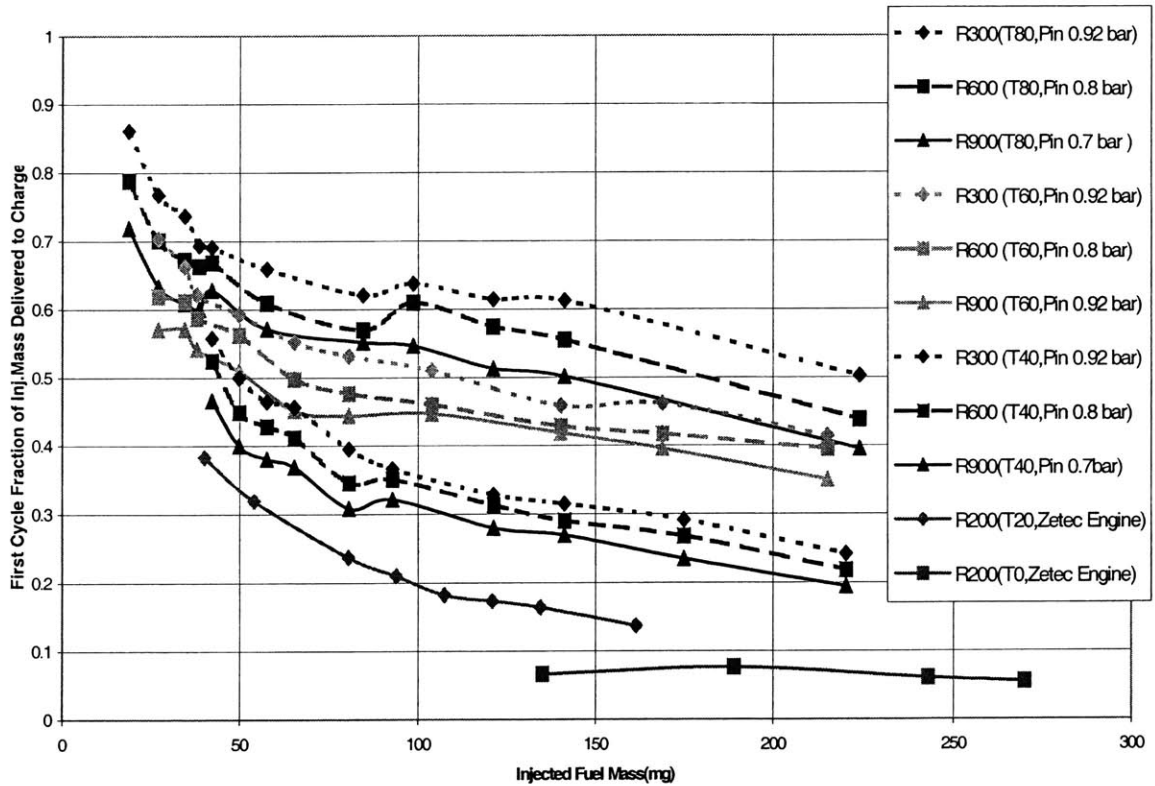
Figure 3.26 Summary of Experimental Result for First Cycle Fraction of Injected Mass delivered to Charge
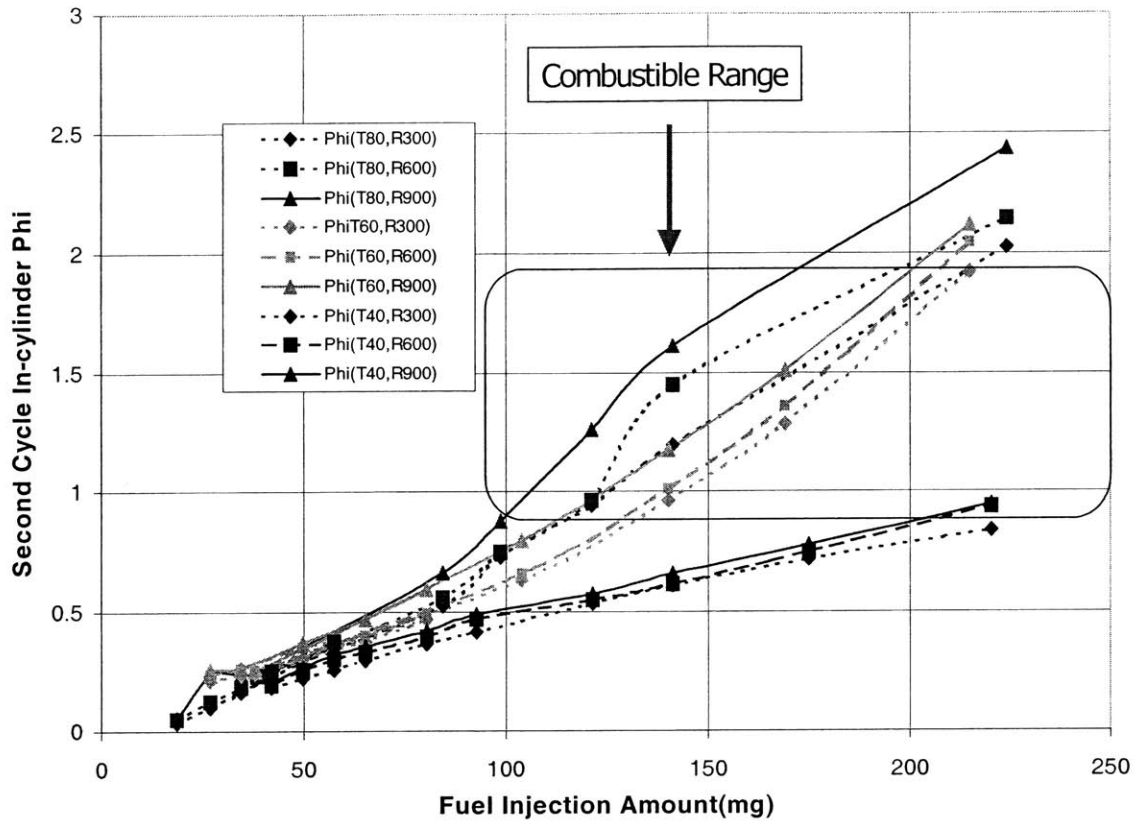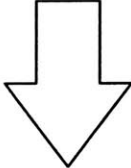
Figure 3.27 Summary of Experimental Results for Second Cycle In-cylinder φ

DISTRIBUTION OF MIXTURE MASS
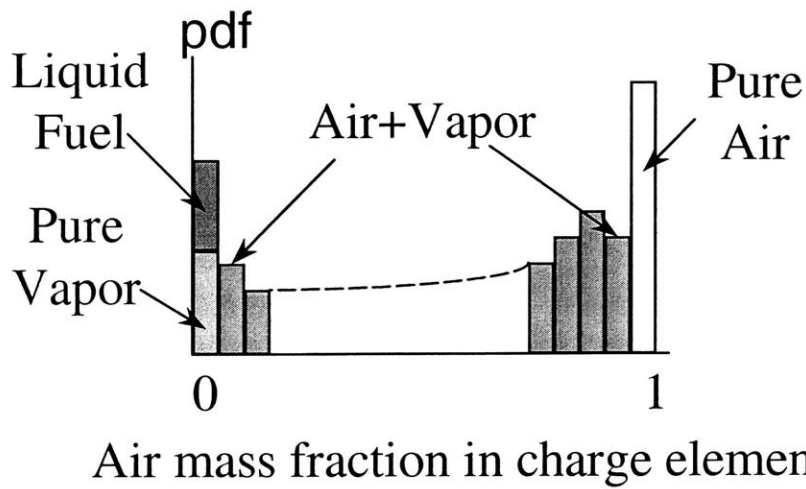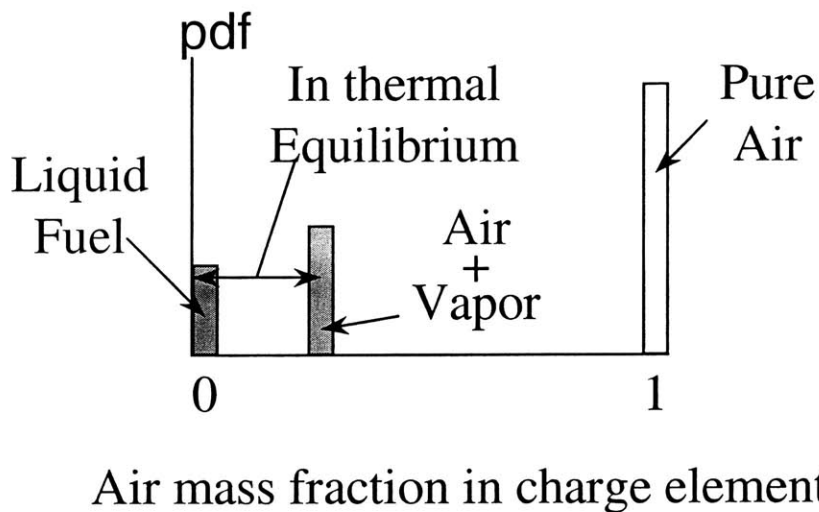
Figure 3.28 Concept of Mixture Preparation Model Based on Effectively Equilibrated Air Mass Fraction

Limited Heat Transfer Mixture Preparation Model
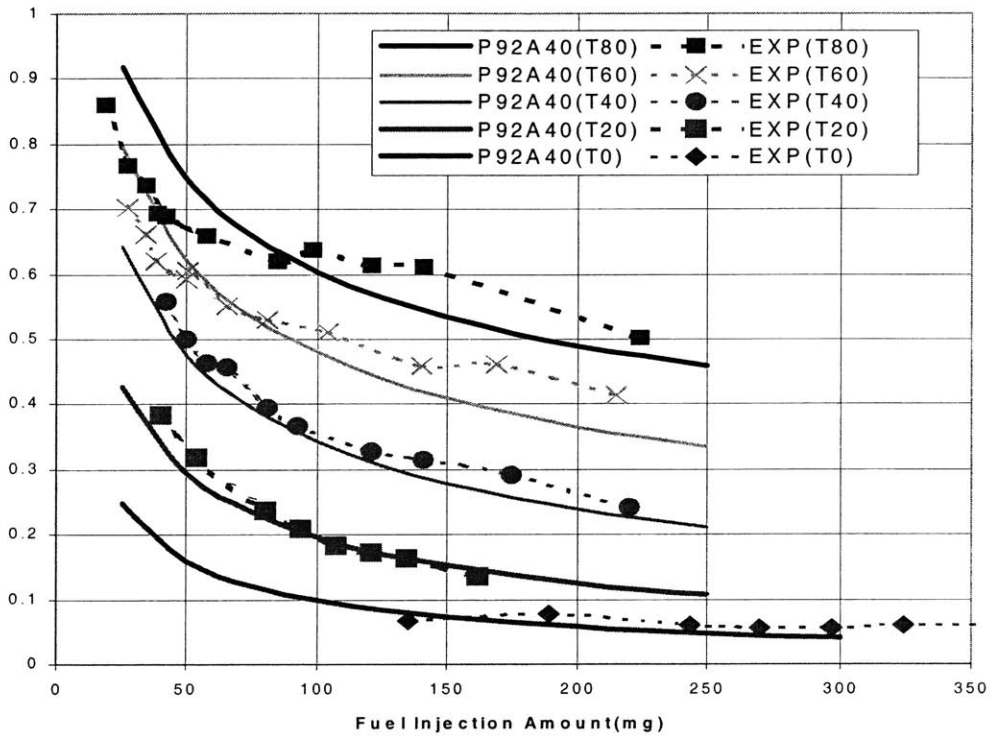
Figure 3.29 Comparison Between Limited Heat Transfer Model Simulation Results and Experimental Results at different Engine Coolant Temperature

Chapter 4

Heat Release and Work Transfer

4.1 Introduction

The heat release and work transfer, as measured by the Indicated Mean Effective Pressure (IMEP), in the cranking cycles are governed by the charge air fuel ratio, the engine speed, and the combustion wall temperature. Through these parameters, the charge available energy, the combustion process, and the combustion phasing are all affected. Because of the engine speeds, coolant temperatures, and air/fuel ratios at cranking may differ substantially from the values at normal operation, the engine cranking behavior needs to be characterized. The IMEP as a function of spark timing, and fuel air equivalence ratio typical of normal engine operation (1500 rpm, 0.4 bar intake pressure) is shown in Fig.4.1. Note that the IMEP is relatively insensitive to the spark timing which controls the combustion phasing.

4.2 Combustion at different cranking speeds

4.2.1 Difficulty in steady state combustion at very low speed.

Figure 4.2 and figure 4.3 show the pressure traces at two experimental conditions, one at 200 rpm and one at 900 rpm with the intake pressure set at 0.7 bar. While the pressure trace in the experiment at 900 rpm shows robust combustion from cycle to cycle, the pressure trace in the 200 rpm experiment shows substantial misfired cycles. The fuel air equivalence ratio for this experiment as measured by the Horiba Lambda sensor in the exhaust port indicated an average value at stoichiometric. Thus the mixture preparation process should not be the cause.

We attribute the misfires due to the presence of a large quantity of residual gas inside the cylinder at lower rpm. The amount of residual gas during steady state operation is controlled by the valve overlap period, the ratio of the intake to the exhaust pressure, and the engine speed which governs the time available for the back-flow process. Figure 4.4 illustrates the volumetric efficiency based on the inlet air density at different engine speed and intake pressure. It can be seen from the graph that the volumetric efficiency at lower engine speed is very sensitive to the intake pressure. Changing the intake pressure from 1 to 0.5 bar at 900 rpm will decrease the volumetric efficiency by 22% while changing the intake pressure at 200 rpm will decrease the volumetric efficiency by more than 80%. The reason for this is

that at lower engine speed the residual mass fraction is very large and also that the throttle is almost fully closed to reduce the manifold pressure which results in extremely poor engine breathing capability.

4.2.2   Effect of Fuel Injection Amount in Skip Injection Mode

The last section deals with the difficulty of having a robust combustion at low speed continuous operation because of the high level of residual. In the first cycle of cranking, however, there is almost no residual presents inside the cylinder because during the engine shut-off period most of the residual gases has already been purged out of the cylinder. Therefore this section deals with the effect of increasing the fuel injection amount on the combustion process during the first cycle of cranking which is simulated using the skip firing method described in chapter 2.

Figure 4.5 and figure 4.6 show the effect of increasing the fuel injection amount at constant speed. The x-axis indicates the injected fuel equivalence ratio which is defined as the amount of fuel injected divided by the stoichiometric amount of fuel required based on the amount of air induction. It should be noted that the injected fuel air equivalence ratio doesn't exemplify the true in-cylinder fuel air equivalence ratio. The combustion can not be initiated unless a certain minimum amount of fuel is injected (1.8 injected fuel air equivalence ratio in figure 4.5 and 2.2 in figure 4.6). The minimum amount of fuel injection is, however, not very accurate due to coupling with the mixture preparation process. A constant amount of fuel injection (fuel pulse width) may result in 0.05 difference in-cylinder fuel air equivalence ratio. Since the combustion process is highly dependent on fuel air equivalence ratio especially near the lean limit, the variation of fuel air equivalence ratio causes significant variation of imep. As we increase the fuel injection amount the variation in imep gets smaller and the average imep becomes larger. Figure 4.7 indicates the effect of engine coolant temperature on gross imep. While figure 4.5 and 4.6 suggests that the minimum amount of fuel injection is influenced by the engine speed, it should also be noted that the engine temperature was not held constant in both experiments. Figure 4.7 shows that for a constant engine speed and injected fuel air equivalence ratio, increasing the engine temperature from 20° C to 40° C will raise the imep from 2.3 bar to 6.5 bar due to better mixture preparation process. In hindsight after in-cylinder fuel air equivalence ratio measurement was available, 2.27 injected fuel air

equivalence ratio still corresponds to in-cylinder fuel air equivalence ratio of 0.85 (lean) at 40°C ECT.

Figure 4.8 shows the effect of increasing cranking speed on average first cycle imep during the skip firing mode. In general Imep increases with the fuel injection amount until it reaches certain value (40 mg at 80°C ECT) before it begins to drop in magnitude. Notice that since the spark timing is set at TDC, the Imep presented in this graph contain the differences in combustion phasing, in-cylinder fuel air ratio, and air mass so that it has a very complex nature which is typical of actual cranking condition. There is no significant difference in imep at lower amount of fuel injection for the 3 different engine speeds. At lower amount of fuel injection higher engine speed tends to induce higher in-cylinder fuel air equivalence ratio but this effect is compensated by the fact that higher engine speed tends to result in lower manifold pressure. Therefore at lower amount of fuel injection these 2 opposing phenomena cancel each other and as a direct result, the imep does not change with engine speed. At higher fuel injection amount, higher engine speed still increases the in-cylinder fuel air equivalence ratio but now increasing the in-cylinder ϕ more than stoichiometric value reduces the imep. Hence, at higher amount of fuel injection higher engine speeds tends to produce a lower gross imep. In order to isolate the governing phenomena, attempts have been made to isolate the parameter one by one. First to isolate the effect of in-cylinder fuel air equivalence ratio, the graph in figure 4.8 was simply re-plotted in figure 4.9 using the in-cylinder phi as the x-axis. Figure 4.9 indicates that for the same in-cylinder ϕ, the imep increases as we decreases the cranking speed. We attribute this phenomenon due to the difference in the total air mass (intake pressure) and combustion phasing. Lower engine speed is coupled with higher map (0.92 bar for 300 rpm and 0.7 bar for 900 rpm), which causes for the same in-cylinder ϕ, more available fuel and hence higher imep.

To look at the pure effect of combustion phasing, the imep is normalized by the intake pressure which is a measure of the charge mass. The results are shown in Fig.4.10. At lower in-cylinder phi, the effect of combustion phasing is not clear. This is due to the fact that at low in-cylinder ϕ, the heat release rate is relatively slow in term of crank angle even for engine speed as low as 300 rpm. After the fuel air equivalence ratio becomes greater than 1, the TDC spark timing seems to be beneficial to the higher engine speed operation due to better heat

release profile. The difference in combustion phasing at higher in-cylinder ϕ seems to be constant at approximately 1.5 normalized imep for 300 and 900 rpm.

4.2.3 Effect of Spark Timing

Spark Sweep to find the MBT timing for different engine speed and different rpm in skip firing modes is shown in figure 4.11, figure 4.12, and figure 4.13. Generally there is a clear difference between the imep for in-cylinder $\phi = 0.8$ and $\phi = 1$ with the higher imep for in-cylinder ϕ equals to 1. The difference in imep is however, is highly dependent on the engine speed. At 300, 600, and 900 rpm the imep's differences for $\phi=1$ and $\phi=0.8$ are approximately 2, 1.1, and 0.8 bar respectively. The relatively large different in imep in 300 rpm experiment result is due to the higher manifold pressure value. The imep's difference between in-cylinder fuel air equivalence ratio of 1 and 1.2 is not so substantial with $\phi = 1.2$ resulting in slightly smaller Imep. The MBT Spark Timing is found to be 10, 15, and 20 BTDC for stoichiometric mixture at 300, 600, and 900 rpm. Figure 4.14 shows the location of peak cylinder pressure at different cranking speeds for stoichiometric mixture. When the spark timing is advanced from a certain value (-20, -25, -30 ATDC for 300, 600, and 900 rpm), the peak cylinder pressure location is located roughly at TDC. This is due to the fact that the pressure increase due to combustion ends before top dead center and the gas is further compressed by the piston until top dead center which result in highest in-cylinder pressure occurring at top dead center. Retarding the spark timing from those certain values delays the peak cylinder pressure locations. In general increasing the cranking speed causes the peak cylinder pressure location to move toward the end of the expansion stroke.

4.3 Heat Release Analysis

4.3.1 Introduction of Heat Release Model

A heat release analysis can be used to estimate the equivalent amount of fuel burned and the equivalent fuel mass fraction burned. The term equivalent fuel mass fraction burned is used because the analysis calculates the combustion energy release relative to the fuel heating value. Hereafter, the prefix "equivalent" is dropped.

The heat release model used in this project was based on the heat release model developed by Gatowski et al. at Massachusetts Institute of Technology [20]. The single zone

analysis uses the energy balance method to determine the burned rate from measured cylinder pressure. The approach uses the First Law of Thermodynamics and several submodels to relate the overall energy balance to the measured pressure and accounts for additional effects such as heat transfer to the cylinder wall and the crevice flow. The model is further revised by Cheung and Heywood [21] by using an effective specific heat ratio which was calibrated against a two-zone engine simulation model. The method worked fairly well in normal engine operation, but some adjustments are needed for engine speed typical of cranking. Specifically the effective specific heat ratio during the expansion stroke was adjusted to account for the relatively low exhaust gas temperature at engine speed typical of cranking.

4.3.2 Burn Release Rate and Burn Duration

The normalized burn rate and the fuel burned mass fraction for 300 rpm, 600 rpm, and 900 rpm at different fuel air equivalence ratios were shown in fig 4.15, 4.16, 4.17, 4.18, 4.19, 4.20. The normalized burn rate is defined as the rate of energy released per crank angle degree divided by the total fuel energy in the charge.

The fuel mass fraction burned is defined as the total energy released divided by the initial energy content of the fuel. The peak fuel mass fraction burned is almost the same between fuel air equivalence ratio of 1 and 0.8 but the peak fuel mass fraction for fuel equivalence ratio of 1.2 is slightly lower due to incomplete combustion. The incomplete combustion occurs due to the limited amount of air in the cylinder which causes emissions problem. Although CO emissions level is not measured in this project, incomplete combustion at high fuel air equivalence ratio has been identified as a major source of CO emissions.

Figure 4.21 and figure 4.22 show the effect of increasing cranking speed on the burn rate and the fuel mass fraction burned at stoichiometric mixture. The burn profile confirm that the heat release schedule is better (not too fast) at the higher engine speeds. The peak burned rate as well as the burn duration changes when the cranking speed is increased from 300 to 900 rpm. These figures help to understand why the higher engine speed gain from combustion phasing at higher fuel air equivalence ratio as shown in the previous section. The peak fuel mass fraction burned stays approximately constant for 3 different cranking speeds. In summary, the heat release analysis shows that increasing the cranking speed will effect the burn rate but has only a modest effect on the total fuel mass fraction burned.

4.3.3 Location of 50% fuel mass fraction burned

There are a few empirical indicators for MBT spark timing at normal operation. First, at MBT spark timing, the 50% fuel mass fraction burned is normally located between 7 to 10 degree after Top Dead Center. Second, the coefficient of variation of the Imep at MBT timing is small. The peak cylinder pressure at MBT spark timing is normally located at 15 ~ 17 degree after Top Dead Center.

Using the heat release analysis, the location of 50% mass fraction burn for lower cranking speed has been identified. Figure 4.23 illustrate the location of 50% mass fraction burned at different fuel air equivalence ratio. In general retarding the spark timing also retards the location of 50% mass fraction burned. Comparison across different fuel air equivalence ratio indicates there is no significant difference between fuel air ratio of 1 and 1.2. The location of 50% fuel mass fraction burned for 0.8 fuel air equivalence ratio seems to indicate a more retarded location compared to the 2 higher fuel air equivalence ratios. While the imep plot has indicated that the MBT timing for 300 rpm and stoichiometric operation occurs at 10 BTDC, the location of 50% fuel mass fraction burned for this particular spark timing was found to be around 5° ATDC, which is slightly more advanced than the normal practice.
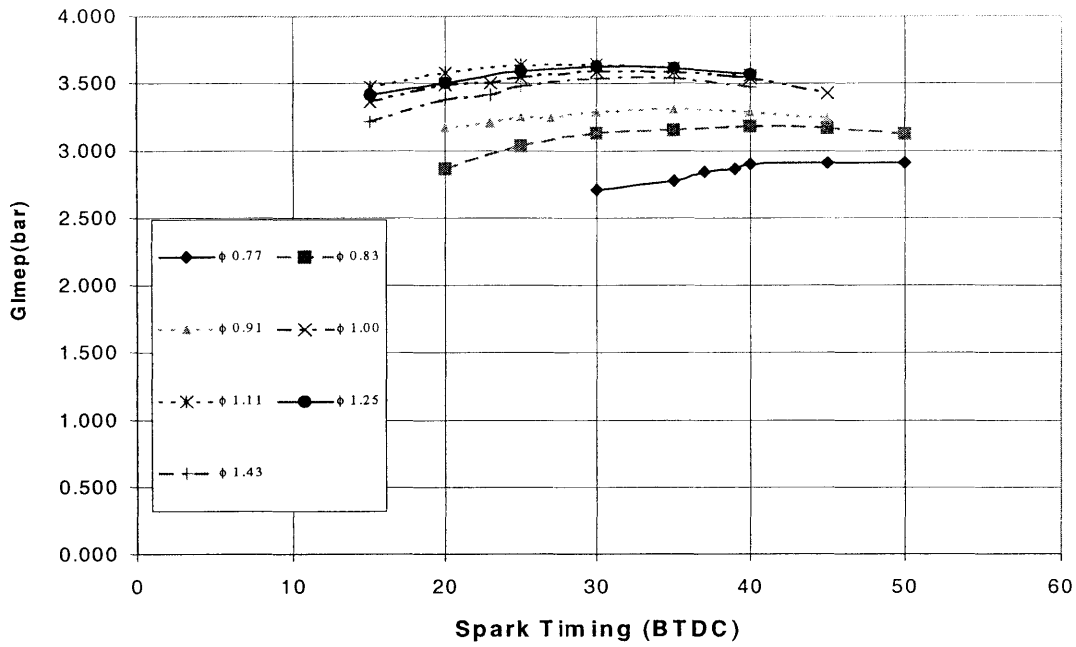
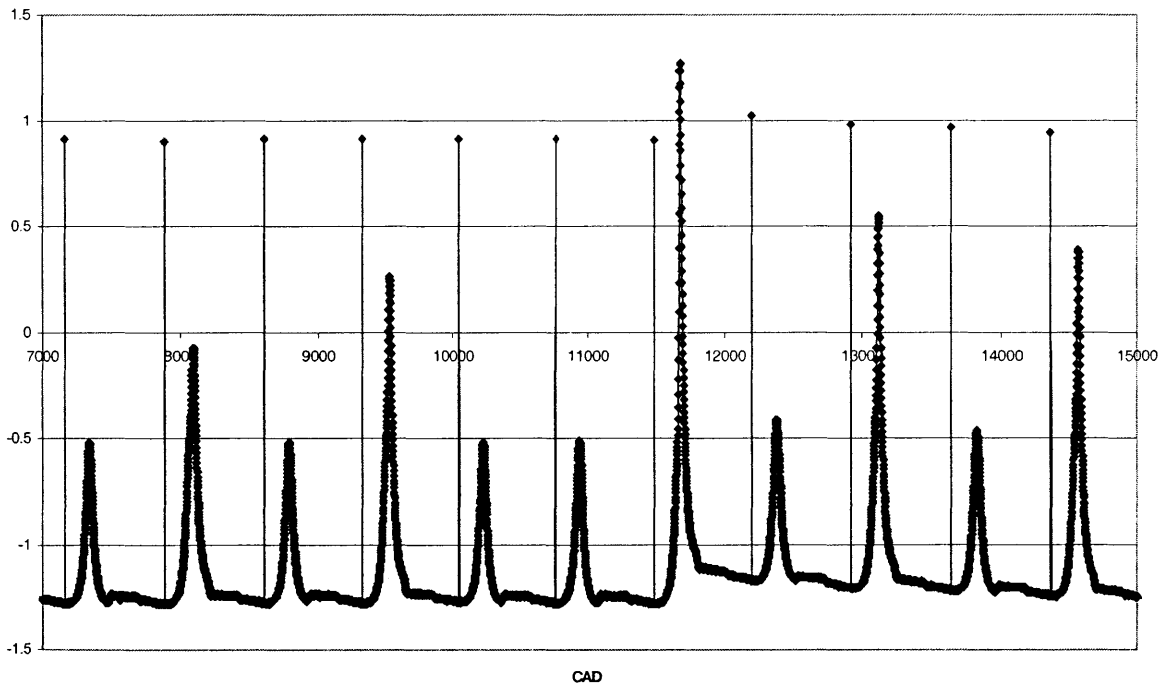Figure 4.1 Spark Sweep in Continuous Firing Mode
1500 rpm, MAP 0.4 bar

Figure 4.2 Combustion Instability at 200 rpm
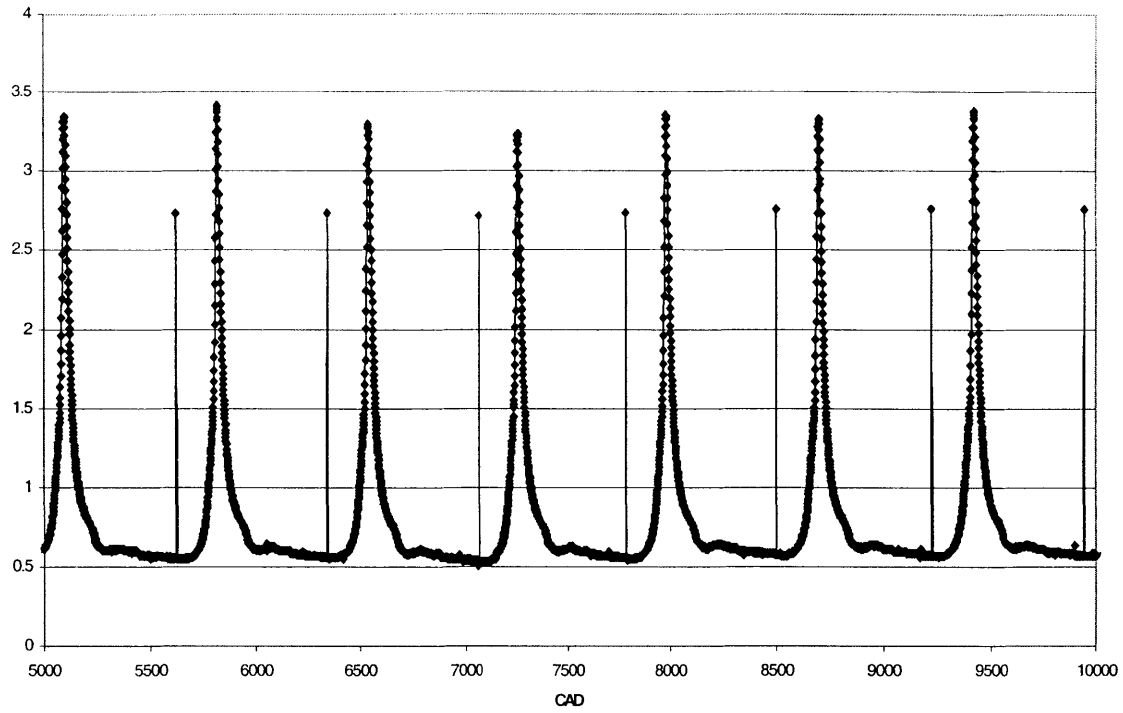0.7 bar MAP, 15 °BTDC Spark Timing, Exhaust Horiba λ=1

69

Figure 4.3 Combustion Stability at 900 rpm
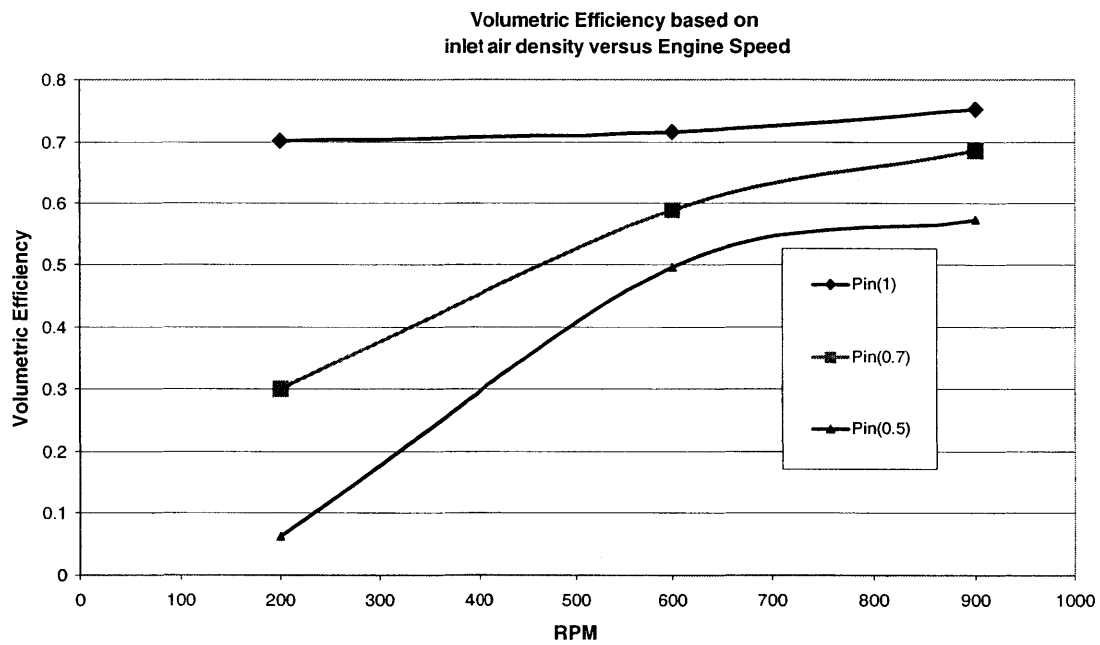0.7 bar MAP, 15 °BTDC Spark Timing, Exhaust Horiba λ = 1

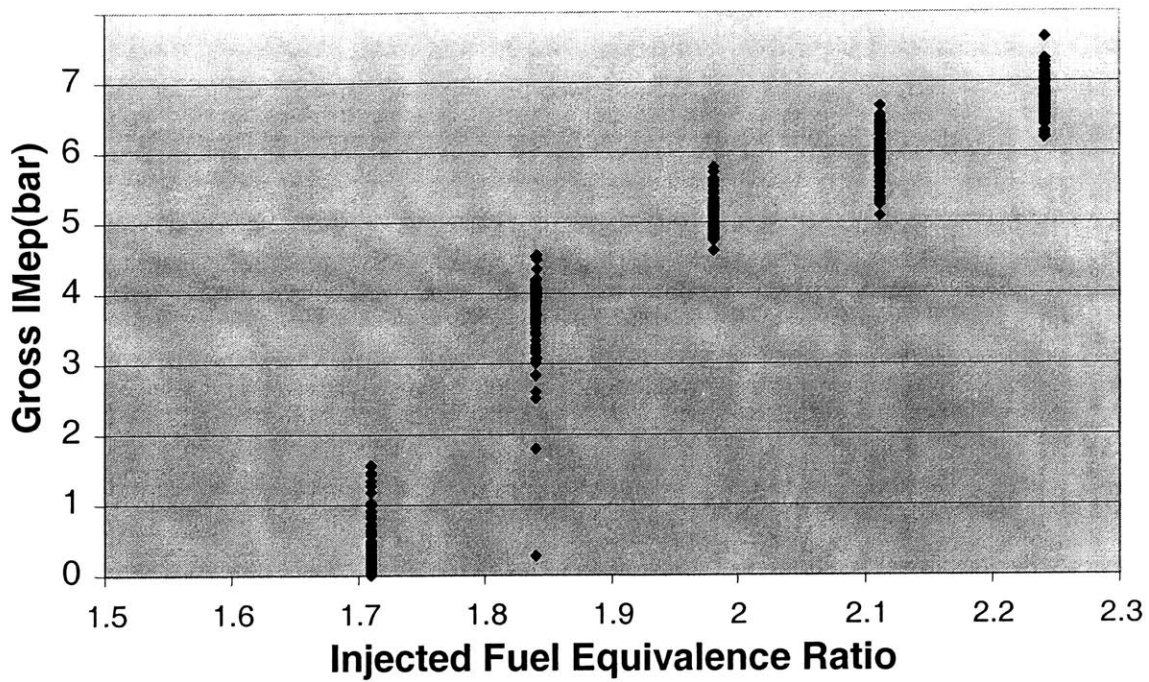Figure 4.4 Volumetric Efficiency at Low Cranking Speed

Figure 4.5 Fuel Injection vs Gross imep
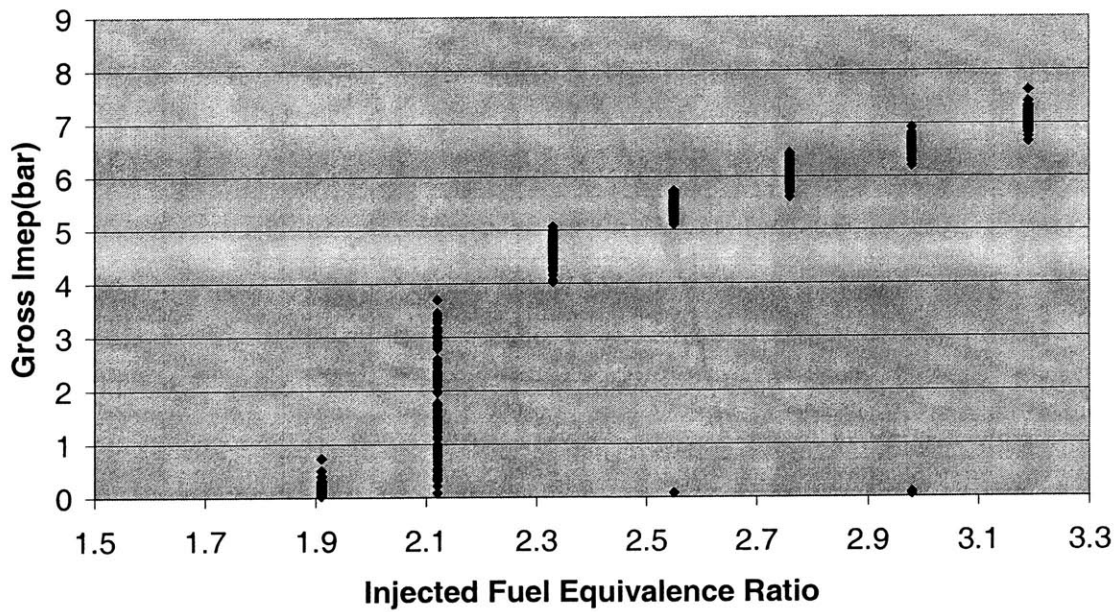200 rpm, 0.95 bar MAP, 100 cycles, 20 ° BTDC Spark Timing, 28° C ECT

Figure 4.6 Fuel Injection vs Gross Imep
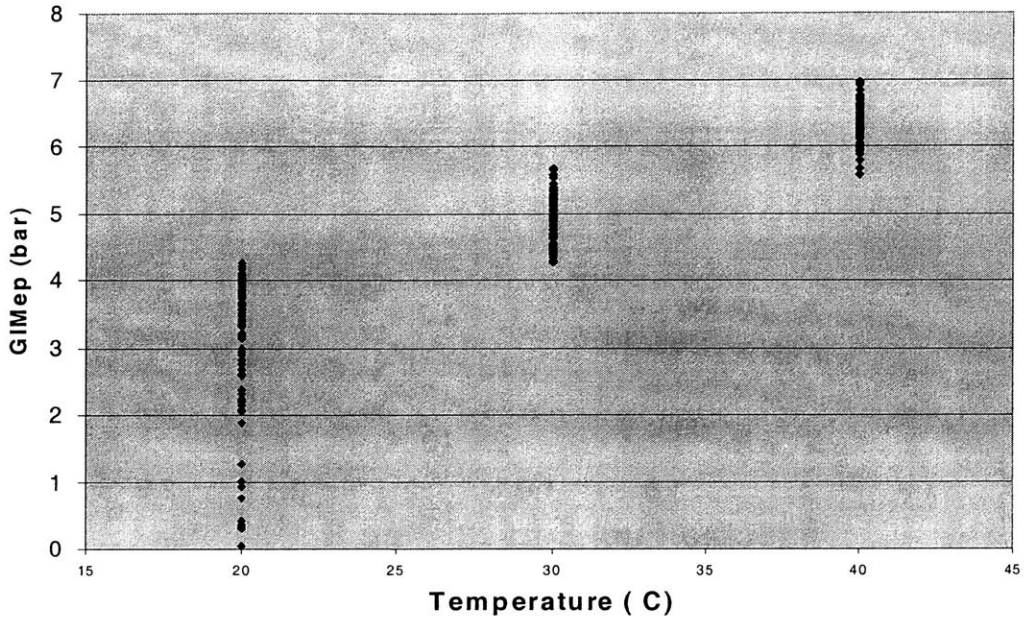700 rpm, 0.7 bar MAP, 100 cycles, 20 °BTDC Spark Timing, 22 °C ECT

Figure 4.7 Temperature Effect on Gross Imep
Injected Fuel Air Equivalence Ratio 2.27, MAP 0.9 bar, 200 rpm, Spark 20 BTDC
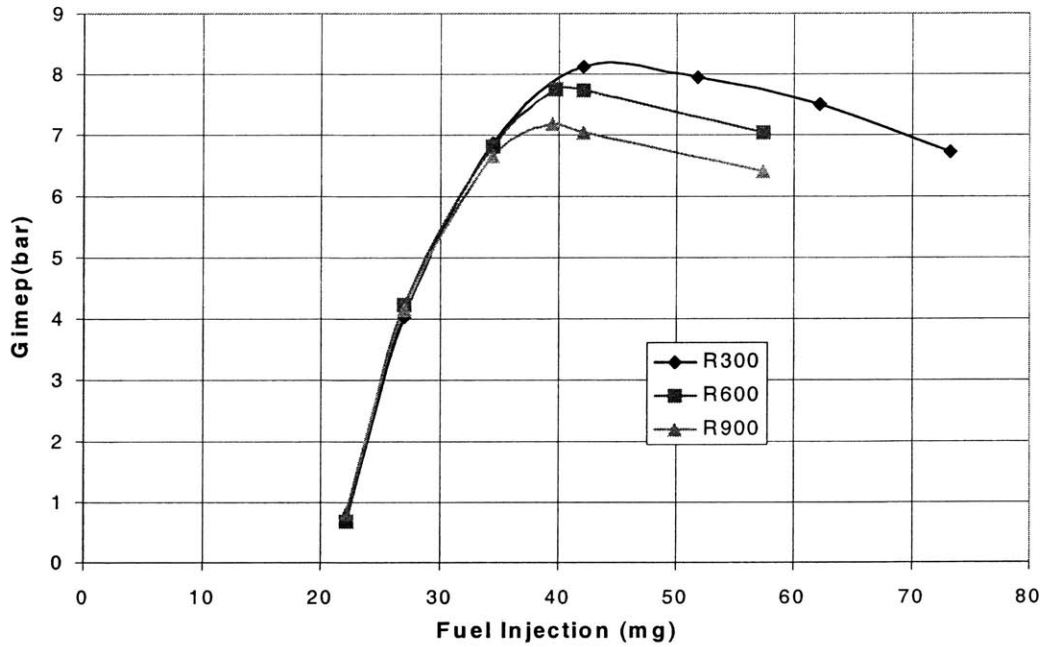

Figure 4.8 Effect of Cranking Speeds on First Cycle Combustion
TDC Spark, 80° C ECT, MAP is Coupled with Speed
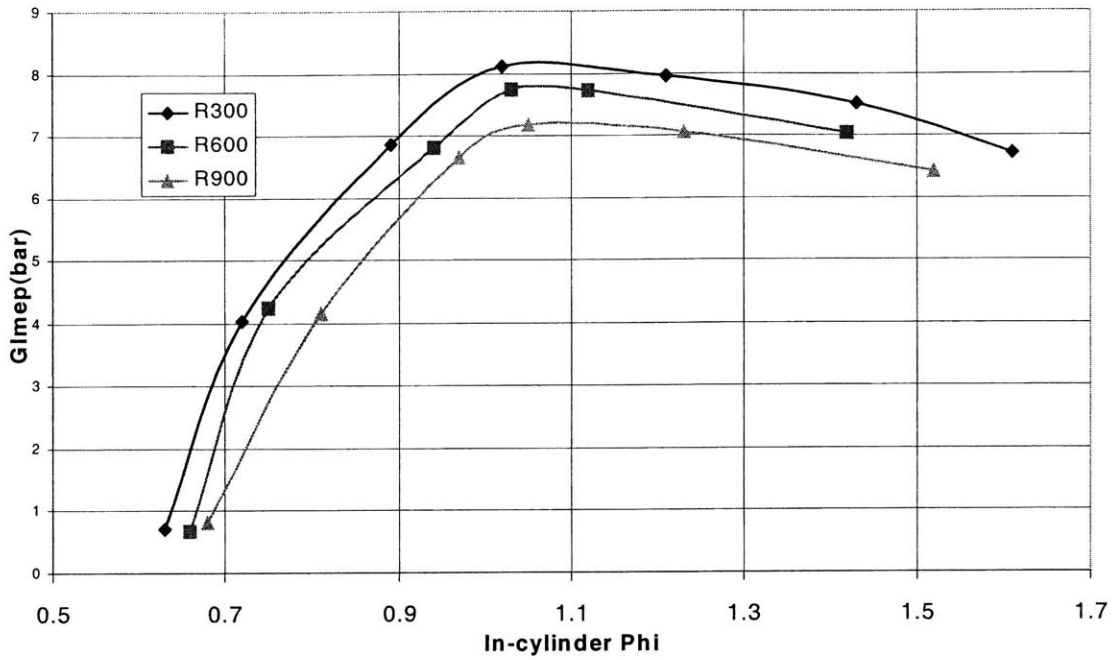
Figure 4.9 Effect of Cranking Speeds on First Cycle Combustion
TDC Spark, 80° C ECT, MAP is Coupled with Speed
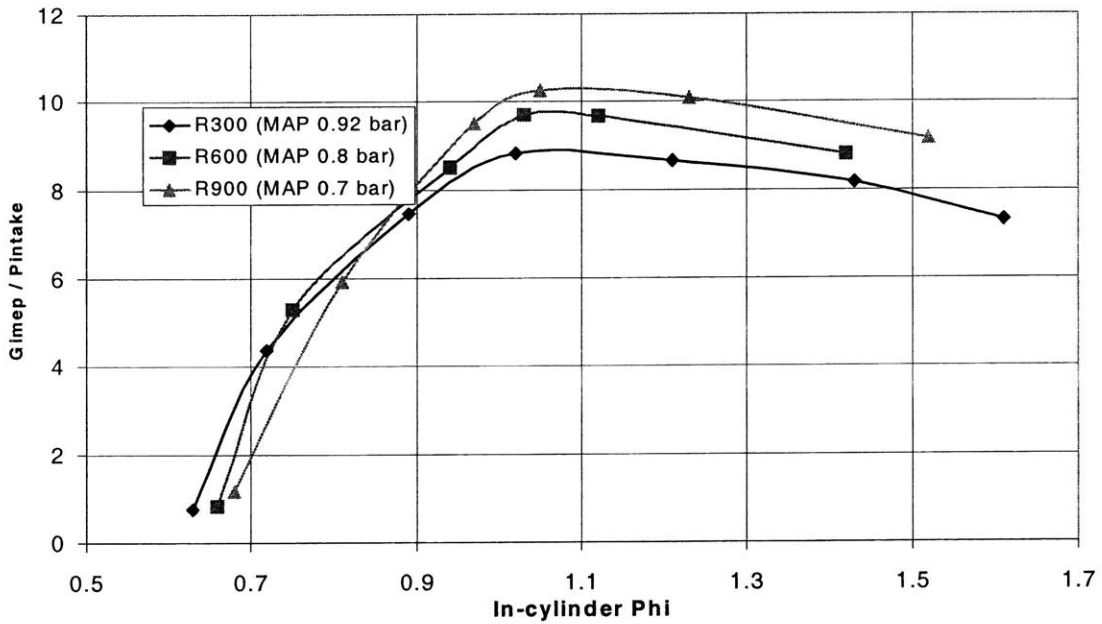
Figure 4.10 The Effect of Combustion Phasing on Imep
TDC Spark, 80° C ECT, MAP is Coupled with Speed
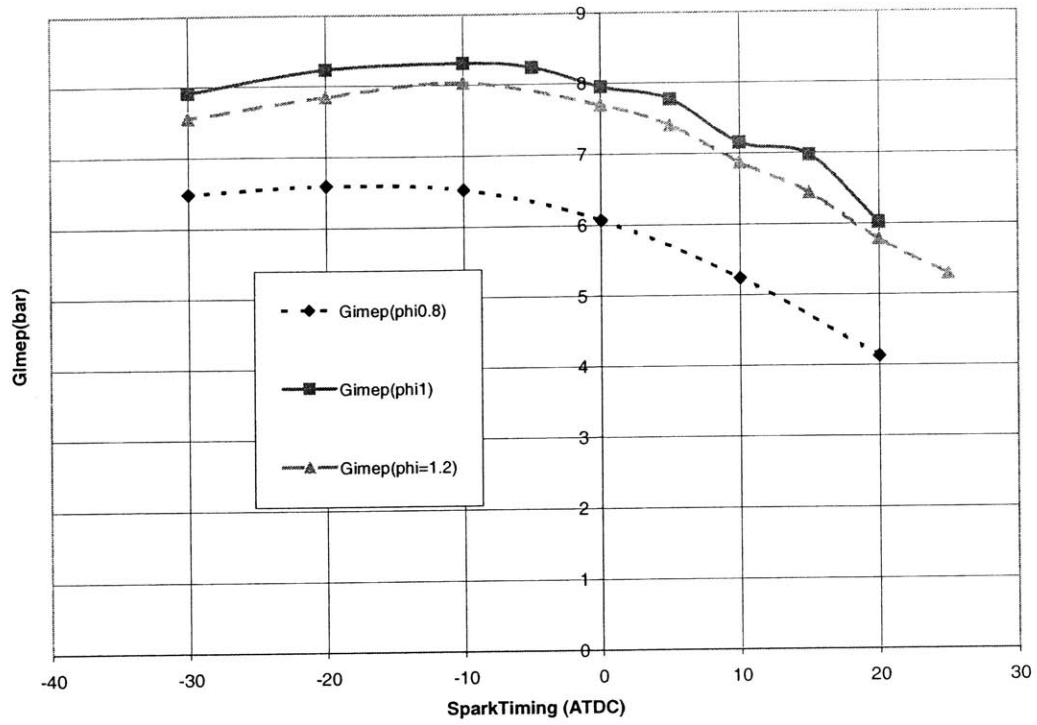
Figure 4.11 First Cycle Simulation Spark Sweep at 300 rpm
0.92 bar MAP, 60° C ECT
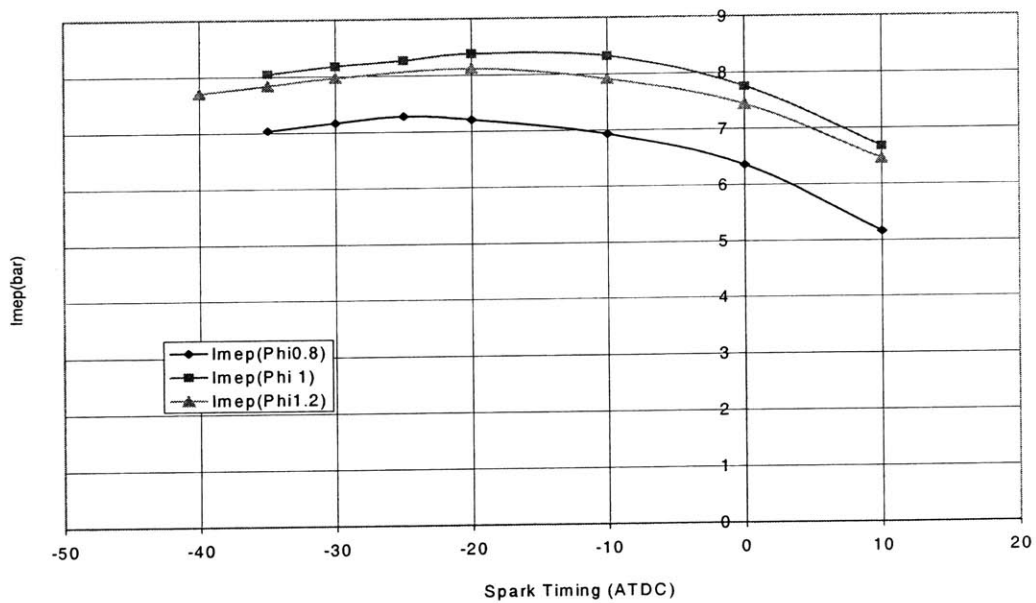
Figure 4.12 First Cycle Simulation Spark Sweep at 600 rpm
0.8 bar MAP, 60 °C ECT

74
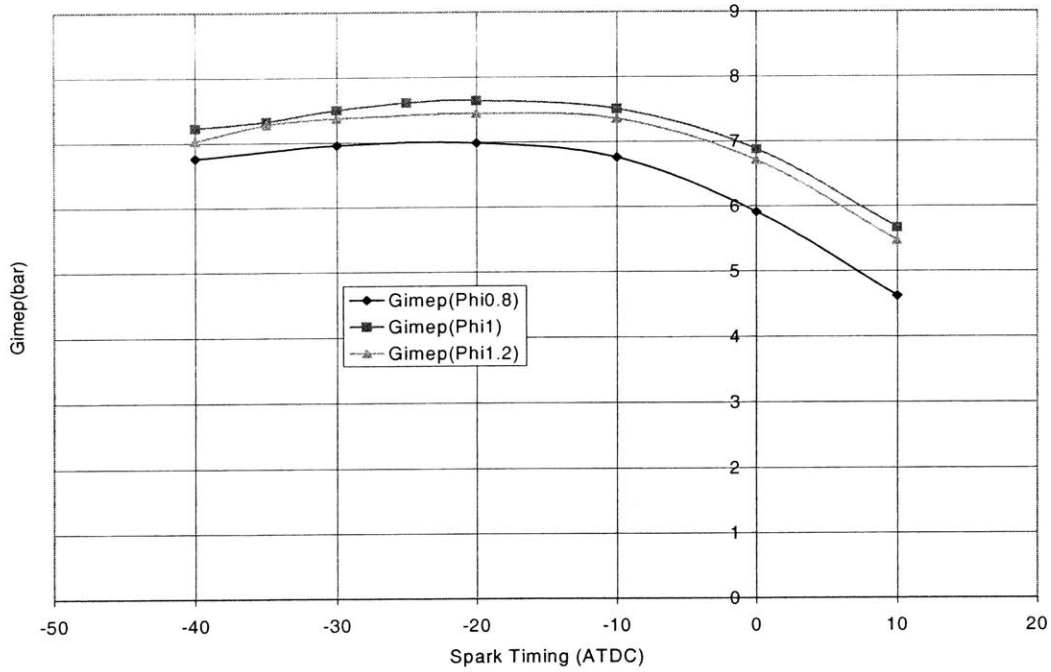
Figure 4.13 First Cycle Simulation Spark Sweep at 900 rpm
0.7 bar MAP, 60 °C ECT
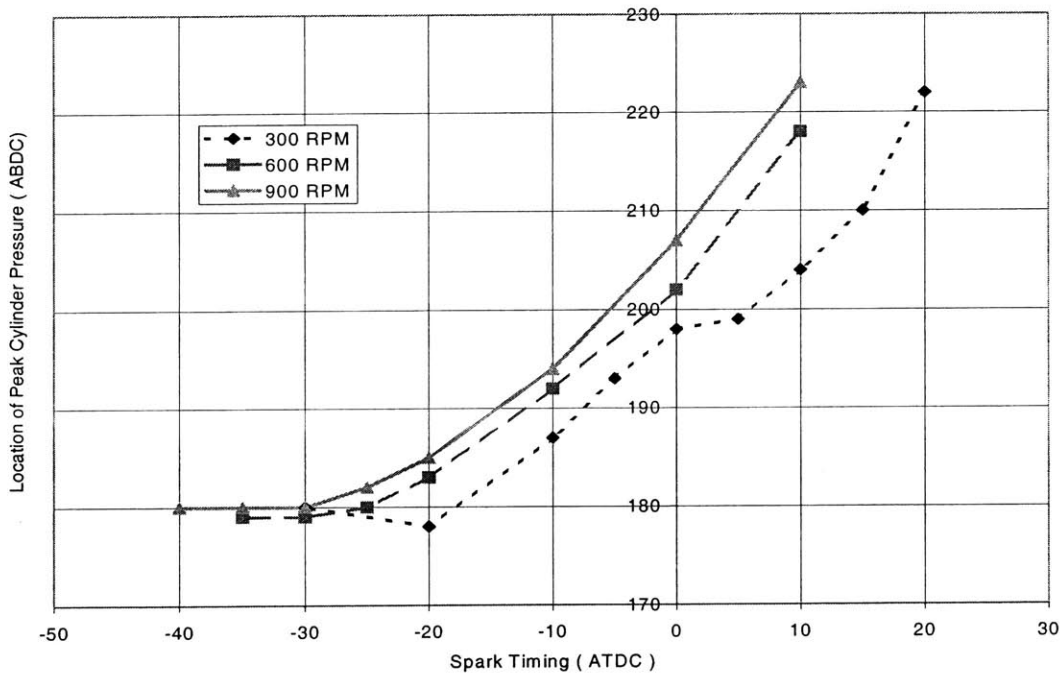
Figure 4.14 Peak In-cylinder Pressure Location at Different Cranking Speeds
Stoichiometric Mixture, 60 °C ECT
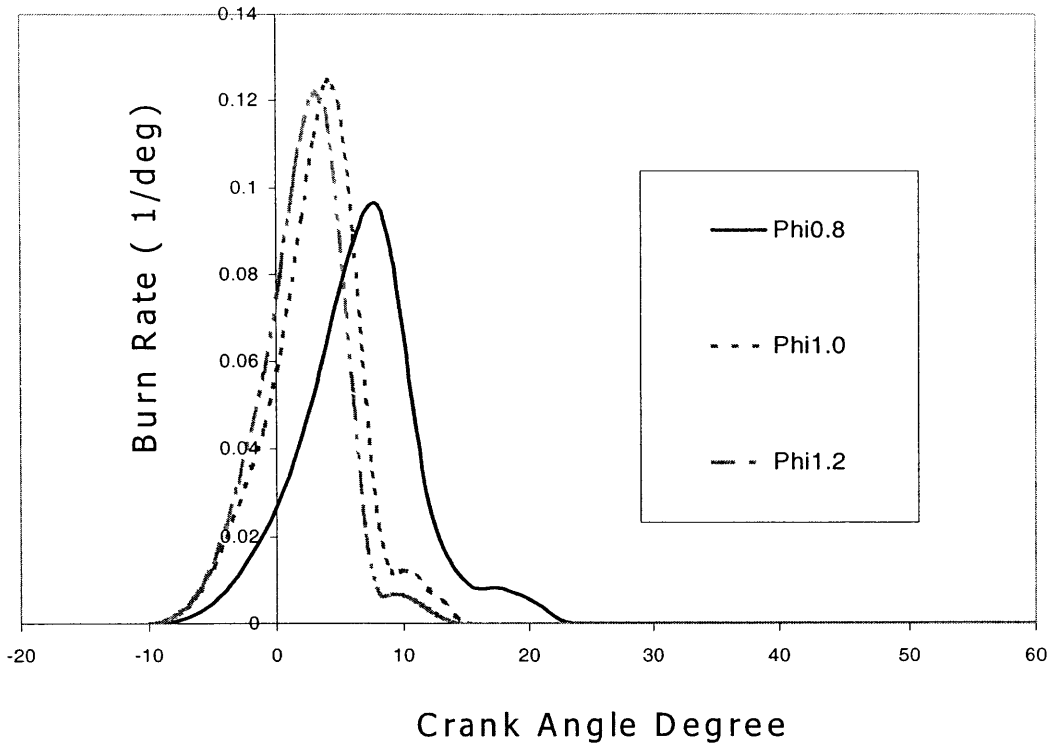
Figure 4.15 Burn Profile at 300 RPM
10 BTDC Spark Timing, MAP 0.92 bar
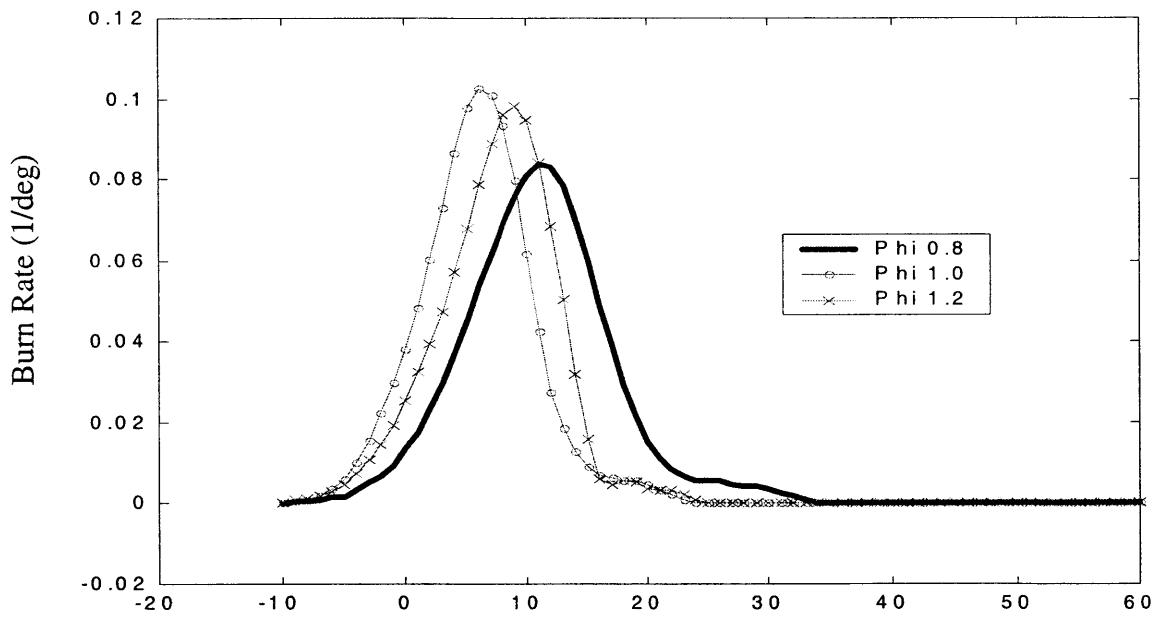
Figure 4.16 B urn Profile at 600 RPM
10 BTDC Spark Timing, MAP 0.8 bar
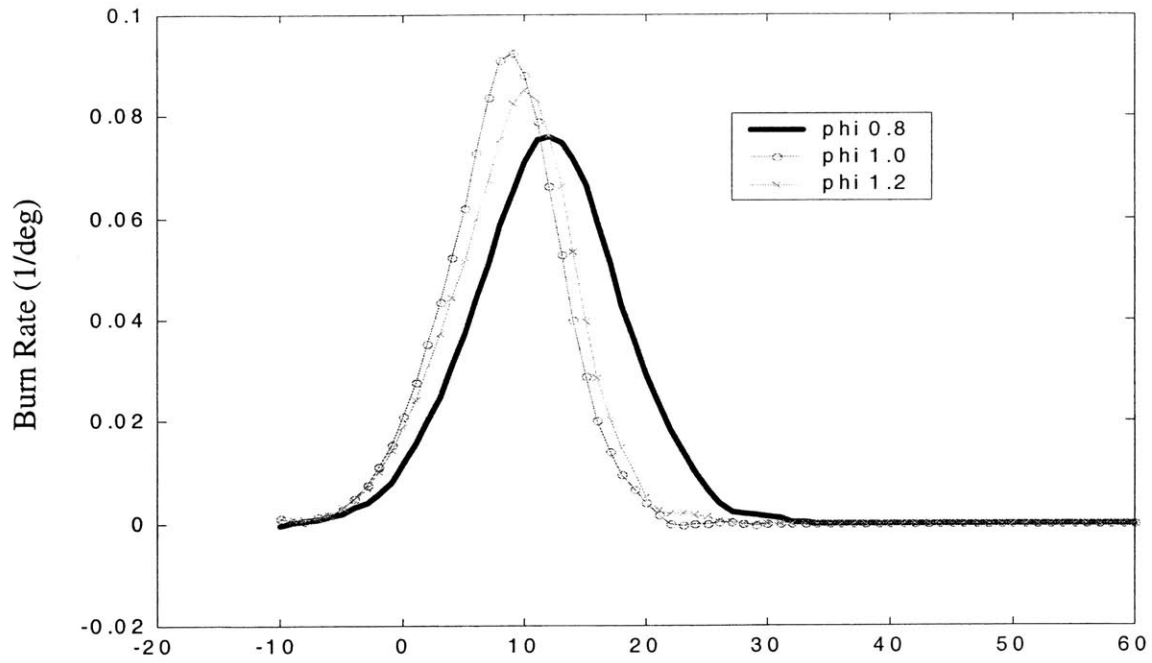
Figure 4.17 Burn Profile at 900 RPM
10 BTDC Spark Timing, MAP 0.7 bar
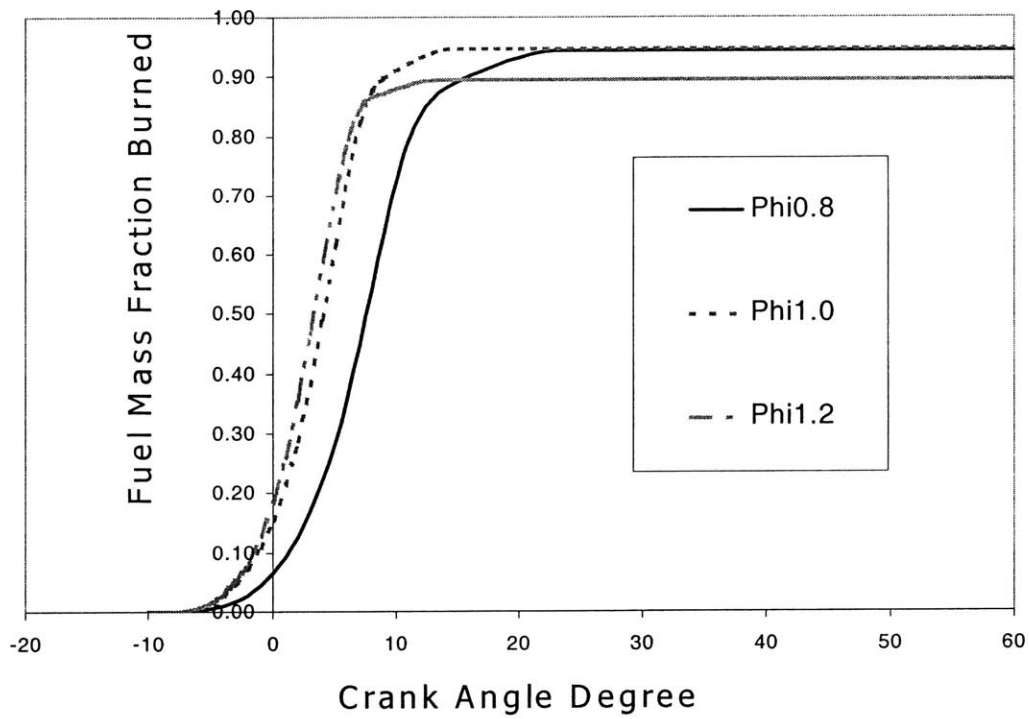
Figure 4.18 Mass Fraction Burned Profile at 300 RPM
10 BTDC Spark Timing, MAP 0.92 bar
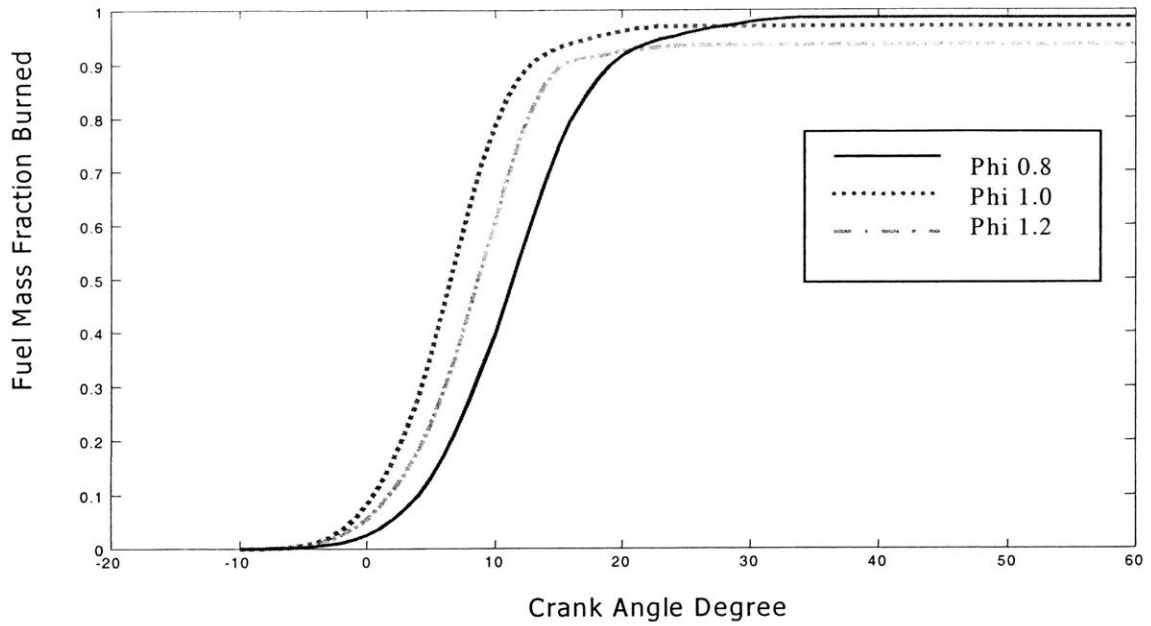
Figure 4.19 Fuel Mass Fraction Burned at 600 RPM
10 BTDC Spark Timing, MAP 0.8 bar
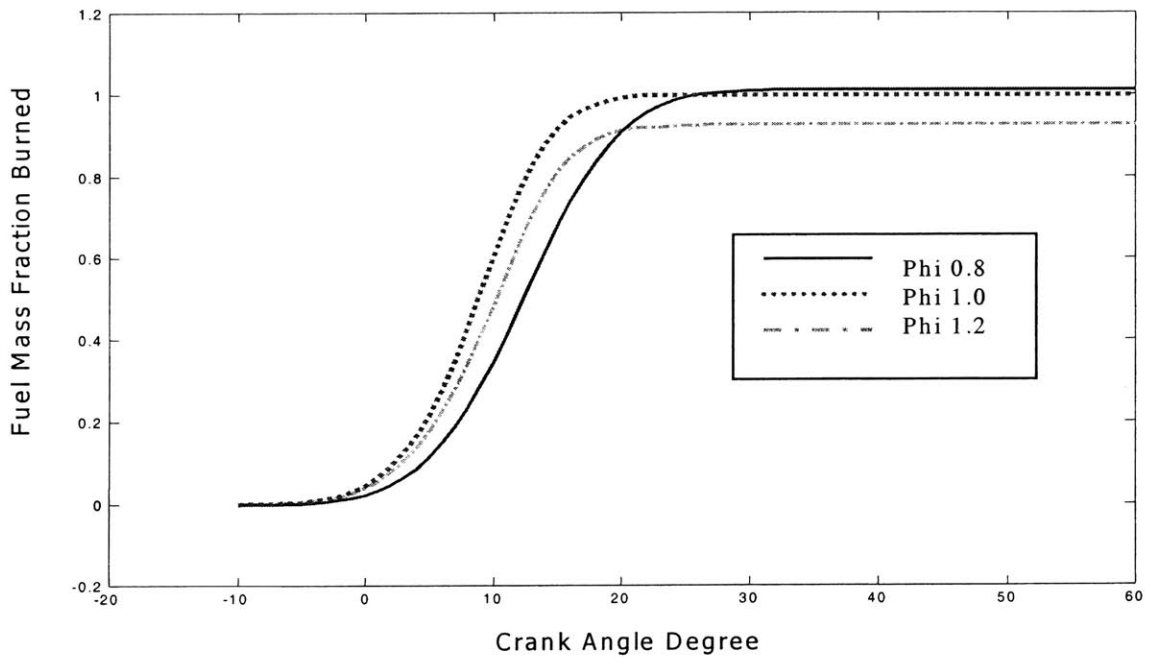
Figure 4.20 Fuel Mass Fraction Burned Profile at 900 rpm
10 BTDC Spark Timing, MAP 0.7 bar
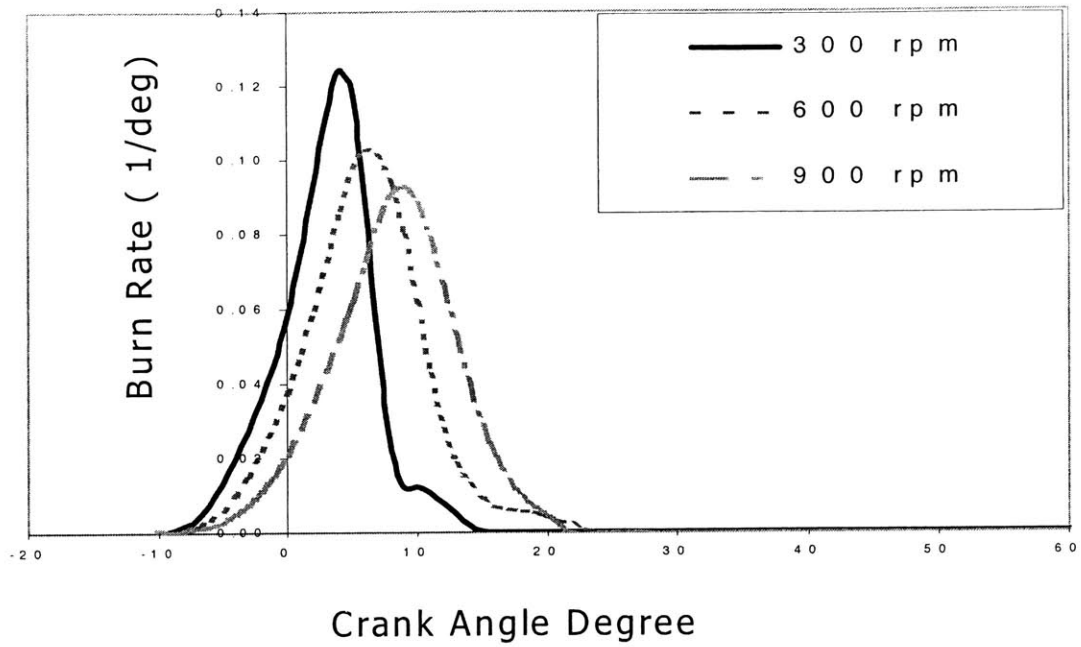
Figure 4.21 Effect of cranking speed on burn profile
Spark Timing 10° BTDC, $\phi = 1$, ECT 60° C
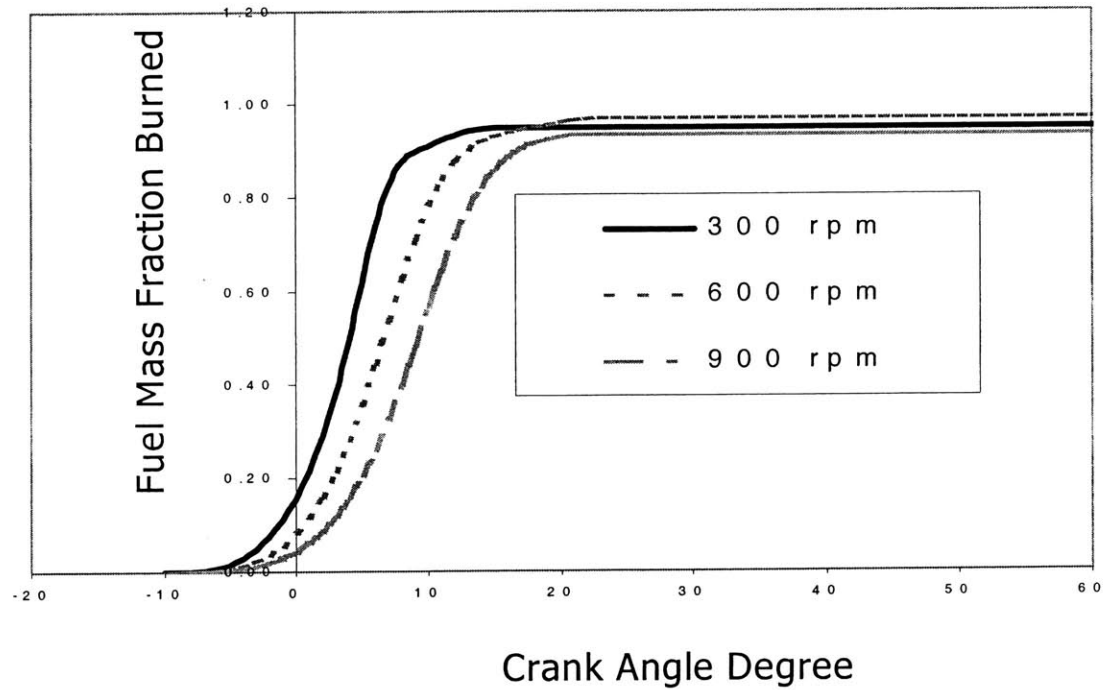
Figure 4.22 Effect of cranking speed on fuel mass fraction burned
Spark Timing 10° BTDC, $\phi = 1$, ECT 60° C

Figure 4.23 Location of 50% Mass Fraction Burned
300 rpm, 0.92 bar MAP, 60° C

Chapter 5

HYDROCARBON EMISSIONS

5.1   Introduction

Hydrocarbon (HC) emissions during cranking is of particular concern because of the unusual operating condition and that the catalyst is not active. While all the HC mechanisms under normal operating conditions [22] apply but with different magnitudes because of the cranking thermal environment, there are additional features with the cranking p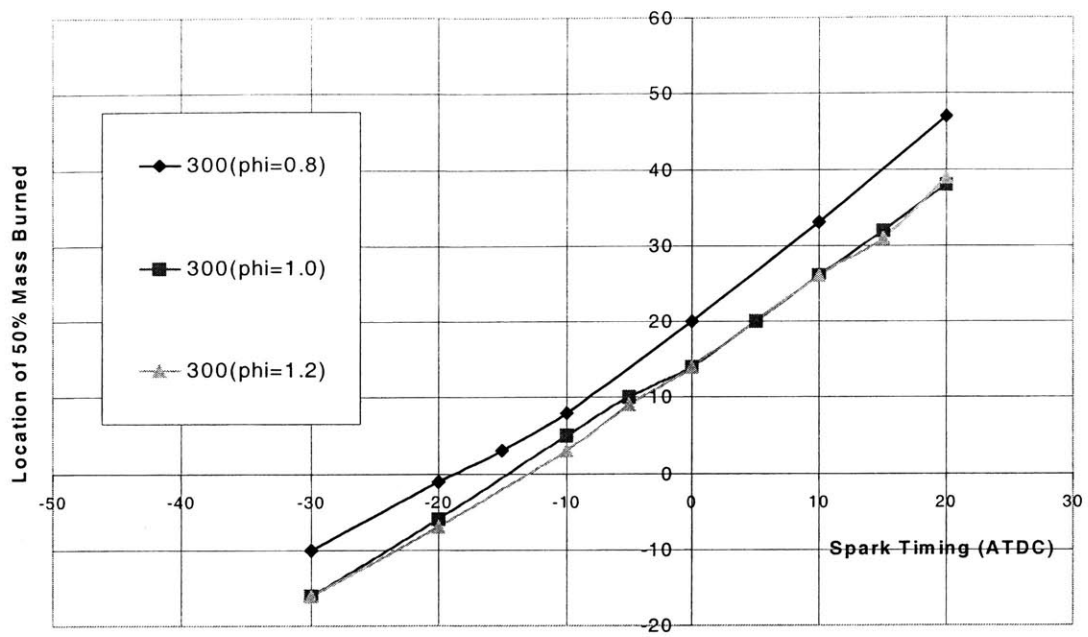rocess that contribute to HC emissions. For example, the substantial liquid fuel entering into the cylinder. This fuel (especially the ones that is deposited around the exhaust valve) could escape combustion and could exhaust as unburned HC. This chapter assesses the magnitude of the Engine-Out Hydrocarbons (EOHC) as a function of the cranking conditions.

5.2   Effect of Different Cranking Speeds

Fig 5.1 shows a typical exhaust Fast FID signal with the engine operating in the skip injection mode. The charge did not fire in the second cycle and resulted in a very high HC level (which saturated the detector); the HC of the subsequent cycles decreased. The first cycle HC emissions level is enlarged in figure 5.2. After the exhaust valve closing the HC level was constant due to lack of exhaust gas motion and the sampling tube sampled the same exhaust gas with time. The signal rose rapidly when the second cycle in-cylinder gas exhausted. The amount of fuel injection in figure 5.1 was modest (34 mg) and therefore combustion was not initiated in the second and subsequent cycles. This fact results in high HC emissions level in the exhaust stroke. The signal for the first cycle combustion process is further enlarged in figure 5.3 and figure 5.4. Figures 5.3 and 5.4 appear to be similar to the hydrocarbon emissions during steady state operation. The first peak is due to crevice gases near the exhaust valve seats [23], namely those around the exhaust valve seat, adjacent head gasket, and spark plug. The second peak which can not be observed in every experiment is very likely due to the crevice gases near the piston top land [24]. The final peak is due to the

vortex of crevice gases "scrolled off the cylinder wall by the piston during the exhaust stroke which exit the cylinder last ".

The effect of increasing cranking speed on hydrocarbon emissions at different coolant temperature as a function of fuel injection is illustrated in figure 5.5, figure 5.6, and figure 5.7. The spark timing was set to top dead center and the data point was an average EOHC level of between 40 to 150 cycles. When the amount of fuel injection exceeded the lean combustion limit, there was substantial drop in HC emissions level. This was due to the several misfires in the lean region. Each misfired cycle can have EOHC level of 50000 ppmC$_1$ and therefore, could significantly effect the average EOHC level.

Increasing the cranking speed cause a lower level of EOHC due to 2 factors: the intake pressure effect and the combustion phasing effect. As we increase the cranking speed the intake pressure in a typical closed throttle start-up strategy decreases. Lower intake pressure will lead to lower peak cylinder pressure during the combustion process. Since the flame can not reach the crevices during normal combustion process, lower peak cylinder pressure will reduce the unburned HC amount that escaped normal combustion by filling the crevices and therefore contribute to the reduction of EOHC level at higher cranking speed. For a fixed spark timing, increasing the cranking speed will reduce the EOHC level through combustion phasing. A fixed spark timing is translated into spark retard in higher engine speed operation which reduce the EOHC emission due to better post flame oxidation mechanism.

However with large amount of fuel injection, higher cranking speed tends to result in higher EOHC level through mixture preparation effect. As discussed in chapter 3, higher engine speed will result in higher in-cylinder fuel air ratio. In the rich region, the higher the in-cylinder ϕ, the worse the extent of incomplete combustion be. Hence higher engine speed tends to induce higher EOHC level for rich mixture.

5.3   Effect of Engine Coolant Temperature

Figure 5.8, figure 5.9, and figure 5.10 shows the result of increasing the coolant temperature at different cranking speed as a function of fuel injection amount. At high engine coolant temperature the EOHC level decreases rapidly at lower amount of fuel injection but also increases more rapidly with larger fuel injection due to mixture preparation effect. At high engine coolant temperature for the same amount of fueling, the in-cylinder value is

higher due to better mixture preparation process. This phenomenon results in smaller amount of fuel injection is necessary to reach the lean limit of combustion and hence, major reduction of EOHC level is reached at lower amount of fuel injection. Similar phenomenon can also be identified at rich limit of combustion which result in rapid EOHC level increase at lower fueling with higher engine coolant temperature. Since the mixture preparation process is the major controlling factor, it is only reasonable to look at the effect of in-cylinder fuel air equivalence ratio on EOHC level.

5.4   In-cylinder Fuel Air Equivalence Ratio vs EOHC

The effect of in-cylinder ϕ versus the EOHC was shown in figure 5.11. When in-cylinder ϕ is used instead of fuel injection amount the EOHC level fit a bowl shaped curved, regardless the engine coolant temperature or engine speed. The sharp increase in EOHC in the low in-cylinder ϕ region was due to misfires. A rather flat curve with a slight upward slope with ϕ follows. This portion represents the robust combustible range. At the very rich region, incomplete combustion occurs and the EOHC level increases sharply again. The rather flat region is the condition where the real cranking should take place. Fig 5.11 indicates that higher engine speed will result in lower EOHC emissions due to the lower peak cylinder pressure and better combustion phasing. Higher engine coolant temperature will also lead to lower EOHC emissions level due to better post flame oxidation process.

5.5   Spark Timing Effect on Hydrocarbon Emissions

Fig 5.11 examines the spark timing effect on HC emissions at different cranking speeds, where the fuel injection amount is set to 41.8 mg and engine coolant temperature set at 60°C. In general, retarding the spark timing will lower the EOHC level due to better post-flame oxidation. With retarded spark timing, less work is extracted from the mixture and but the total energy released is more or less the same. Therefore, more energy is converted to the combustible gas sensible energy which makes the exhaust gas temperature higher with retarded spark timing. Higher exhaust gas temperature will enhance the post-flame oxidation process and therefore reduce the HC emissions level. Retarding the spark timing from 25° BTDC to 10° ATDC decreases the EOHC from 3400 to 2800 ppm C1 at 300 rpm and from approximately 3100 to 2500 ppm C1 at 600 and 900 rpm. There is no substantial difference

observed in the EOHC level for 600 and 900 rpm case. This result suggest that there is a threshold for engine speed above which increasing the cranking speed will not produce much more benefit on the EOHC level. Therefore, future cranking strategy should assess the possibility of increasing the cranking speed until the threshold speed.
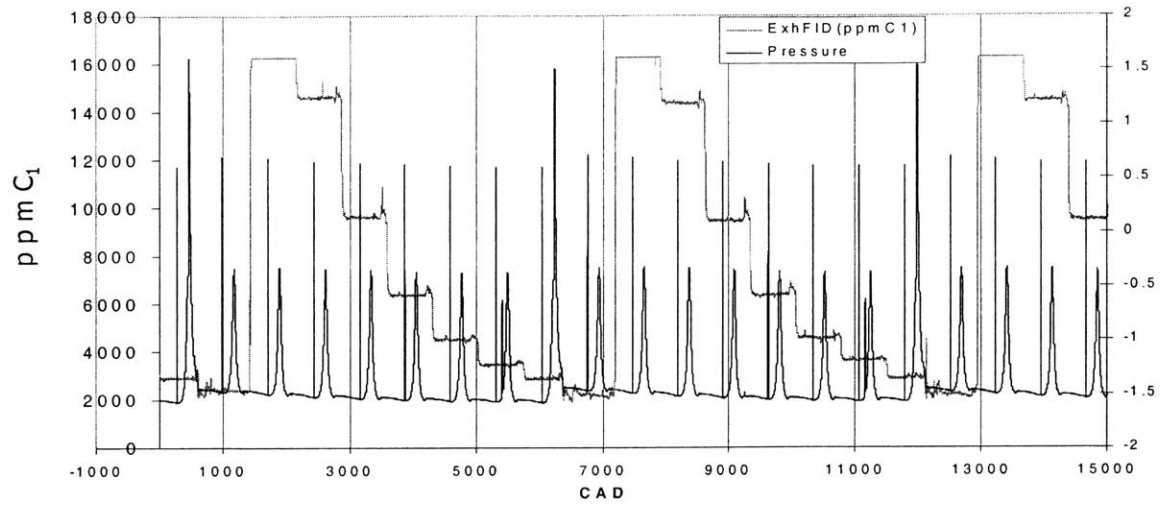
Figure 5.1 Typical Exhaust FFID Signal in Skip Injection Mode
80°C ECT, 300 rpm, 0.92 bar MAP, 34 mg Fuel Injection, TDC Spark
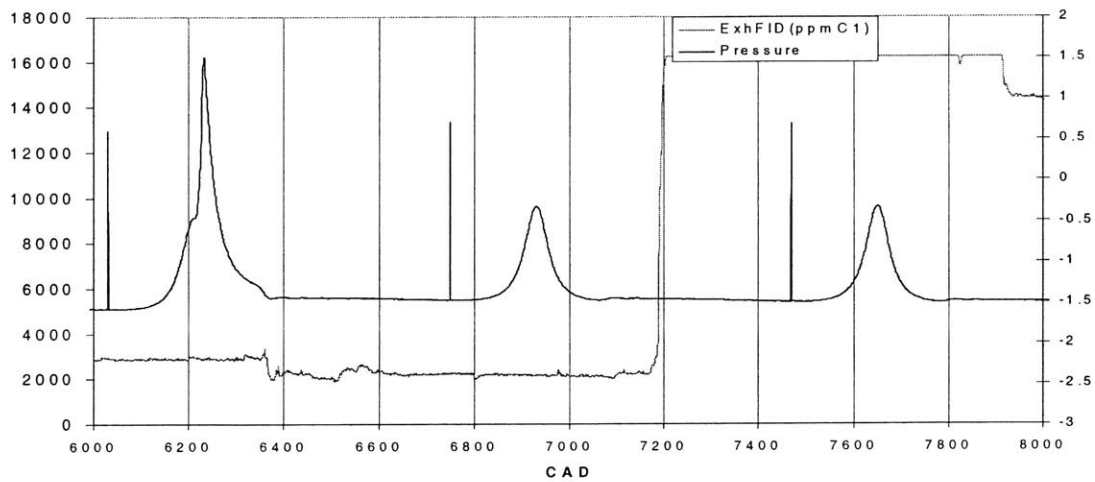
Figure 5.2 Enlarged Exhaust FFID Signal in Skip Injection Mode
80°C ECT, 300 rpm, 0.92 bar MAP, 34 mg Fuel Injection, TDC Spark
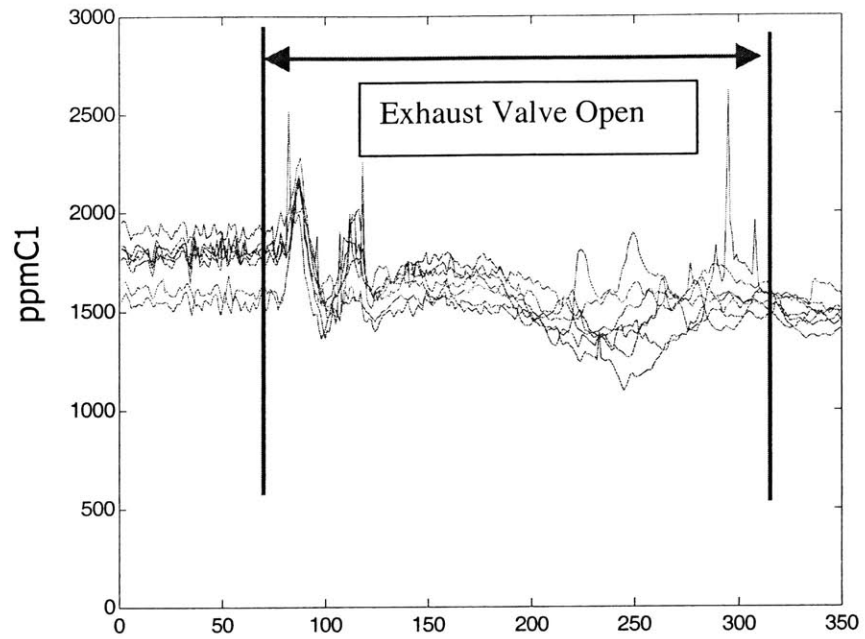
Figure 5.3 FID Signal During Exhaust Valve Open Period
80° C ECT, 600 RPM, 0.8 bar MAP, TDC Spark, 35 mg Fuel Injection
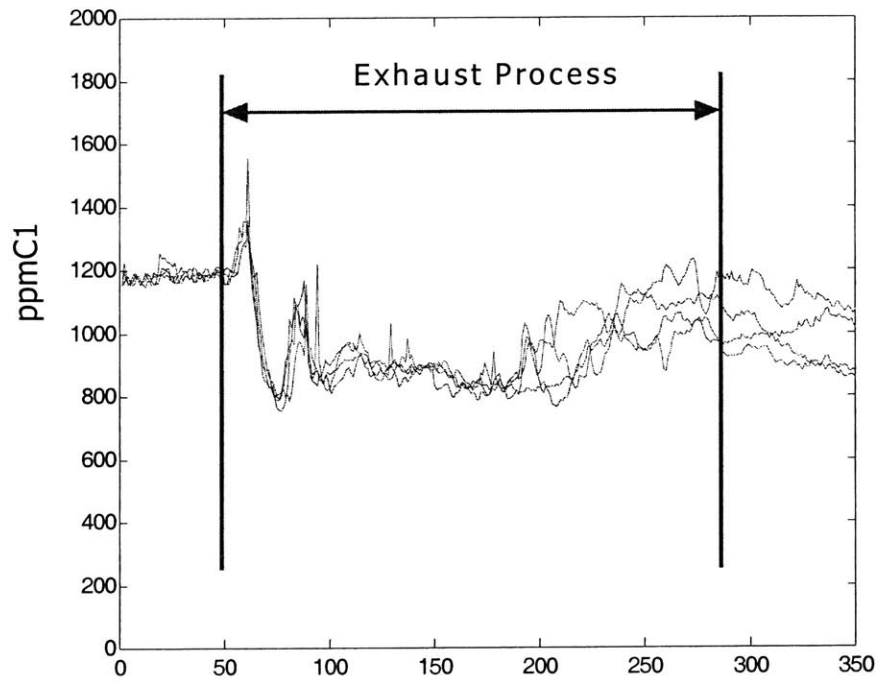
Figure 5.4 FID Signal During Exhaust Valve Open Period
80° C ECT, 900 RPM, 0.7 bar MAP, TDC Spark, 35 mg Fuel Injection
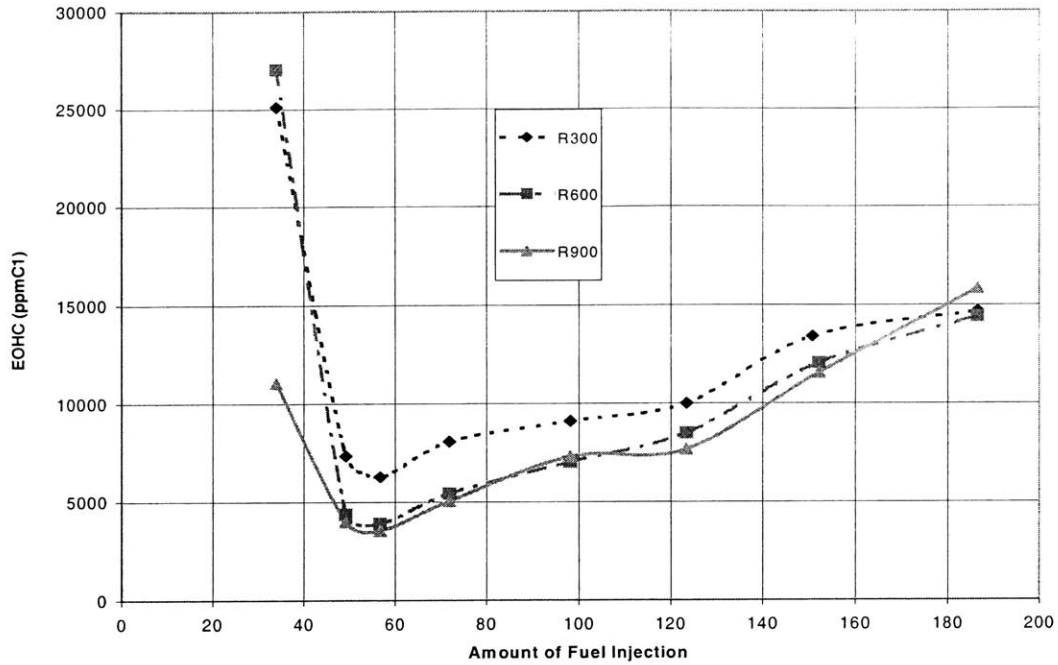
Figure 5.5 Effect of Cranking Speed on EOHC
40 °C ECT, TDC Spark
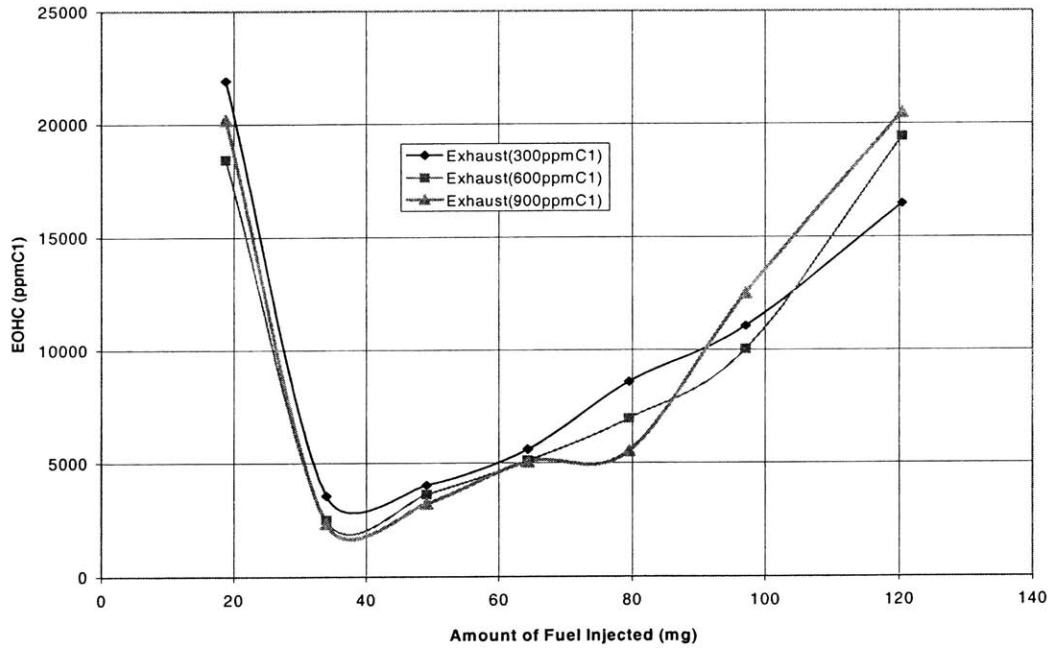
Figure 5.6 Effect of Cranking Speed on EOHC
60 °C ECT, TDC Spark
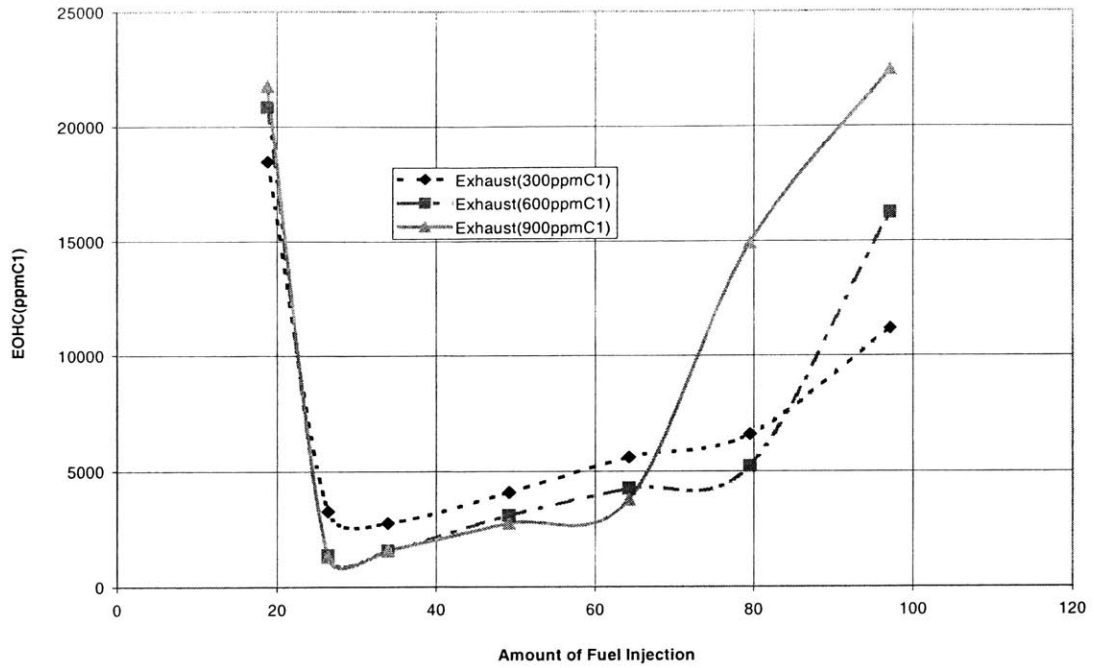
Figure 5.7 Effect of Cranking Speed on EOHC
80 °C ECT, TDC Spark
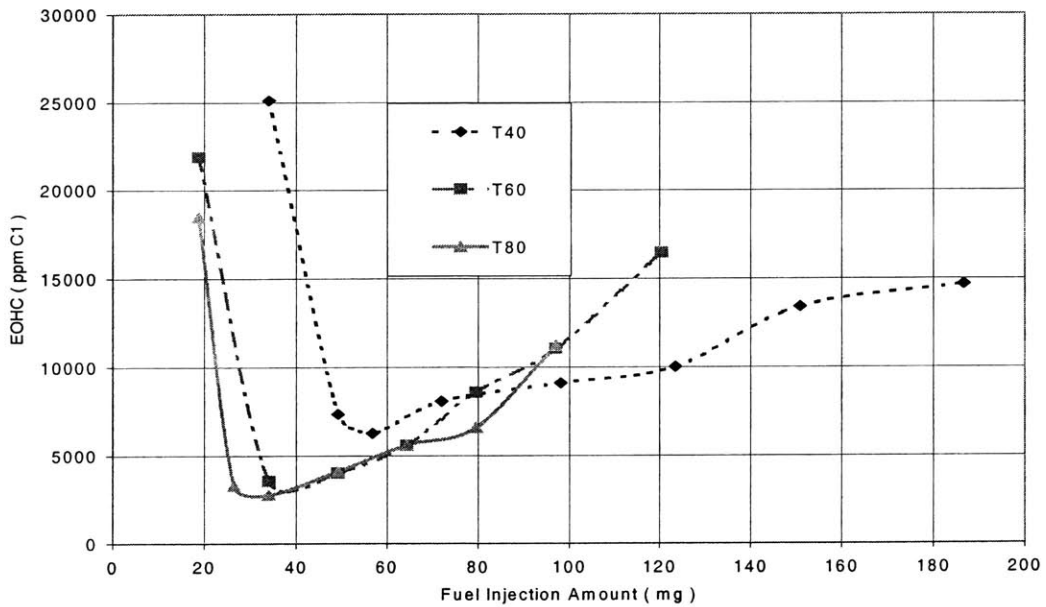
Figure 5.8 Effect of Engine Coolant Temperature on EOHC
300 RPM, 0.92 bar MAP, TDC Spark Timing
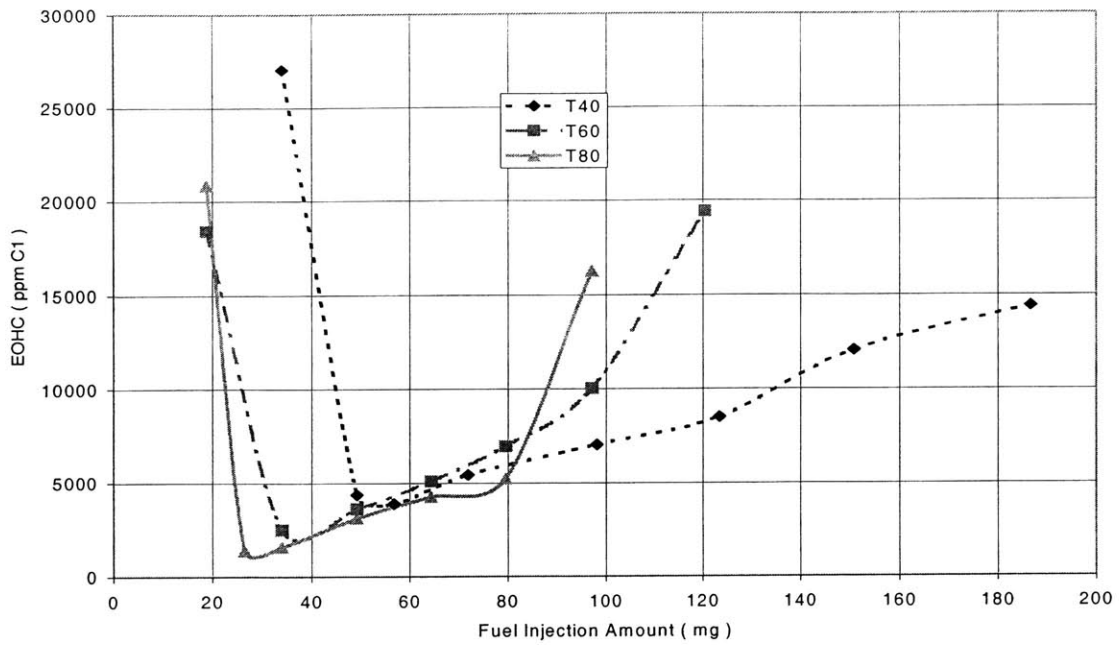
Figure 5.9 Effect of Engine Coolant Temperature on EOHC
600 rpm, 0.8 bar MAP, TDC Spark
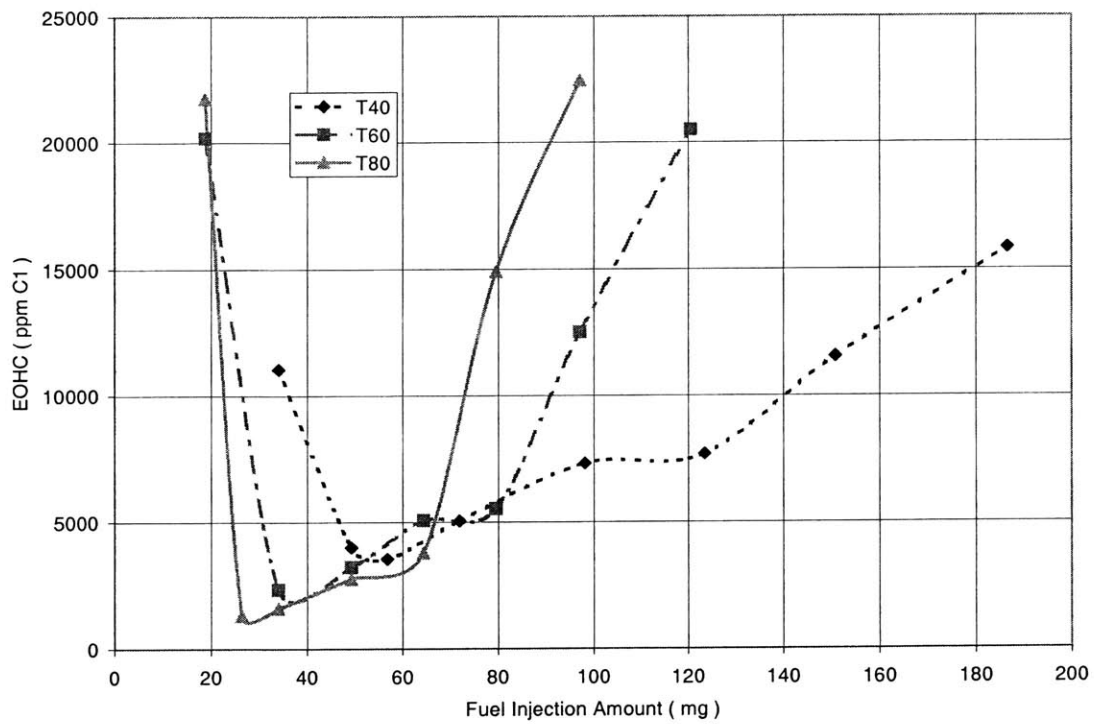
Figure 5.10 Effect of Engine Coolant Temperature on EOHC
900 rpm, 0.7 bar MAP, TDC Spark
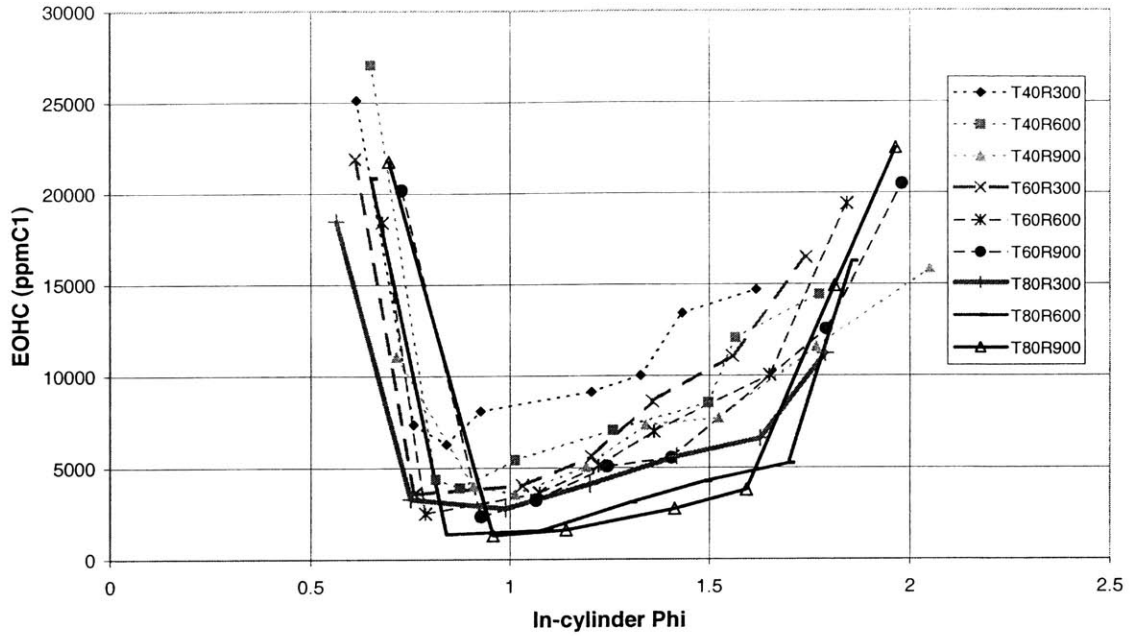
Figure 5.11 In-cylinder Fuel Air Ratio vs EOHC
TDC Spark Timing
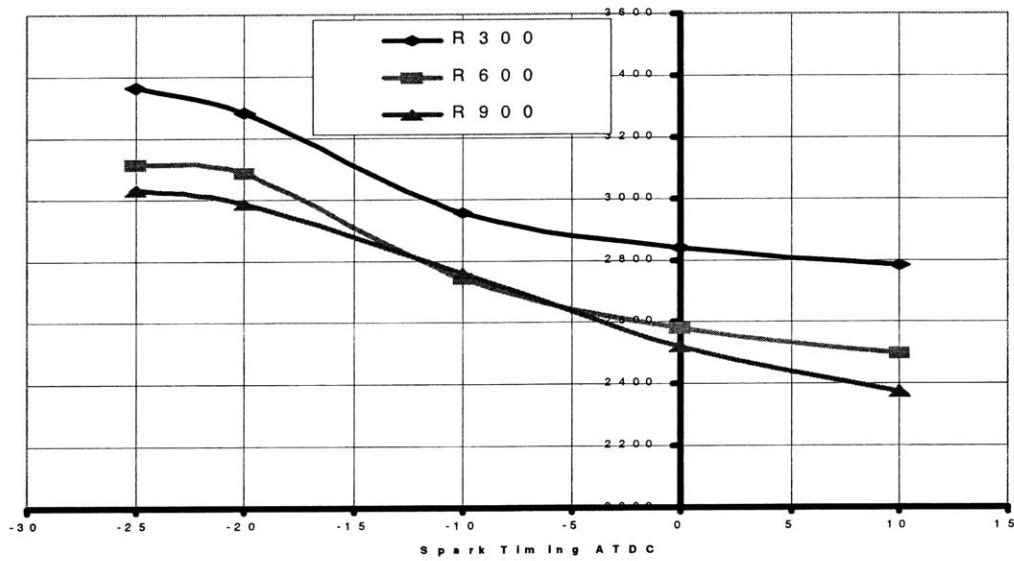
Figure 5.12 Spark Timing Effect on EOHC
60 ° ECT, 41.8 mg fuel injection

Chapter 6
SUMMARY & CONCLUSIONS

6.1 Conclusions

6.1.1 Mixture Preparation

- The mixture that enters the cylinder in the initial phase of the intake process is rich and it may contain some liquid droplets. The air-fuel mixing process continues inside the cylinder during the compression stroke. At spark ignition, limited mixture inhomogeniety may still present.

- For the same amount of fuel injection, there is cycle-to-cycle variation in the first cycle in-cylinder fuel-air equivalence ratio. The standard deviation of the variation in the first cycle ϕ is slightly larger than normal engine operation due to the complex nature of wall wetting and fuel puddle forming mechanisms in the first-cycle.

- Larger amount of fuel injection will result in higher first and second cycle in-cylinder ϕ. The fraction of the injected fuel mass in the charge is, however, lower because of the limiting of the vaporization process.

- Increasing the cranking speed will increase the first and second cycle in-cylinder ϕ due to lower intake pressure and higher air velocity but the effect seems to be modest ($\sim$ 10% in the 300 – 900 rpm range). The effect is more noticeable when a large amount of fuel is injected. The increase in the second cycle in-cylinder ϕ is attributed to the fact that more fuel is left in the port at higher engine speed.

- Increasing the engine coolant temperature increases the first cycle in-cylinder ϕ due to better evaporation.

- The engine starts to fire at fuel air equivalence ratio as low as 0.65 but the lean limit for robust combustion occurs approximately at in-cylinder ϕ of 0.8. There is no significant change in the lean limit of robust combustion at different coolant temperatures or engine speeds.

- A mixture preparation model based on that the evaporation process is mixing limited was constructed and it fit the experimental data very well. While the simple model does not account for all the details that effect the mixture preparation, the good

agreement with the experimental result implies that mixture preparation process is indeed controlled by the vaporization process.

6.1.2 Combustion

- It is difficult to achieve robust combustion with continuous operation at low speed, part load, due to the high residual gas fraction. The residual gas fraction is due to the high backflow in the valve overlap period which is extensive at low speed.

- The combustion process at different cranking speeds for typical start-up strategy is complex due to the combined effect of different MAP, combustion phasing, and in-cylinder fuel air equivalence ratio.

- At modest amount of fuel injection for the first firing cycle, the imep values at 3 different cranking speeds for the same amount of injected fuel were almost the same. The reason is that at higher engine speed, the intake pressure is lower but the fuel air-equivalence ratio is higher therefore the same level of imep is observed. However, at higher amount of fuel injection the imep is higher for lower engine speed since the effect of intake pressure dominated the combustion phasing effect.

- Higher engine speed will create benefit from better combustion phasing only when the in-cylinder fuel air equivalence ratio is richer than the stoichiometric value.

- The highest imep value occurs at in-cylinder fuel air ratio between 0.95 ~ 1.1 with the highest value of about 8 bar when the engine speed is 300 rpm with the intake pressure set at 0.92 bar.

- The burn rate analysis indicated that the combustion during the first cycle of cranking is much faster (in terms of crank angle) than normal. There are 2 reasons for this phenomenon. The low engine speed results in slower rotation. Another reason is that no residual gas is presence during the first cycle of cranking. The 0 ~ 10 % burned duration is very short (2~5 CAD) compared to normal combustion process.

- The total mass fraction burned however, is not influenced by the engine speed.

- Higher fuel air equivalence ratio leads to higher burn rate especially at the lean region. There is not much difference between the burn profile between the fuel air equivalence ratio of 1 and 1.2 but there is definite difference between in-cylinder ϕ of 0.8 and 1.

The peak mass fraction burned is lower for in-cylinder ϕ of 1.2 due to the lack of air to complete the combustion process at the rich region.

- The MBT timing for continuous firing for the Nissan Engine indicated the MBT timing at around 30 BTDC for stoichiometric mixture. The leaner the mixture the more advance is the MBT timing.

- The MBT timing for the first cycle occurs at 20 BTDC for 900 rpm stoichiometric mixture and shifted to 10 BTDC for 300 rpm stoichiometric mixture. The location of 50% mass fraction burned is at about 5 ATDC for the 300 rpm case which is slightly more advance than the normal result at 7~10 ATDC for steady state operation.

6.1.3 Hydrocarbon Emissions

- The in-cylinder fuel air equivalence ratio seems to be the most important parameter in controlling the EOHC level. When plotted against the in-cylinder fuel air equivalence ratio the curve for EOHC level looks like a bowl. The rapid decrease in the EOHC is due to the lean combustion limit where no misfires occur after certain level of in-cylinder ϕ, the rapid increase in EOHC is due to partial burn or incomplete combustion.

6.2 Direction of Future Work

While this project has evaluated the effect of increasing the cranking speed on mixture preparation, combustion, and hydrocarbon emissions, there are still a few things that can be done to cover a wider range of data and to validate some of the ideas. Specifically future experimental research should focus on:

- Identifying the effect of increasing cranking speed at lower engine coolant temperature. While increasing the engine speed seems only has a modest effect on mixture preparation, it may be significant enough at lower engine temperature where a large amount of fuel injection is necessary even to increase the fuel air equivalence ratio by 0.1

- Further research needs to be conducted in order to elucidate some discrepancies between this experimental result with previous experimental results in term of first cycle imep value at low engine speed. While previous investigation by Bridgette

Castaing and Jim Cowart indicated the imep decreased with cranking speed, this project clearly indicated that the imep value is higher at low speed operation due to the higher intake intake pressure. The answer may lie in the different configuration of engine (4 cylinders with actual cranking vs single cylinder driven at constant speed by a dynamometer)

REFERENCES

[1] Stanglmaier, R.H., Hall, M.J. and Mattews, R.D., " In-Cylinder Fuel Transport during the First Cranking Cycles in a Port Injected 4-Valve Engine", SAE Paper 970043, 1997.

[2] Takeda, K., Yaegashi, T., Sekiguchi, K., Sakito, K., Imatake, N., " Mixture Preparation and HC Emissions of a 4-Valve Engine with Port Fuel Injection During Cold Starting and Warm-up", SAE Paper 950074, 1995

[3] Morishima, R., Asai, K, "Mixture Strength at Cranking Cycles of Gasoline Engine Starting", SAE Paper 920235, 1992

[4] Henning, C., Fischer, Giles, J., Brereton, " Fuel Injection Strategies to Minimize Cold-Start HC Emissions ", SAE Paper 970040

[5] Henein, N.A., Tagomori, M.K., Yassine, M.K., Asmus T.W., Thomas, C.P., and Hartman P.G., "Cycle-by-Cycle Analysis of HC Emissions During Cold Start of Gasoline Engines", SAE Paper 952402, 1995

[6] Brigitte, M., Castaing, Jim, S., Cowart, and, Wai, K.,Cheng, "Fuel Metering Effects on Hydrocarbon Emissions and Engine Stability During Cranking and Start-up in a Port Fuel Injected Spark Ignition Engine", SAE Paper 2000-01-2836, 2000

[7] Cowart, Jim, "Mixture Preparation Behavior in Port Fuel Injected Spark Ignition Engines during Transient Operation ", MIT Press, Cambridge, MA, 2000

[8] Castaing, Brigitte, " Fuel Metering Effects on Hydrocarbon Emissions and Engine Stability During Cranking and Start-up in a Port Fuel Injected Spark Ignition Engine", MIT Press, Cambridge, MA, 2000

[9] Heywood, J.B., Internal Combustion Engine Fundamentals, McGraw-Hill Book Co., 1988

[10] Lee, G.R., Morley, C., "Fuel-Wall Impaction as a Mechanism of Increased Hydrocarbon Emissions from Fuel Heavy Ends ", SAE Paper 952523, 1995

[11] Shayler, P.J., Davies, M.T., Colechin, M.J.F., "Intake Port Fuel Transport and Emissions: The Influence of Injector Type and Fuel Composition ", SAE Paper 961996, 1996

[12] Oda, K., Hosono, K., Isoda, T., Aihara, H., Kojima, K., Shibata, G., " Effect of

Gasoline Composition on Engine Performance ", SAE Paper 930375, 1993

[13]   Al-Roub, M., Farrell, P.V., Senda, J., " Near Wall Interaction in Spray Impingement ", SAE Paper 960863, 1996

[14]   Maier, G., Witting, S., Manz, P., "Influence of Air-Assisted Fuel Injection on the Mixing Preparation within the Intake Ports of SI-Engines ", SAE Paper 982523, 1998

[15]   Rik Wairo, Cheng, Wai.K., "EGR Correlation for Spark Ignition Engines ", Final Report DaimlerChrysler Challenge Fund Project, 2000

[16]   Quader, Ather A., Majkows, Richard F., "Cycle-by-Cycle Mixture Strength and Residual-Gas Measurement During Cold Starting ", SAE Paper 1999-01-1107, 1999

[17]   Ikas, A. Gerhard, "Mixture Preparation Model for a Port Fuel Injected Spark Ignition Engine During the First Cycle of Cranking ", MIT Press, 2001

[18]   Guezennec, Yann G., Hamama, Wajdi, "Two-Zone Heat Release Analysis of Combustion Data and Calibration of Heat Transfer Correlation in an I.C. Engine ", SAE Paper 1999-01-0218, 1999

[19]   Rassweiler, G.M., and Withrow, L., "Motion Pictures of Engine Flames Correlated with Pressure Cards ", SAE Trans. Vol. 42, pp. 185 ~ 204, 1938

[20]   Gatowski, J A. Balles, E. N., Chun, K. M. Nelson, F. E., Ekchian, J.A., and Heywood, J.B., " Heat Release Analysis of Engine Pressure Data ", SAE Paper 841359, 1984.

[21]   Cheung, Hon Man, "A Practical Burn Rate Analysis for Use in Engine Development and Design ", MIT Press, Cambridge MA, 1993

[22]   Cheng, Wai.K, D.Hamrin, J.B Heywood, S.Hochgreb, M. Min, and M. Norris, "An Overview of Hydrocarbon Emissions Mechanism in Spark-Ignition Engines ", SAE Paper 932708, 1993

[23]   Stache, I., Alkidas, A.C., " The Influence of Mixture Preparation on HC Concentration Histories from a S.I. Engine Running Under Steady-State Conditions", SAE Paper 972981, 1997

[24]   Seabrook, J., Nightingale, C., Richardson, S.H., "The effect of Engine Variables on Hydrocarbon Emissions – An Investigation with Statistical Experiment Design and Fast Response FID Measurements ", SAE Paper 961951, 1996